THE JOHNS HOPKINS UNIVERSITY

DEPARTMENT OF PHYSICS

LASER RAMAN SCATTERING STUDIES OF CRYSTALS

including: Light Scattering Studies of the Alpha-Beta Phase Transition in Quartz

Final Report on Contract Nonr 4010(06)
ARPA Order Number 306-63

July 15, 1969

Baltimore, Maryland 21218

185

I) Historical Summary of The Project

In May 1963, Professor G. H. Dieke of The Johns Hopkins University submitted a proposal to the Office of Naval Research for a laser excited Raman spectroscopy program. He intended to apply Raman spectroscopy to the study of the crystal phonon field, primarily as a means of gaining further insight into the interactions occurring in laser materials. A research and development task order effective 16 June 1963 directed that "The contractor . . . . . shall employ laser techniques to study the structure of crystals, principally fluorescent. One technique to be employed will be the use of Raman scattering to measure the phonon spectra of various crystalline substances."

During the first year of this contract Professor Dieke and Dr. Wilbur Peters carried out a series of stimulated Raman scattering experiments using a Korad giant pulse ruby laser. These experiments were not completed, however, and were succeeded during the following year by spontaneous Raman scattering experiments utilizing a Spectra-Physics 8 mw C. W. He-Ne laser.

Dr. Dieke died suddenly on August 25th 1965, and responsibility for the work was taken over by Dr. H. Z. Cummins who subsequently became principal investigator. At that time, a Spectra-Physics Model 125 He-Ne laser producing 70 mw of 6328 A radiation was acquired for an exciting source. Subsequently a Spectra-Physics Model 140 one watt argon ion laser was added to the apparatus, along with a Spex tandem grating monochromator and modern "photon counting" electronics.

Project Personnel

Dr. Gerhardt H. Dieke	Principal Investigator (16/June/63 - 25/Aug./65)
Dr. Herman Z. Cummins	Principal Investigator (25/Aug./65 - 15/June/69)
Dr. Wilbur Peters	Visiting Professor 1963-64
Dr. A. Roger Gee	Research Associate 1964-65
Dr. Ramanaiah V. Kolluri	Research Associate 1966-67
Donald O'Shea) Stephen Shapiro)	Graduate Student Research Assistants
Doris LeBrun) Arthur Weinman)	Summer Assistants
Irene Keesler) Ruth Rapoport) Elsa Clark)	Secretaries (Part Time)
Earl Williams	Crystal Technician (Part Time)

Ph. D. Degrees Earned

Donald C. O'Shea (June 1968) "Raman Scattering Experiments in Strontium Titanate"

Stephen Shapiro (June 1969) "Light Scattering Studies of the Alpha-Beta Phase Transition in Quartz"

Publications Resulting in Whole or in Part from This Project

1) "Raman Scattering and Fluorescence in Calcium Fluoride," A. Roger Gee, Donald C. O'Shea and Herman Z. Cummins. Solid State Communications 4, 43 (1966).

2) "Dewar for Use in Crystal Raman Spectroscopy," A. Roger Gee and Donald C. O'Shea. Rev. Sci. Instr. 37, 670 (1966).

3) "Brillouin Scattering Spectra of Crystalline Quartz, Fused Quartz and Glass," Stephen M. Shapiro, Robert W. Gammon and Herman Z. Cummins. Appl. Phys. Letters 9, 157 (1966).

4) "Visual Observation of Ferroelectric Domains in TGS," Stephen M. Shapiro, Robert W. Gammon and Herman Z. Cummins. Appl. Phys. Letters 10, 113 (1967).

5) "Temperature Dependent Raman Spectrum of Strontium Titanate," Donald C. O'Shea, R. V. Kolluri and Herman Z. Cummins. Solid State Communications 5, 241 (1967).

6) "Raman Scattering Study of the Alpha-Beta Phase Transition in Quartz," Stephen M. Shapiro, Donald C. O'Shea and Herman Z. Cummins. Phys. Rev. Letters 19, 361 (1967).

7) "Laser Light Scattering Spectroscopy" in: Proceedings of the International School of Physics "Enrico Fermi" XLII Course, 1967. (Academic Press - to be published).

8) "Temperature Dependence of the Raman, Brillouin and Rayleigh Scattering in Quartz," S. M. Shapiro and H. Z. Cummins; "Spatial Variation in the Raman Spectrum of $SrTiO_3$," D. C. O'Shea and H. Z. Cummins; "Brillouin Scattering Study of the Ferroelectric Phase Transition of KH_2PO_4," E. M. Brody and H. Z. Cummins. In: Proceedings of the International Conference on Light Scattering Spectra of Solids, New York University, September 1968; G. B. Wright, Editor. (In Press)

9) "Critical Opalescence in Quartz," S. M. Shapiro and H. Z. Cummins. Phys. Rev. Letters 21, 1578 (1968).

I) Historical Summary of The Project

In May 1963, Professor G. H. Dieke of The Johns Hopkins University submitted a proposal to the Office of Naval Research for a laser excited Raman spectroscopy program. He intended to apply Raman spectroscopy to the study of the crystal phonon field, primarily as a means of gaining further insight into the interactions occurring in laser materials. A research and development task order effective 16 June 1963 directed that "The contractor . . . . . shall employ laser techniques to study the structure of crystals, principally fluorescent. One technique to be employed will be the use of Raman scattering to measure the phonon spectra of various crystalline substances."

During the first year of this contract Professor Dieke and Dr. Wilbur Peters carried out a series of stimulated Raman scattering experiments using a Korad giant pulse ruby laser. These experiments were not completed, however, and were succeeded during the following year by spontaneous Raman scattering experiments utilizing a Spectra-Physics 8 mw C. W. He-Ne laser.

Dr. Dieke died suddenly on August 25th 1965, and responsibility for the work was taken over by Dr. H. Z. Cummins who subsequently became principal investigator. At that time, a Spectra-Physics Model 125 He-Ne laser producing 70 mw of 6328 A radiation was acquired for an exciting source. Subsequently a Spectra-Physics Model 140 one watt argon ion laser was added to the apparatus, along with a Spex tandem grating monochromator and modern "photon counting" electronics.

The contract was extended year by year until reaching final termination on June 15, 1969.

II) Scientific Summary

Initial efforts aimed at exploiting stimulated Raman scattering for investigating crystal phonon fields were abandoned after one year for two reasons: (1) Stimulated scattering tends to occur preferentially in one mode, and the other (weaker) modes are never seen, and (2) the giant pulse required for producing stimulated scattering frequently destroys the crystal.

During the second year, a spontaneous Raman scattering apparatus was constructed using a Spectra-Physics Model 115 8 mw He-Ne laser as the exciting source. The initial experiments with the apparatus were on calcium fluoride and calcium tungstate crystals doped with erbium and samarium. These materials are also used as the active medium in lasers. The many lines which were observed in the laser-excited spectra, however, were found to be caused by fluorescence rather than by Raman scattering. Therefore rare-earth doped crystals were not studied further, and attention turned to the Raman spectra of pure crystals, and particularly to the modifications occurring in the vicinity of a crystalline phase transition.

The systems studied included calcium fluoride, calcium tungstate, second order Raman scattering in numerous crystals, strontium titanate,

potassium dihydrogen phosphate and quartz. The technical results of these experiments have been presented in previous reports, and many have been published in the scientific literature. (See list of publications above.)

The two major efforts of this project have been the Raman studies of strontium titanate and quartz in the vicinity of their respective phase transitions. The quartz work which has been the principal undertaking during the past two years is covered in detail in the remainder of this report.

III) Light Scattering Studies of The Alpha-Beta Phase Transition in Quartz

This section which completes this report gives a detailed account of the quartz work. The text was prepared by Stephen M. Shapiro and was submitted by him to The Johns Hopkins University in June 1969 in a slightly expanded form in partial fulfillment of the requirements for the Ph. D. degree.

LIGHT SCATTERING STUDIES OF THE ALPHA-BETA PHASE TRANSITION IN QUARTZ

ABSTRACT

On the basis of early theoretical and experimental investigations of the alpha-beta phase transition in crystalline quartz (T_t = 573°C), it has been accepted that the transition is second order, the quartz crystal exhibits critical opalescence at the transition temperature, and the 207 cm^{-1} Raman active, zone center optic vibration is the soft mode responsible for the phase transition.

We have studied the Raman and Brillouin spectra of crystalline quartz from 20°K to 873°K (600°C) with special attention devoted to the alpha-beta transition region.

The Raman spectra of alpha quartz reveal 12 lines of E symmetry whereas group theory predicts 8. Scott and Porto showed that the additional lines are due to a lifting of the LO-TO degeneracies of some of the E vibrations. There is little change in the frequency of the E vibrations with increasing temperature.

The A_1 spectrum of alpha quartz reveals 5 lines whereas group theory predicts 4. The lowest frequency A_1 line appears to play a dominant role in the phase transition since its frequency decreases from 147 cm^{-1} at room temperature to 30 cm^{-1} in the transition region. At the transition temperature this line disappears from our spectra. On cooling from the high temperature phase, there is a temperature hysteresis since the mode suddenly reappears at a temperature 1 C° lower than the temperature at which it disappears on heating. The frequency of the

207 cm^{-1} line decreases to 162 cm^{-1} at the transition temperature and is still present in the beta phase. Group theory appears to be violated in the beta phase since only one A_1 vibration is allowed and two lines are observed. Scott attributed the anomalous temperature dependence of the 147 cm^{-1} and 207 cm^{-1} excitations to anharmonic coupling of the soft zone center phonon and two zone edge acoustic phonons. The extra line in the alpha and beta phases is a second order Raman line and does not violate the group theoretical calculations which are for $\vec{q} = 0$.

Since the frequency of the soft mode does <u>not</u> decrease continuously toward zero as the transition temperature is approached, the "opalescence" is not due to diverging fluctuations associated with the soft optic mode as had been proposed by Ginzburg.

In the Brillouin scattering experiments, acoustic phonons propagating in the [100], [010], [001], and [110] directions were studied. The various elastic constants measured agreed with the results of ultrasonic experiments. For each propagation direction studied, the longitudinal acoustic modes exhibited a decrease in frequency of 10 to 20% on heating the crystal from room temperature to the transition temperature, and then an abrupt increase. On cooling there is a gradual change in the frequency of the phonons. Since no acoustic mode becomes unstable at the transition temperature, the observed "opalescence" is not due to diverging fluctuations associated with an acoustic vibration.

The temperature hysteresis observed in the Raman and Brillouin experiments suggests that quartz undergoes a first order transition rather than a second order transition.

Observations of the Rayleigh scattered light at the transition temperature showed that the large increase in the elastic scattering is due to essentially static inhomogeneities in the index of refraction. Two possible sources of the inhomogeneities are domain boundaries between the two members of the Dauphiné twins coexisting in the quartz crystal, or the formation, on heating, of beta quartz regions within the alpha quartz crystal.

TABLE OF CONTENTS

TABLE OF CONTENTS (Continued)

LIST OF TABLES

LIST OF ILLUSTRATIONS

LIST OF ILLUSTRATIONS (Continued)

LIST OF ILLUSTRATIONS (Continued)

BLANK PAGE

INTRODUCTION

It has long been known that crystalline quartz undergoes a phase transition at 573°C. At this temperature the crystal changes from the low symmetry or alpha phase, belonging to the trigonal system ($D_3 \equiv 32$), to the high symmetry or beta phase, belonging to the hexagonal system ($D_6 \equiv 622$). Also, at this temperature there are anomalous changes in many of the properties of quartz, one of these being the intensity of the scattered light. Yakovlev et al observed the spectrally unresolved scattered light and reported an increase in intensity of $\sim 10^4$ over the room temperature scattered light intensity, and because of the appearance of the scattering column under white light illumination interpreted this phenomenon as critical opalescence. Ginzburg applied Landau's theory of second order phase transitions to quartz and calculated the increase in scattered light intensity at the transition temperature, obtaining a value which agreed with experiment. It thus appeared that quartz underwent a second order phase transition and exhibited critical opalescence at the transition temperature.

The present investigation explores the temperature dependence of the spectral components of the scattered light in an effort to understand the dynamics of the alpha-beta phase transition and determine the cause of the opalescence.

In Chapter I we study the symmetry and properties of quartz. Group theory is used to calculate the normal modes of vibration and the

displacement and mode correlation charts. The alpha-beta phase transition is discussed and Ginzburg's theory of the quartz transition is presented.

In Chapter II we discuss the Raman scattering experiments performed on crystalline quartz. Following a brief introduction on the classical theory of the Raman effect, the past Raman experiments on quartz are reviewed. The apparatus used in the present investigation is described, and the results of the temperature dependent experiments are presented and discussed.

In Chapter III we discuss the Brillouin scattering experiments performed on crystalline quartz. In reviewing the theory of Brillouin scattering in solids, we discuss the elastic and photoelastic behavior of solids. The past experiments are reviewed and the apparatus used is described. The chapter concludes with the results of the Brillouin studies.

In Chapter IV, the Raman and Brillouin experiments in the transition temperature region (570°C - 576°C) are reported. In addition, the results of the visual observations of the Rayleigh scattering are discussed and the probable cause of the "opalescence" is reported.

Finally, in Chapter V we summarize the results of our light scattering investigations of quartz.

CHAPTER I

CRYSTALLINE QUARTZ: STRUCTURE AND PROPERTIES

The molecular unit comprising all forms of silica is SiO_2. The difference between crystalline quartz and the other forms of silica is the particular arrangement of three molecular units to form one unit cell. The translation of this cell in three directions in space will generate a crystal whose space group is one of the 230 allowed space groups.

Fig. I-1 shows the six principal phases of silica (1). The name quartz applies to that form of silica stable up to 867°C. Alpha, or low quartz is the stable modifications of SiO_2 up to 573°C. At this temperature quartz undergoes a transition to the beta, or high quartz phase with an increase in the space group symmetry. From 867°C to 1470°C tridymite is the stable form of silica. Cristabolite, the highest symmetry form, is stable from 1470°C up to the melting point of silica, 1723°C. It is possible for the high temperature forms of silica to exist at room temperature, but only in a metastable state. A well known example is vitreous silica, or fused quartz, which is liquid SiO_2 cooled under conditions such that it doesn't crystallize. A detailed discussion of the various modifications of silica and their properties is given by Sosman (1). We report only the light scattering experiments performed on quartz and its alpha-beta transition.

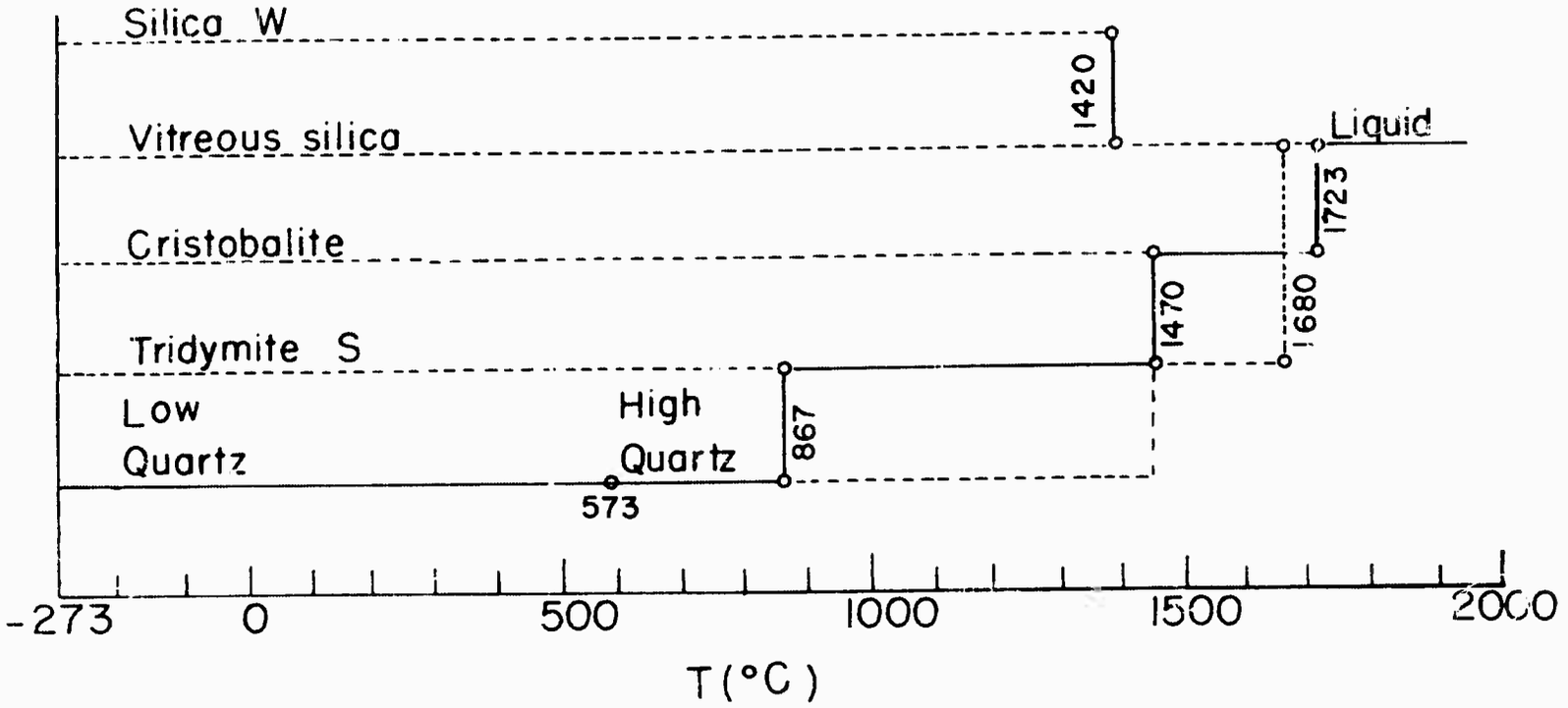

Fig. I-1. The various modifications of Silica. The solid lines represent stable states; the dashed lines metastable and unstable states.

The remainder of this section discusses the structure and properties of alpha and beta quartz. Group theory is used to cal ulate the symmetry of the normal modes of vibration and to infer the directions of the atomic displacements in the various modes. Finally, the currently accepted theory of the alpha-beta phase transition is discussed.

A. LOW TEMPERATURE (ALPHA) QUARTZ

1. Symmetry

Alpha, or low quartz is a member of the trigonal crystal system and possesses a point symmetry of $D_3(\equiv 32)$ called the trigonal trapezohedral (2). The crystals belonging to this point group have a triad axis denoted as the Z (or c) axis and three twofold axes in the plane perpendicular to Z. The commonly used set of orthogonal axes established by the IRE (3) to describe many of the physical properties of quartz are the triad axis as Z, one of the twofold axes designated as X, and Y is defined as perpendicular to Z and X. Often the X,Y,Z axes are referred to as a, b and c. Many crystallographers use a different set of axes to describe quartz: X and Y are two of the three twofold axes making an angle of 120° with one another, and Z is the threefold axis.

To understand the features of the structure and the interrelations that exist in crystalline quartz, a projection of the crystal structure onto the x-y plane, looking down the c axis, is useful. This projection is shown in Fig. I-2 (4).

To describe the positions of the silicon and oxygen atoms, four parameters are needed. Since each silicon atom is situated on the twofold X axis, one parameter, u, the distance from the Z axis to the silicon atom defines the silicon's position. This number is a fraction

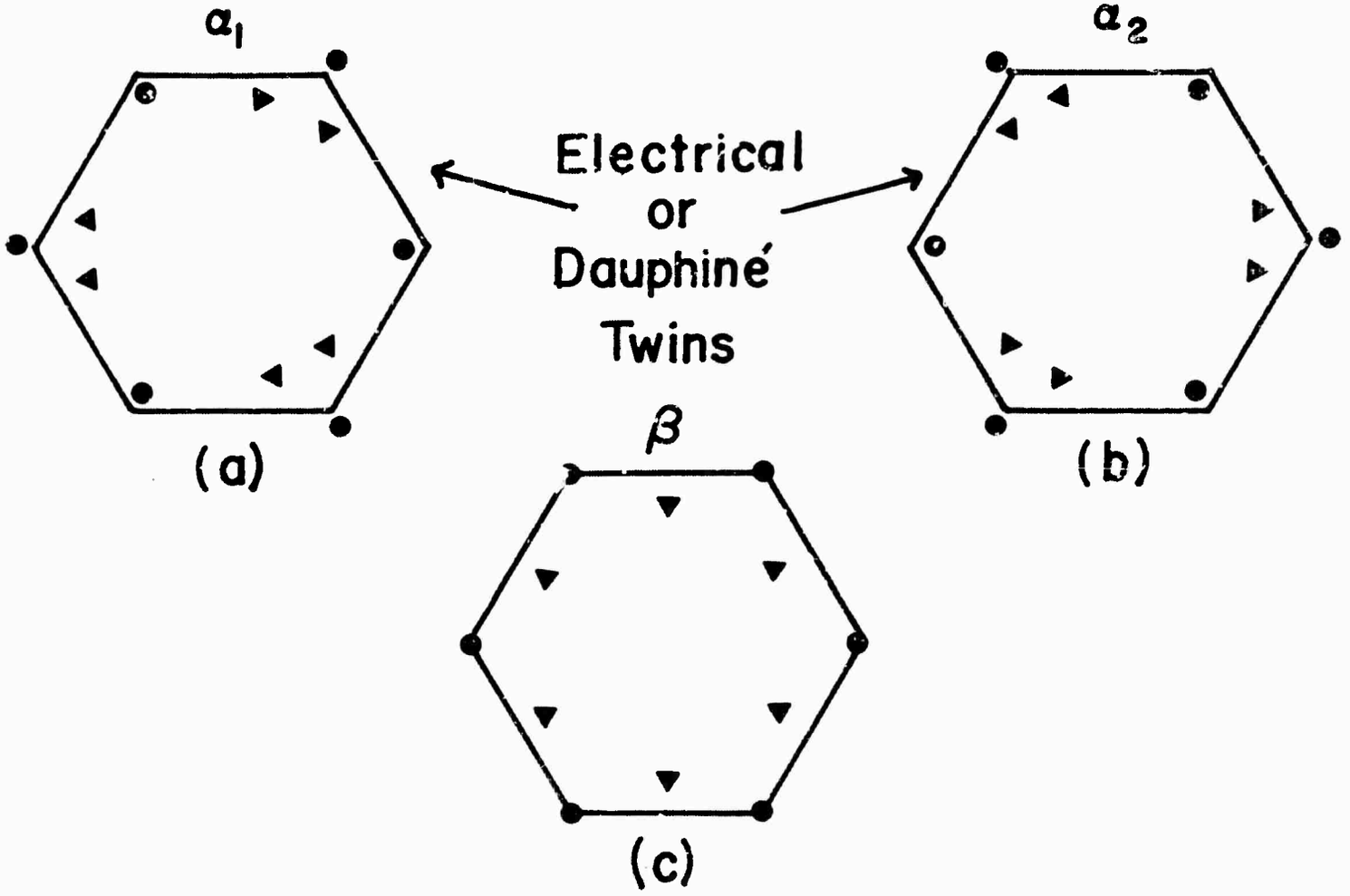

Fig. I-2. x-y projection of the quartz structures showing the relationship between the electrical or Dauphiné twins (a and b) and beta quartz (c): ● . silicon atoms; ▲ : oxygen atoms.

of the lattice parameter in the X direction. Once one silicon atom is positioned, the others are generated by the symmetry elements. The general position, x,y,z, of one oxygen atom is required, and the rest are generated by symmetry. x and y are given in terms of fractions of the lattice parameter a, and the coordinate z is given in terms of a fraction of the lattice parameter in the Z direction, c. It is necessary to note that the fractional coordinates of the atoms in alpha quartz are given in relation to the crystallographers' set of axes, the non-orthogonal XYZ system mentioned above. Appendix A gives the crystallographic information regarding the structure of quartz. In addition, other properties of quartz useful in later discussions are tabulated.

So far we have limited the discussion to the point symmetry, i.e., the symmetry described by keeping one point in the unit cell fixed. This allows only rotations, reflections and rotatory reflections. There are 32 allowed point groups (5). If we allow translations to be combined with these 32 point groups, the 230 space groups are generated. Alpha quartz is enantomorphic in that there are two space groups to which alpha quartz belongs: $D_3^6(P3_221)$ and $D_3^4(P3_121)$ (2). The former contains a symmetry operation which is a rotation of 120° about Z followed by a translation in the Z direction of 2/3 of the cell edge, c. Another rotation and a 2/3 translation will bring the atom 1/3 of the way into the next cell. Since the cells are identical, if the atom is in one cell it is in all of them, so the atom is placed in the starting cell. The third operation moves the atom to the position corresponding to where it started. The combined operation of a rotation and translation creates a screw axis which, in this case, is a left handed screw axis. $D_3^4(P3_121)$ contains a symmetry operation which is a 120° rotation followed by a translation of 1/3 the cell edge, generating a right handed screw axis.

The space group $D_3^6(P3_221)$ corresponds to left handed quartz and $D_3^4(P3_121)$ corresponds to right handed quartz. Since quartz is also optically active, the names of the different forms tell how the plane of polarization is rotated when light travels along the optic axis. When these two enantomorphic forms of quartz exist simultaneously in a crystal the crystal is said to be twinned. This type of twinning is referred to as Brazilian, or optical twinning (1). Since these optical twins rotate the plane of polarization in different directions, they can easily be detected with crossed polaroids. In our experiments, all samples used were free of optical twinning.

The other major type of twinning, the Dauphiné, or electrical, twin is less easily detected and, as the name suggests, affects the electrical properties of quartz. The two members of this twin are related by 180° rotation about the Z axis as shown in Figs. I-2a and I-2b. The space group symmetry properties of each type are the same. Twinning of this type is not revealed by optical tests. However, the X axes (which are the electric axes in the two components) are opposed, and if the two types are present the piezoelectric effect is diminished. Etching and electrical measurements can reveal the existence of Dauphiné twinning.

Several authors have studied electrical twins in quartz crystals with regard to their motion, creation and reduction (1, 6, 7). The general result from these studies is that this type of twinning is extremely difficult to control. More was learned about putting Dauphiné twinning into quartz than removing it!

Dauphiné twinning occurs naturally and can be produced readily at room temperature by a small mechanical shock. River quartz is extensively twinned at the surface as a result of being tumbled in the stream. It is most likely that in the cutting and polishing of our crystals we changed any pre-existing twins and introduced new ones.

The strategy frequently employed for removing Dauphiné twins is to heat quartz well above the alpha-beta transition temperature where the twinned crystal becomes homogeneous, and then control the cooling rate so that twinning does not reappear at lower temperatures (6). The amount of twinning produced is influenced by the rate of cooling through the transition temperature, the size of the sample and the original distribution of the twinning. Frondel found that slow cooling tends to increase the amount of twinning produced and decrease the amount of cracking (6). He found that inversion twinning always occurred in plates of quartz over 1 mm. thick regardless of the cooling conditions. He also found that when quartz is heated above the transition temperature, the crystal retains a memory of what twin it was while in its low temperature phase. This was observed in experiments where quartz was cooled from the beta phase; the crystal was more likely to go back into the same form which it possessed before heating rather than to the other form of the twin. This is apparently due to the strains being created and persisting in the sample when the twinning is lost. Heating the quartz 100°C above the transition temperature does not erase the memory.

Since there are two possible equilibrium positions available for each atom in the alpha phase of quartz (Fig. I-2a and I-2b) corresponding to the two Dauphiné twins, and since electrical twinning should disappear on heating above the transition temperature, the concept of electrical twinning appears to be an important consideration in understanding the phase transition.

In our experiments twinning went uncontrolled. However, the reproducibility of the data within a temperature run where the transition region was traversed several times indicates that either the twinning was changing in the same way each time, or was not affecting the properties being measured.

In the types of twins described above, the Z axis is constant in direction throughout the crystal. Many more types of twins are possible involving variation of the orientation of the Z axis but none are frequent among natural crystals (1). The best known of these is the Japanese twin, its two parts being symmetrical with respect to one of the trigonal bipyramid faces so that the Z axes in the two twins meet at an angle of 104°. These types of twins can be detected by inspection. Crystals used in our experiments were observed to be free of such twinning.

2. Properties

The two properties which have led to extensive studies of quartz are piezoelectricity and optical activity.

Piezoelectricity can be precisely defined as "the electric polarization produced by mechanical strain in crystals belonging to certain classes, the polarization being proportional to the strain and changing sign with it. This is the direct effect. In the converse effect, a piezoelectric crystal becomes strained when electrically polarized by an amount proportional to the polarizing field"(8).

We can express this statement in mathematical terms:

Direct effect:

$$P_h = \sum_{m=1}^{6} e_{hm} x_m$$

$$\text{or} \quad P_h = \sum_{m=1}^{6} d_{hm} X_m$$

Converse effect:

$$X_m = \sum_{h=1}^{3} e_{hm} E_h$$

$$x_m = \sum_{h=1}^{3} d_{hm} E_h$$

where the quantities are defined: E_h is the electric field, P_h the polarization, x_m the strain, and X_m the stress. The third rank tensor quantities, d_{hm} and e_{hm} are the piezoelectric strain and stress constants respectively. h can take on values 1, 2, or 3 and m = 1, 2, 3, 4, 5, or 6. The subscripts are in their reduced form where pairs of subscripts have been replaced by a single subscript, i.e. (9):

$$\{1 \quad 2 \quad 3 \quad 4 \quad 5 \quad 6\}$$

$$\text{for} \quad \{11 \quad 22 \quad 33 \quad 23 \quad 13 \quad 12\}$$
$$\qquad\qquad\qquad\qquad\qquad\quad 32 \quad 31 \quad 21\}$$

From the matrix of the piezoelectric constants (Appendix A) an X or Y compressive or tensile stress in alpha quartz can produce polarization in the X direction only. The sign of the polarization depends on the sign of the stress (tension or compression). The X axis is thus polar and is called the electric axis. For right handed quartz the plus direction is defined as having a positive charge on compression.

A shear stress can produce a polarization in the x or y directions. Since the bottom row of the matrix representation of the piezoelectric tensor contains all zeros no possible stress can produce a polarization along the triad axis.

Quartz is probably the most widely used piezoelectric crystal although the effect is smaller than that in some other crystals such as Rochelle Salt and KDP (8). The reasons for the widespread use of quartz are its abundance, chemical stability, hardness and the ability to cut and polish quartz into any shape.

The optical rotatory power of quartz is 18.5 angular degrees/mm. near 6328 A. As mentioned above, right and left handed quartz will rotate the plane of vibration of the E vector of a plane polarized light beam travelling along the optic axis in opposite directions. The convention used is the following: right handed rotation is a rotation of the electric vector in a clockwise direction looking against the oncoming light. Left handed quartz rotates the vibration plane counterclockwise (10).

In most of our experiments, efforts were made to avoid sending light along the optic axis due to the difficulty in polarization assignments and intensity measurements. Only in the case where a Z phonon was being studied was the optic axis in the scattering plane. In all other experiments, the scattering plane was the x-y plane and the effects of optical activity were avoided.

B. HIGH TEMPERATURE (BETA) QUARTZ

When quartz is heated above 573°C into its high temperature or beta phase, the symmetry of the crystal changes (1). Beta quartz belongs to the hexagonal crystal system with point symmetry $D_6(622)$ (2). Beta quartz is still enantomorphic, $D_6^4(P6_222)$ and $D_6^5(P6_422)$, and has the same helicity as the lower temperature form, i.e., the handedness is preserved. Fig.1-2c shows the basal plane (x-y) projection of the oxygen and silicon atoms. By looking at the special hexagonal unit cell, we see that in order to form the 6 fold axis from the low temperature phase the silicons must move along the two-fold axes to the vertices of the hexagon. The oxygens move nearly perpendicular to the Si - O - Si plane to positions equidistant from the silicons. Thus, in addition to the new six-fold rotation symmetry, a new two-fold symmetry axis lying in the basal plane connecting opposite oxygens is also created.

Because of the higher symmetry of beta quartz, there is only one positional parameter to be determined. This is the x coordinate of one oxygen. The other coordinates are related to this coordinate by symmetry as shown in Appendix A. Since the silicons occupy the vertices of the hexagon, their x,y,z positions are given in terms of small integer fractions of the lattice parameters a and c. Appendix A gives the fractional coordinates for beta quartz, along with other physical properties and constants.

Fig. 1-2 shows the relationship of beta quartz to the two Dauphiné twins of alpha quartz. We see that the atomic positions in the beta quartz are the average atomic positions of the two Dauphiné twins of

alpha quartz.

Since the atomic positions in the beta phase occupy the mean position of the alpha twins, one would expect Dauphiné twinning to disappear on passing into the high temperature phase. This is also expected since the piezoelectric coefficient d_{11} goes to zero as the transition temperature is approached and is zero in the beta phase. Thus, because of the higher symmetry, the polarity of the X axis has disappeared. This is observed, but, as mentioned above, on cooling the crystal "remembers" its twin form due to strains persisting in the high temperature phase (11).

C. NORMAL MODE ANALYSIS OF QUARTZ

In a crystalline solid containing N atoms, there are a total of 3N vibrational motions since each atom has 3 translational degrees of freedom. For macroscopic samples, N is a very large number and there is an extremely large number of modes. The problem of calculating the properties of these modes is reduced to manageable proportions when the translational symmetry of the solid is taken into account. Translational symmetry means that there exist basis vectors such that the crystal structure remains invariant under translation through any vector which is the sum of integral multiples of the basis vectors. The physical arrangement of the whole crystal can be defined if we specify

the contents of a single unit cell. The macroscopic crystal is generated by repeated translations of this unit cell in directions defined by the basis vectors. Since all unit cells are equivalent it is sufficient to consider the motions of the atoms in one unit cell. If there are n atoms in a primitive unit cell, there will be 3n branches of the dispersion curve, frequency of vibration Ω vs momentum q. (In the trigonal and hexagonal crystal systems, corresponding to alpha and beta quartz, the unit cells are primitive.) A typical dispersion curve is shown in Fig. I-3. The three branches with $\Omega \to 0$ as $q \to 0$ are the acoustic branches and the remaining 3n-3 branches are the optic branches. In the dispersion curve, q can take on values from 0 to $\pm 10^8 cm^{-1}$. For those modes that produce light scattering, q is on the order of $10^5 cm^{-1}$, which is small compared to $10^8 cm^{-1}$. Thus the approximation $q \simeq 0$ is made and in the following discussion the term "modes" refers to the 3n modes of vibration with $q = 0$.

If the interatomic forces are known, the vibrational modes can be completely determined. One sets up the dynamical matrix which is the matrix of the coefficients of the quadratic term of the potential energy expansion in terms of particle displacement coordinates. From this matrix the eigenvalues can be computed. A new set of coordinates are defined which are linear combinations of the displacement coordinates. If the transformation matrix, which defines our new coordinates, simultaneously diagonalizes the kinetic and potential energies, then the new coordinates are called the normal coordinates. In terms of these coordinates, the Hamiltonian has the form of a sum of simple

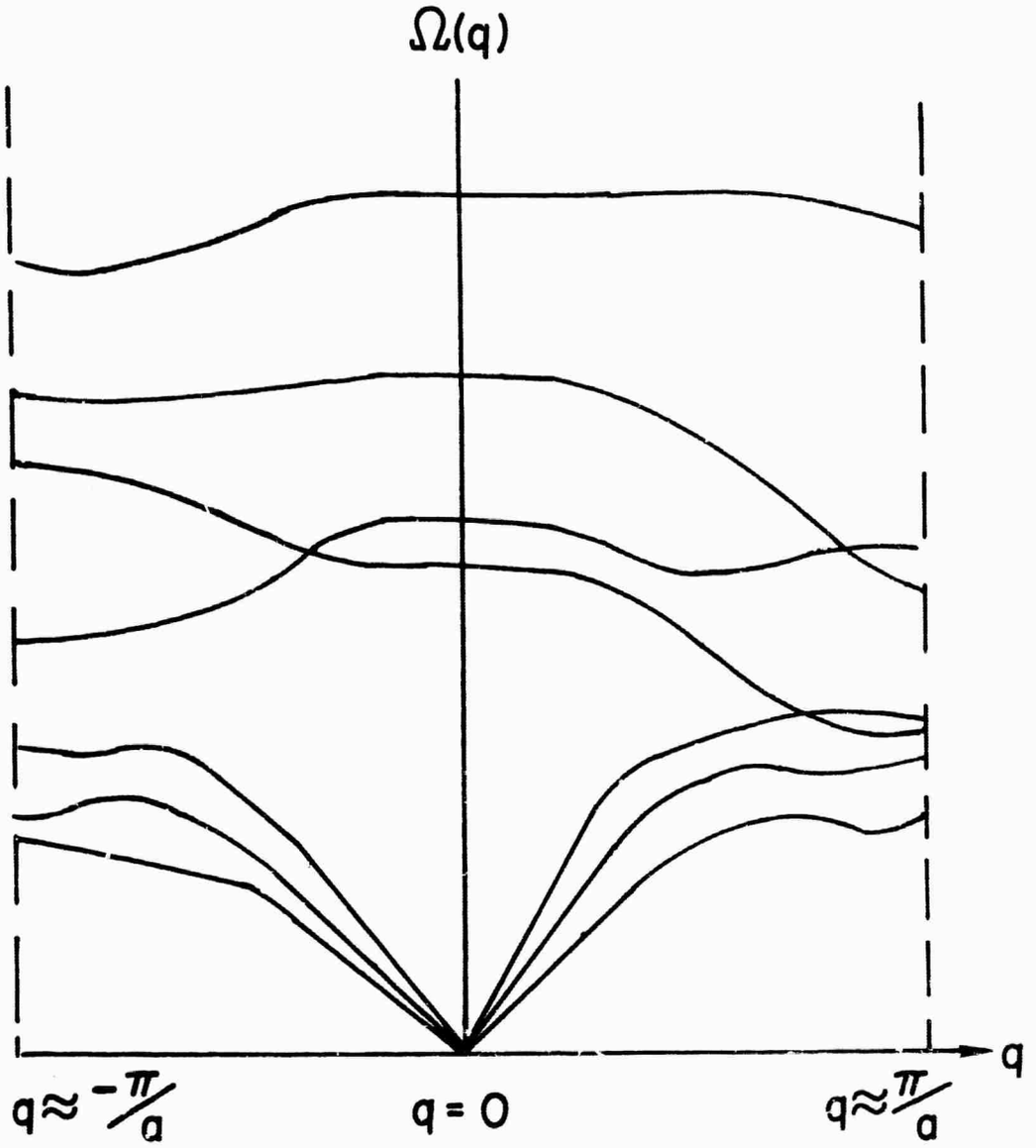

Fig. I-3. A typical dispersion curve for lattice vibrations. Ω is the frequency of the lattice modes and q is the wavevector (proportional to momentum). The 3 branches for which $\Omega \to 0$ as $q \to 0$ are the acoustic branches and the remaining branches are the optic branches.

harmonic oscillator Hamiltonians where the kinetic and potential energies are sums of squares only, without any cross terms. Each normal coordinate corresponds to a vibration of the system with only one frequency. These oscillations are spoken of as the normal modes of vibration (12).

For quartz, there are 9 atoms in a unit cell and 27 normal modes. Although the interatomic forces are not known, they may be estimated on the basis of a model. The calculation, though cumbersome, is possible. On the basis of a valence force model Kleinman and Spitzer calculated the atomic motions and frequencies for the eight nondegenerate modes of vibration of alpha quartz (13).

Since the potential energy function is invariant under the symmetry operations of the full space group of the lattice, restrictions are imposed on the form of the potential and, thus, on the normal coordinates. The normal coordinates will possess certain transformation properties which can be determined by group theory. We can also determine the atomic displacement directions which occur for each normal vibration. In addition, the correlation between the normal modes in alpha and beta quartz can be determined. Group theory, however, cannot yield values for the normal coordinates or the frequencies. These can be found only when the interatomic forces are known.

Because of the translational symmetry and our $q=0$ assumption it is sufficient to consider the crystal point groups. The collection of symmetry operations which leave a crystal invariant, and one point fixed, form a group which is one of the 32 crystal point groups. Each element of the group can be represented by a matrix and the collection

of matrices form a representation of the group. The elements of a group divide into classes. The invariant quantity for equivalent representations of a class is the character, or trace, of the representation. A representation can be reduced if a similarity transformation can be found which puts the representation into block form along the diagonal. If this cannot be done, the representation is said to be irreducible. For each point group the number of irreducible representations equals the number of classes (14).

The invariance of the potential energy under the symmetry operations of the group implies the invariance of the square of a single, nondegenerate normal coordinate, or the invariance of a linear combination of the squares of p normal coordinates which have the same frequency. The former corresponds to a one dimensional representation and the latter to a p dimensional irreducible representation. In general, a frequency is p fold degenerate if the corresponding normal coordinates transform according to a p dimensional irreducible representation.

The characters for the irreducible representations of the 32 different point groups have been tabulated (14). Table I-1 gives the character tables for alpha quartz (D_3) and beta quartz (D_6). These tables show, in addition to the characters of the different classes, the transformation properties of the orthogonal coordinates (x,y,z) and various bilinear forms. These are useful in deriving the selection rules for Raman and Infrared activity. The character table for alpha quartz (D_3) gives the characters for the three classes: the identity element, E; the two possible 120° rotations about the threefold axis,

Table I-1

Character Tables

Alpha Quartz

$D_3(32)$			E	$2C_3$	$3C_2'$
$x^2 + y^2, z^2$		A_1	1	1	1
	z	A_2	1	1	-1
(xz,yz)	(x,y)	E	2	-1	0
$(x^2 - y^2, xy)$					

Beta Quartz

$D_6(622)$			E	C_2	$2C_3$	$2C_6$	$3C_2'$	$3C_2''$
$x^2 + y^2, z^2$		A_1	1	1	1	1	1	1
	z	A_2	1	1	1	1	-1	-1
		B_1	1	-1	1	-1	1	-1
		B_2	1	-1	1	-1	-1	1
(xz,yz)	(x,y)	E_1	2	-2	-1	1	0	0
$(x^2 - y^2, xy)$		E_2	2	2	-1	-1	0	0

$2C_3$; and 180° rotation about the three twofold axes in the x-y plane, $3C_2'$. The irreducible representations are: A_1, a totally symmetric, one dimensional representation in which the displacements of the atoms are invariant under all operations in the group; A_2, a one dimensional representation in which the displacements are symmetric with respect to the threefold rotation, but antisymmetric with respect to the two-fold axes; E, a doubly degenerate, two dimensional representation where the displacements are antisymmetric under C_3 and unsymmetric under C_2'.

There are two methods which can be used to find the number of vibrations of each irreducible representation (or species) for a given solid with a given symmetry. One method involves the consideration of the individual molecules within the crystal and is called the site method (15). The method we will employ is the unit cell analysis of Bhagavantum and Venkatarayudu (16). In this method all the atoms in the unit cell are considered.

We consider an arbitrary displacement of the atoms in a unit cell. The collection of matrices representing the transformation properties of an arbitrary displacement of all the atoms in the unit cell under the symmetry operations of the group is called the total representation. In quartz the total representation is a collection of 27 dimensional matrices.

It can be shown that only those nuclei which remain fixed, or are moved to an equivalent position, under the symmetry elements of the group contribute to the characters of the total representation matrices (14). For a rotation by an angle θ, each atom that is transformed into itself, or an equivalent one, contributes $(1 + 2\cos\theta)$ to the character.

For the classes in alpha quartz (D_3):

$\chi'(E)$	$\chi'(C_3)$	$\chi'(C_2')$
3	0	-1

where $\chi'(\sigma)$ is the contribution to the total character for one atom.

For the classes in beta quartz (D_6):

$\chi'(E)$	$\chi'(C_2)$	$\chi'(C_3)$	$\chi'(C_6)$	$\chi'(C_2')$	$\chi'(C_2'')$
3	-1	0	0	-1	-1

It is now necessary to determine how many atoms are unchanged under the operations of each class. We will use the hexagonal cells in Figs. I-2 and cyclic notation (i.e. (123) means atom 1 is moved to position of atom 2, 2 to 3 and 3 to 1; no atom is unchanged):

Alpha quartz (D_3)

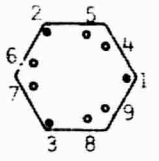

Class	Atoms	Number Unchanged
E	(1)(2)(3)(4)(5)(6)(7)(8)(9)	9
C_3	(123)(468)(579)	0
	(132)(486)(597)	0
C_2'	(1)(23)(49)(58)(67)	1
	(2)(13)(56)(47)(98)	1
	(3)(12)(45)(96)(87)	1

Thus the characters of the total representation $\chi_T(\sigma)$ for the symmetry operations of alpha quartz with 9 atoms in a unit cell:

$\chi_T(E)$	$\chi_T(C_3)$	$\chi_T(C_2')$
9 x 3 = 27	0x0 = 0	1 x(-1) = -1

Doing the same for beta quartz with symmetry D_6: (primed atoms are equivalent to unprimed atoms and each primed and unprimed pair is counted once)

Beta quartz (D_6)

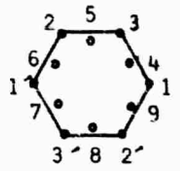

Class	Atoms	Number Unchanged
E	(1)(2)(3)(4)(5)(6)(7)(8)(9)	9
$C_2(\|\|z)$	(11´)(22´)(33´)(47)(58)(69)	3
$C_3(\|\|z)$	(123)(468)(579)	0
	(132)(486)(597)	0
$C_6(\|\|z)$	(13´21´32´)(456789)	0
	(12´31´23´)(987654)	0
$C_2'(\|\|x)$	(3)(3´)(45)(96)(87)	1
	(1)(1´)(49)(58)(67)	1
	(2)(2´)(47)(56)(98)	1
$C_2''(\|\|y)$	(8)(5)(3´2)(11´)(2´3)	3
	(4)(7)(31´)(22´)(3´2)	3
	(6)(9)(12´)(33´)(21´)	3

$\chi_T(E)$	$\chi_T(C_2)$	$\chi_T(C_3)$	$\chi_T(C_6)$	$\chi_T(C_2')$	$\chi_T(C_2'')$
9x3 = 27	3x(-1) = -3	0	0	1x(-1) = -1	3x(-1) = -3

An arbitrary displacement of the atoms in a unit cell can be written as a linear combination of the normal coordinates. The total representation is a linear combination of the irreducible representations. In terms of the characters, the standard reduction formula is (14):

$$\chi_T(\sigma) = \sum_i c^i \chi^i(\sigma) \qquad \text{(I-1)}$$

where $\chi_T(\sigma)$ is the character for the total representations for element σ. $\chi^i(\sigma)$ is the character of the i^{th} irreducible representation of element σ and c_i is the number of times that irreducible representation appears in the reduction of the total representation. To find c_i we multiply both sides of (I-1) by $h_\sigma \chi^i(\sigma)$ (where h_σ is the number of elements in each class), sum both sides over σ and apply the orthogonality condition (14),

$$\sum_\sigma h_\sigma \chi^i(\sigma)\chi^j(\sigma) = g\delta_{ij} \qquad \text{(I-2)}$$

where g is the number of elements in group.

The result is

$$\frac{1}{g}\sum_\sigma h_\sigma \chi_T(\sigma)\chi^i(\sigma) = c_i \qquad \text{(I-3)}$$

Applying (I-3) to reduce the total representations found above:

Alpha quartz (D_3):

$$c_{A_1} = 1/6\ [1x27x1 + 0 + 3x(-1)x1] = 4$$

$$c_{A_2} = 1/6\ [1x27x1 + 0 + 3x(-1)x(-1)] = 5$$

$$c_E = 1/6\ [1x27x2 + 0 + 0] = 9$$

Beta quartz (D_6):

$$c_{A_1} = 1/12\ [1x27x1 + 1x(-3)x1 + 0 + 0 + 3x(-1)x1 + 3x(-3)x1] = 1$$

$$c_{A_2} = 1/12\ [1x27x1 + 1x(-3)x1 + 0 + 0 + 3x(-1)x(-1) + 3x(-3)x(-1)] = 3$$

$$C_{B_1} = 1/12\ [1x27x1 + 1x(-3)x(-1) + 0 + 0 + 3x(-1)x1 + 3x(-3)x(-1)] = 3$$

$$C_{B_2} = 1/12\ [1x27x1 + 1x(-3)x(-1) + 0 + 0 + 3x(-1)x(-1) + 3x(-3)x(1)] = 2$$

$$C_{E_1} = 1/12\ [1x27x2 + 1x(-3)x(-2) + 0 + 0 + 0 + 0] = 5$$

$$C_{E_2} = 1/12\ [1x27x2 + 1x(-3)x2 + 0 + 0 + 0 + 0] = 4$$

Thus the number of each species for alpha and beta quartz is:

Alpha: $4A_1 + 5A_2 + 9E$

Beta: $1A_1 + 3A_2 + 3B_1 + 2B_2 + 5E_1 + 4E_2$

(Since the E modes are doubly degenerate, while the A and B modes are non-degenerate, the number of "degrees of freedom" in either phase is 27.)

To find the number of optic modes we have to subtract the three acoustic modes from the total number. Acoustic modes are a result of a translation of the entire unit cell. Thus the acoustic modes will transform as the coordinates x, y, and z (14). From the character tables we see that for D_3, x, y and z transform as $E + A_2$; and in D_6, x, y and z transform as $E_1 + A_2$. Thus the optic modes are:

Alpha quartz: $4A_1 + 5A_2 + 9E - (E + A_2)$

: $4A_1 + 4A_2 + 8E$

Beta quartz : $A_1 + 3A_2 + 3B_1 + 2B_2 + 5E_1 + 4E_2 - (E_1 + A_2)$

: $A_1 + 2A_2 + 3B_1 + 2B_2 + 4E_1 + 4E_2$

1. Displacement Correlation Charts

The displacement directions of the atoms in each of the normal modes can be determined once the transformation properties of the normal modes are known. This determination is made by comparing the characters of the irreducible representations of the symmetry group at the site of each atom (called the site group) with the characters of the irreducible representation of the point group of the lattice (17). Since each site group must be a subgroup of the lattice point group, each site group will have symmetry elements (i.e. classes) in common with the point group. For each one dimensional representation of the point group of the lattice we can find a one dimensional representation of the site group, such that the characters for the classes in common will be equal. By inspection of the character table we can determine which particular one dimensional representation of the lattice point group and the site group have the same characters. For each p ($p > 1$) dimensional irreducible representation of the lattice point group, we can find either i) a single p dimensional irreducible representation of the site group, or ii) a linear combination of m ($m < p$) dimensional irreducible representations of the site group such that the characters for the common classes will be equal. Again, by inspection of the character tables, the correlation between the p dimensional irreducible representation of the lattice point group and the irreducible representations of the site group can readily be determined. In constructing the displacement correlation chart (Table I-2), the above correlations between the irreducible representations of the lattice point group and the site groups are represented by straight lines.

Table I-2

Displacement Correlation Charts

(a) Alpha Quartz

O	$3SiO_2$	Si
Site	Lattice	Site
C_1	D_3	C_2*

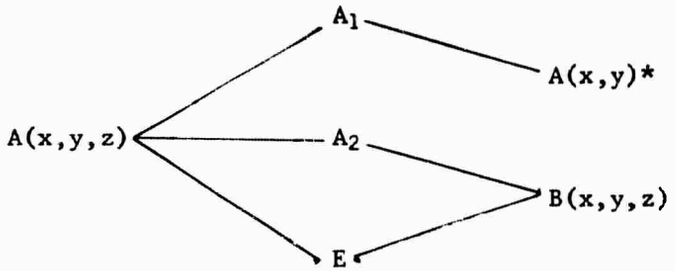

* In the character tables for C_2, z transforms as A. However, this is for the twofold axis parallel to z. In quartz, the twofold axis is parallel to x.

(b) Beta Quartz

O	$3SiO_2$	Si
Site	Lattice	Site
C_2	D_6	D_2

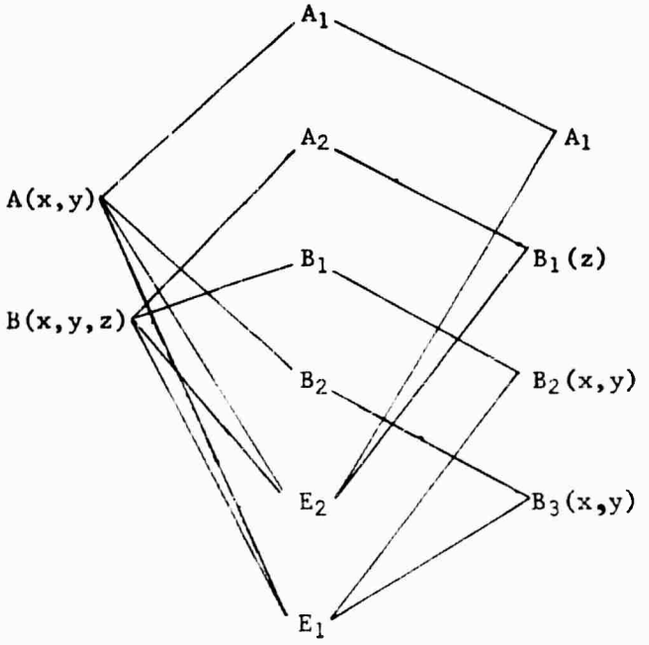

If a given species of vibration of the lattice is correlated with an irreducible representation of the site group which transforms as a component of a vector (x, y, or z), then motion of the atom is allowed in that vector component direction. If the lattice vibration is correlated with an irreducible representation of the site group which does not transform as any component of a vector, then the atom cannot move.

The above discussion is now applied to quartz. Table I-2 shows the displacement correlation chart for alpha and beta quartz. In alpha quartz the site symmetry of the oxygens is C_1 (the identity group) and the site symmetry of the silicons is C_2 (2, 18). Next to the irreducible representations of the site group are the vector components which transform according to that particular representation. From this chart we see that in all the normal modes of the lattice, the direction of motion of the oxygens is not restricted. For the A_1 modes, the motion of the silicons is limited to the x-y plane while for A_2 and E modes, the displacement directions of the silicons are not restricted. These conclusions agree with Kleinman and Spitzer's valence force model calculations of the atomic motions associated with the A_1 and A_2 modes (13). Figs. I-4a-4d are xy projections of the calculated particle displacements for the 4 A_1 modes and show our measured frequencies at room temperature. In the 4 A_1 modes, the z component of the silicon atoms is zero.

In the correlation chart for beta quartz the site symmetry of the oxygens is C_2 and of the silicons is D_2. We see that in the A_1 mode of vibration the silicons cannot move and the oxygens move only in the x-y plane. In the B_1 modes the silicons move only in the x-y plane and

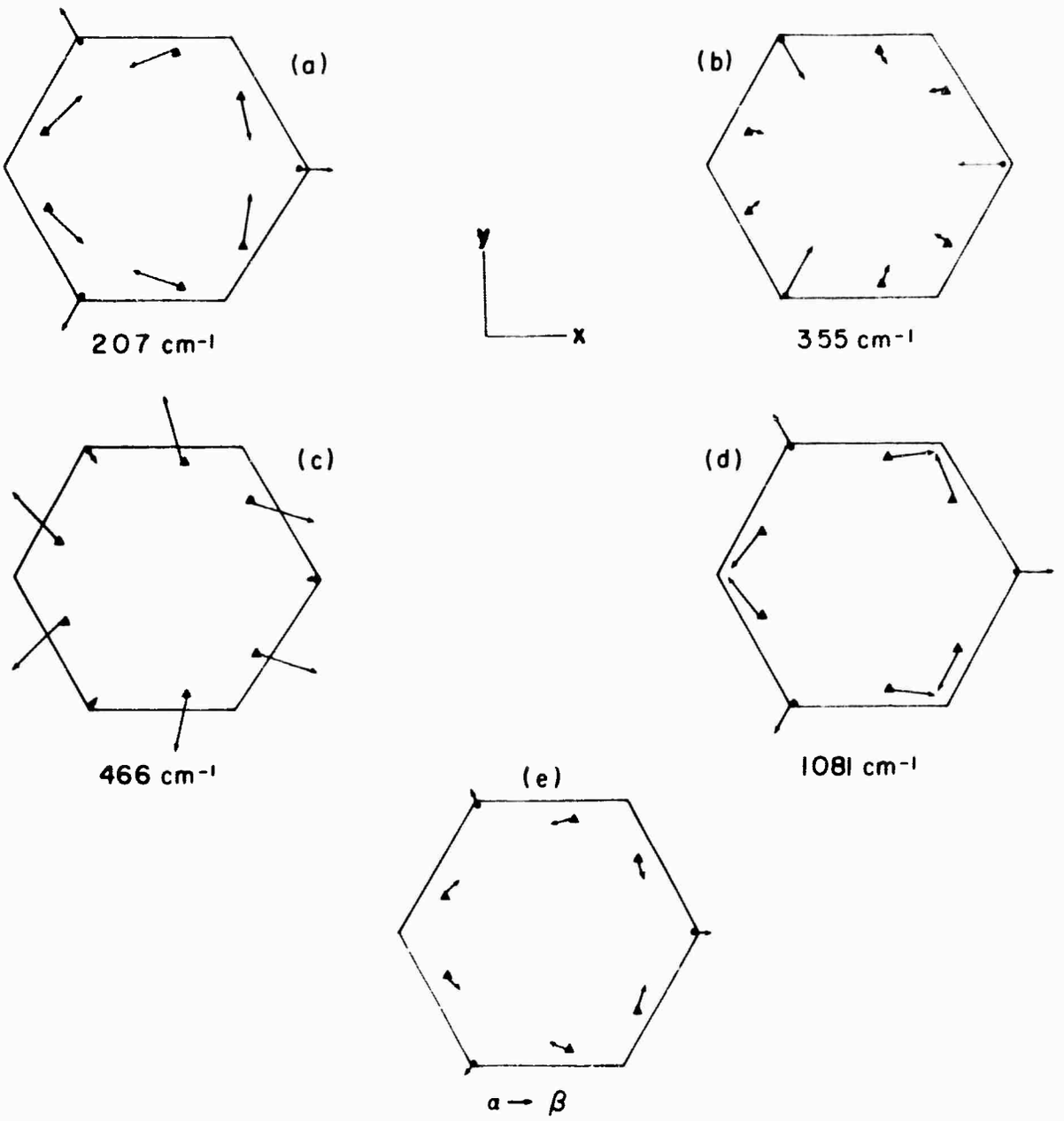

Fig. I-4. (a-d) Atomic displacements in the x-y plane for the four A_1 vibrations based on the calculations of Kleinman and Spitzer (13). The numbers are our measured values of the room temperature frequencies. (e) The atomic displacements necessary to change from alpha to beta quartz. These are most closely approximated by the 207 cm^{-1} vibration.

the oxygen motion is unrestricted. In the E_1 and E_2 modes there are no restrictions on the directions of atomic motion.

2. Mode Correlation Chart

Another type of correlation chart relates the normal modes of the high and low temperature phases. This chart has physical significance only when the fractional changes in the normal coordinates and frequencies which occur at the transition are very small. Under this condition the transformation properties of the vibrations in the two phases are related. This is the case for second order transitions where the normal coordinates and frequencies change continuously as the transition region is traversed. (In fact the Landau theory is based on the continuous change of state of the crystal (19)). If the transition is first order, where there may be a large, discontinuous change in the interatomic forces in going from the high phase to the low phase, there can be a large mixing of the different normal coordinates in the low temperature phase. Because of this mixing there may be no correlation of a normal vibration in the high temperature phase with a particular normal vibration in the low temperature phase.

For quartz, the evidence suggests that the transition is first order (20). However, from Young's measurements of atomic positions as a function of temperature, we conclude that any discontinuous change in the normal coordinates is small. Thus the symmetry properties of the normal vibrations of the two phases will be closely related and we can construct a meaningful mode correlation chart.

Since the lattice point group of alpha quartz is a subgroup of the point group of beta quartz, there will be classes in common. We determine, from the character tables, which irreducible representations of alpha and beta quartz have equal characters for classes in common. The result is shown in Table I-3. The underlined species are the irreducible representations whose associated modes are Raman active. The 8 doubly degenerate Raman active E modes of alpha quartz become 4 E_1 modes (Raman and infrared active) and 4 E_2 modes (Raman active and infrared inactive) in the β phase. The 4 A_2 modes (Raman inactive, infrared active) become 2 A_2 modes (Raman inactive, infrared active) and 2 B_2 modes (Raman and infrared inactive). Of the four totally symmetric, Raman active A_1 modes (room temperature frequencies: 207, 355, 466 and 1081 cm^{-1} (21, 22)) only one is Raman active in the beta phase. The remaining three become Raman and infrared inactive B_1 modes.

From the mode and displacement correlation charts, we can infer to which species the transition mode belongs.

In order to change from the beta to the alpha phase, the silicons move in the x-y plane only: the z coordinates remain unchanged.[20] From the displacement correlation chart for alpha quartz (Table I-2a) we see that all three species of vibration allow motion in the x-y plane and in the A_2 and E vibrations the silicon atoms can also move in the z direction. In the beta to alpha transition the silicons again move only in the x-y plane. From the beta quartz correlation chart (Table I-2b) this can be a B_2, E_1, or B_1 vibration. Thus the mode associated with the transition is an A_1, A_2, or E mode of alpha quartz which, from Table I-3, becomes a B_1, B_2 or E_1 mode, respectively, of beta quartz.

TABLE I-3

QUARTZ

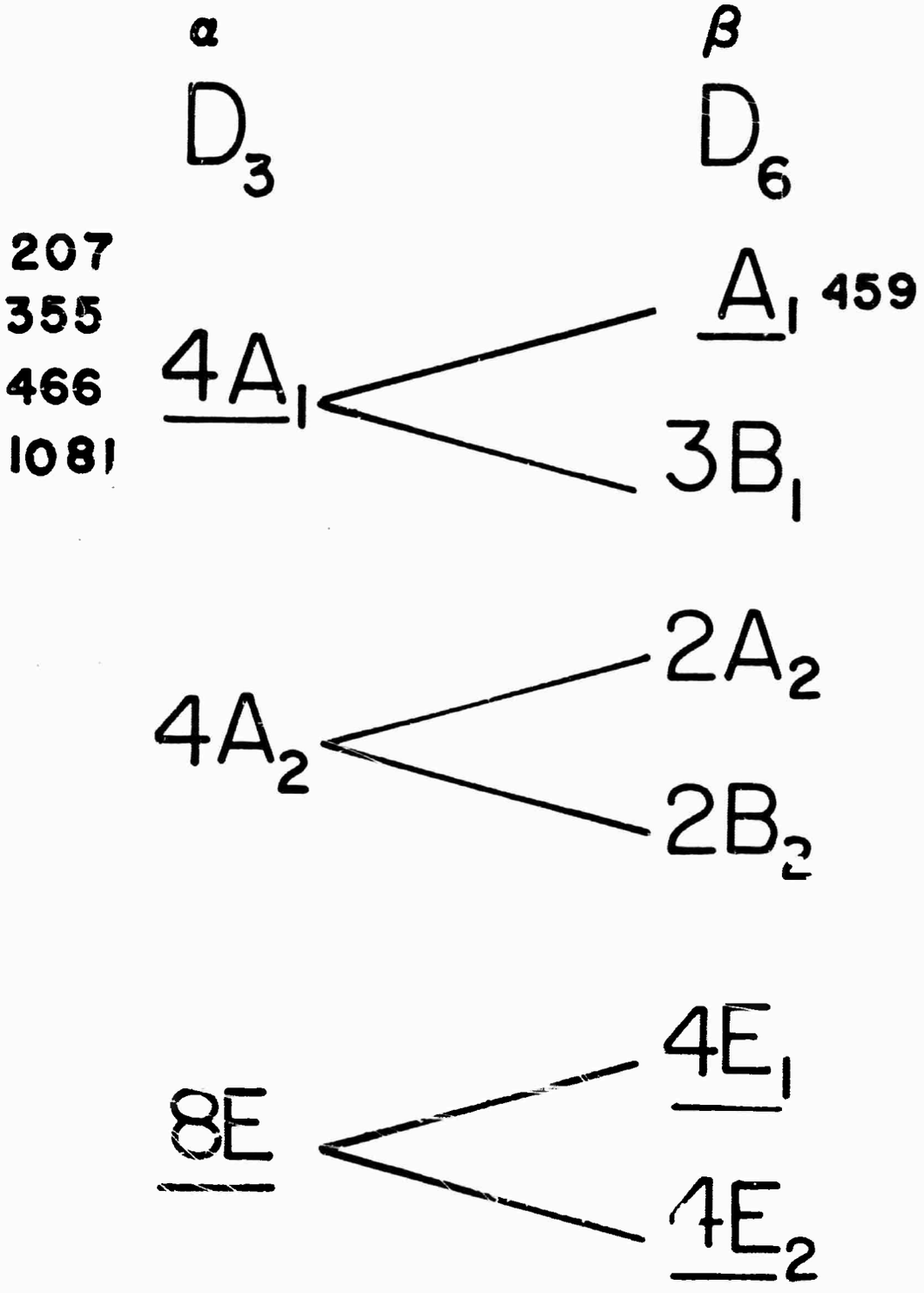

This is as far as group theory can go. To gain more information about which is the transition mode. one relies on experiments or calculations. Kleinman and Spitzer's calculation of the particle displacements in the A_2 vibrations show that the silicons move in the z direction (13). Thus the A_2 species in alpha quartz (B_2 in beta quartz) do not contain the transition mode. The transition mode is of either A_1 or E species of alpha quartz. Again, appealing to the Kleinman and Spitzer calculation of the particle displacements for the A_1 vibrations we see that the 207 cm^{-1} vibration most closely resembles the atomic motions necessary to change alpha quartz into beta quartz (13) (compare Figs. I-4a with I-4e). The assignment of the 207 cm^{-1} vibration as the transition mode agrees with the experimental observations (23) where the properties of the 207 cm^{-1} vibration possess a strong temperature dependence, which is what one would expect of a transition mode. (Other complications are introduced due to a coupling of the 207 cm^{-1}, q=0 phonon with two $q \neq 0$ phonons. This will be discussed in the next chapter.)

D. THE ALPHA-BETA TRANSITION OF QUARTZ

The transition between alpha and beta quartz at atmospheric pressure occurs at 573 ± 1°C (1). Within 50 C° of this temperature many of the physical properties of quartz show a strong temperature dependence. Among these are the specific heat (24), molar volume (25), coefficient of thermal expansion (26), piezoelectric coefficients (27) and elastic constants (28). The most extensive study of quartz done in recent years was an X-ray analysis of the transition by Young, who measured

the fractional coordinates of the atomic positions (see Ch. 1, Sec. A, and Appendix A) at several temperatures from room temperature up to 650°C (20).

As we shall demonstrate shortly, discontinuities in some of the properties of quartz are expected in the transition region (19). To study these discontinuities requires high temperature resolution. The relative temperature resolution in the above experiments was never better than 2 C° and many of the experiments were performed with the temperature changing. Under these conditions it was impossible to study effects occurring within 1 C° of the transition and any discontinuity occurring very near the transition temperature would not be observed.

The atomic motions which result in a change from D_3 to D_6 symmetry can be determined from a study of the special hexagonal cells of alpha and beta quartz (Figs. I-2). The silicons move along the twofold (X) axes to occupy positions on the vertices of the hexagon. This creates a new sixfold rotation axis. Each silicon is now shared by two unit cells. At the same time each oxygen within a sector moves to occupy a position equidistant from neighboring silicons which leads to the creation of additional twofold axes in the x-y plane.

A conceptual picture of the atomic motions during the transition is given by studying the SiO_4 tetrahedra. Alpha and beta quartz are built up of SiO_4 tetrahedra joined at all corners. The transition can be pictured as a rearrangement of the oxygens about the silicon to form a regular tetrahedron. Conversely, we describe the transition beta to alpha, as a "puckering" of the SiO_4 tetrahedra from

the regular arrangement of the oxygens in the beta phase to the distorted shape in the alpha phase. This picture is useful if one wants to compare quartz with the first order transition in ferroelectric $BaTiO_3$ (29).

Another picture of the transition is obtained by considering the electrical twins of alpha quartz. This leads to a definition of an order parameter to describe the transition. From Fig. I-2 we see that the average atomic positions in the beta phase lie midway between the two alpha phase equilibrium positions. Thus the motions of the atoms will be along the lines connecting the atomic positions in the two twins of quartz. Two parameters, one for the silicons and one for the oxygens, define these motions. In terms of fractional coordinates and lattice vectors they are:

$$\vec{\gamma} = \vec{r}^{\,\alpha}_{si} - \vec{r}^{\,\beta}_{si} = [\tfrac{1}{2} - \mu]\,\vec{a} \qquad \text{(I-4a)}$$

which is motion along the X axis, and:

$$\vec{\delta} = \vec{r}^{\,\alpha}_{ox} - \vec{r}^{\,\beta}_{ox} = [(x_\alpha - x_\beta)^2 + (y_\alpha - \tfrac{x}{2}\beta)^2 + (y_\alpha - \tfrac{x}{2}\beta)(x_\alpha - x_\beta)]^{\frac{1}{2}}\,\vec{a} + (z - \tfrac{\ell}{c})\,\vec{c} \qquad \text{(I-4b)}$$

which is motion essentially in the y-z plane. Since the X parameters in the alpha and beta phases are very nearly the same, there is little change in the X direction of the oxygen atoms. γ and δ are positive if the vector points toward the α_1 position of the atom and negative if toward the α_2 position (Fig. I-2). Thus the sign of γ or δ will determine which twin the crystal belongs to. It is also seen (by definition) that the value of γ and δ will be zero in the high

temperature phase. Thus, γ or δ will serve as an order parameter in a phenomenological description of the transition. They can have either sign below the transition, go to zero continuously or discontinuously at the transition temperature, and are zero above the transition temperature. The temperature dependence of these quantities, calculated from Young's data, is shown in Fig. I-5 (20).

Landau presented a phenomenological description of second order phase transitions (19). He expanded the thermodynamic potential, Φ, in terms of powers of the order parameter η:

$$\Phi(\eta) = \Phi_o + A\eta + a\eta^2 + B\eta^3 + \frac{b}{2}\eta^4 + C\eta^5 + \frac{c}{6}\eta^6 + \ldots \qquad (I-5)$$

The coefficients are assumed to be functions of temperature and stress. From the equilibrium conditions

$$\left(\frac{\partial\Phi}{\partial\eta}\right)_{\eta_o} = 0 \; ; \quad \left(\frac{\partial^2\Phi}{\partial\eta^2}\right)_{\eta_o} > 0$$

certain restrictions are imposed on the coefficients:

i) $A=0$ to satisfy the equilibrium condition $(\partial\Phi/\partial\eta)_{\eta_o} = 0$ for $\eta_o = 0$ at any temperature in the high temperature phase

ii) a; In the symmetric, high temperature phase the minimum of Φ corresponds to $\eta=0$. This requires $a>0$. In the low temperature phase the equilibrium state corresponds to $\eta_o \neq 0$. This requires $a<0$. Thus a is assumed to have the temperature dependence $a=a'(T-T_t)$ where T_t is the transition temperature.

iii) $B=0$, to insure the existence of a minimum of Φ at the transition temperature.

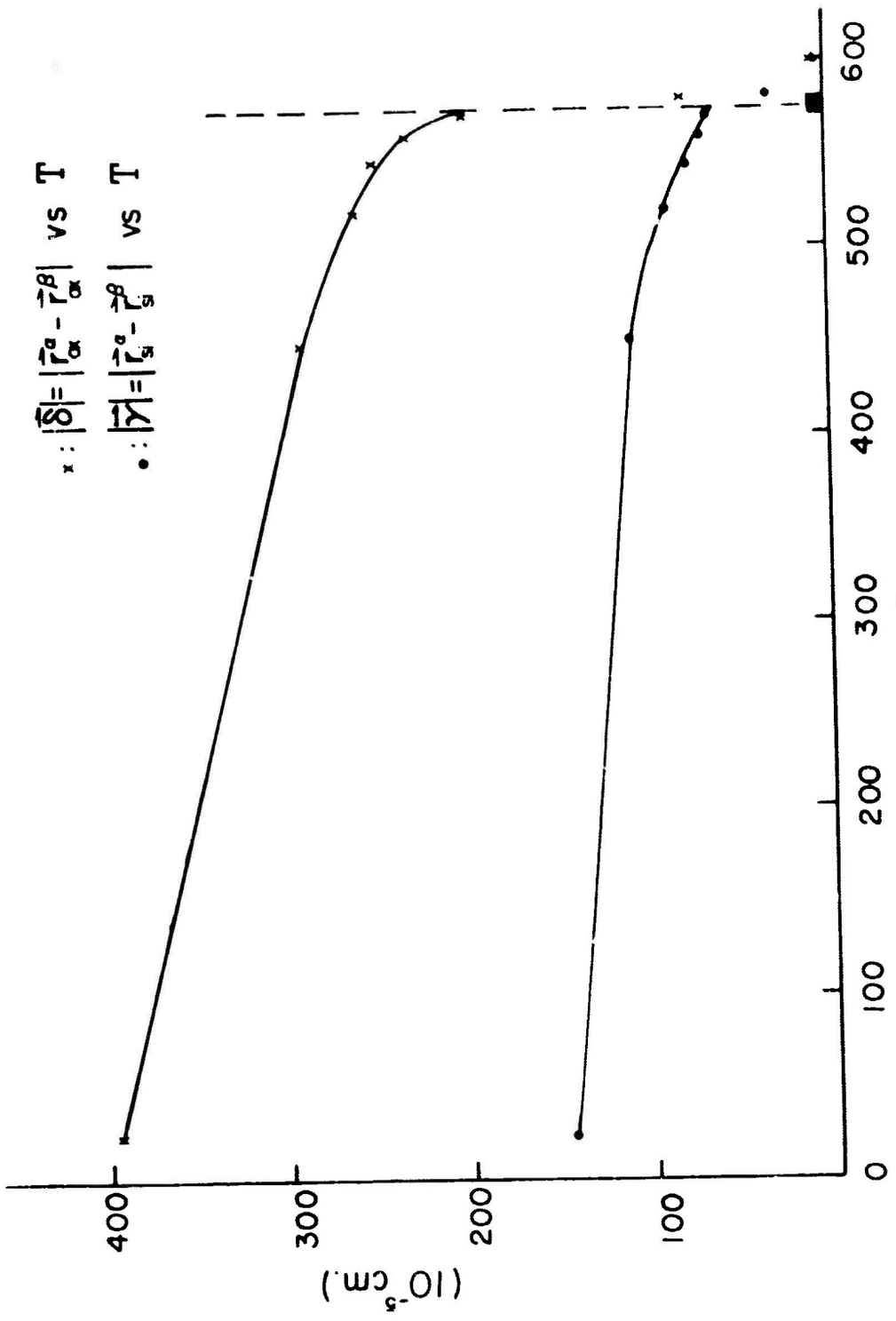

Fig. I-5. The temperature dependence of $|\gamma| = |r_{si}^{\alpha} - r_{si}^{\beta}|$ and $|\delta| = |r_{ox}^{\alpha} - r_{ox}^{\beta}|$ based on Young's X-ray measurements (20).

iv) b; In a second order transition (the type that Landau studied) b>0. In a first order transition b<0. b=0 corresponds to a transition at the Curie critical point (19).

v) C; We assume C=0. If C were different from zero the thermodynamic potential associated with one value of the order parameter in the low temperature phase (either $+\eta$ or $-\eta$) would be lower than the energy associated with the other value.

vi) c>0 to satisfy the equilibrium condition $(\partial^2\Phi/\partial\eta^2)_{\eta_o} > 0$ for large values of η.

The thermodynamic potential is rewritten:

$$\Phi(\eta) = \Phi_o + a\eta^2 + \frac{b}{2}\eta^4 + \frac{c}{6}\eta^6 \qquad \text{(I-6)}$$

The coefficients are related to measurable quantities. Their physical significance depends on the system being studied. For example: in a ferroelectric transition, a^{-1} is proportional to the dielectric susceptibility; in a magnetic transition a^{-1} is proportional to the magnetic susceptibility; in a liquid, a^{-1} is proportional to the compressibility (30).

The thermodynamic potential, $\Phi(\eta)$, is plotted in Fig. I-6. The double minimum in the low temperature phase corresponds to the two equilibrium values of the order parameter ($\pm\eta$). The single minimum in the high temperature phase corresponds to $\eta=0$.

The phenomenological description of the transition involves determining how the double well in the low temperature phase changes into the single well as the temperature is increased. If b>0, we have a

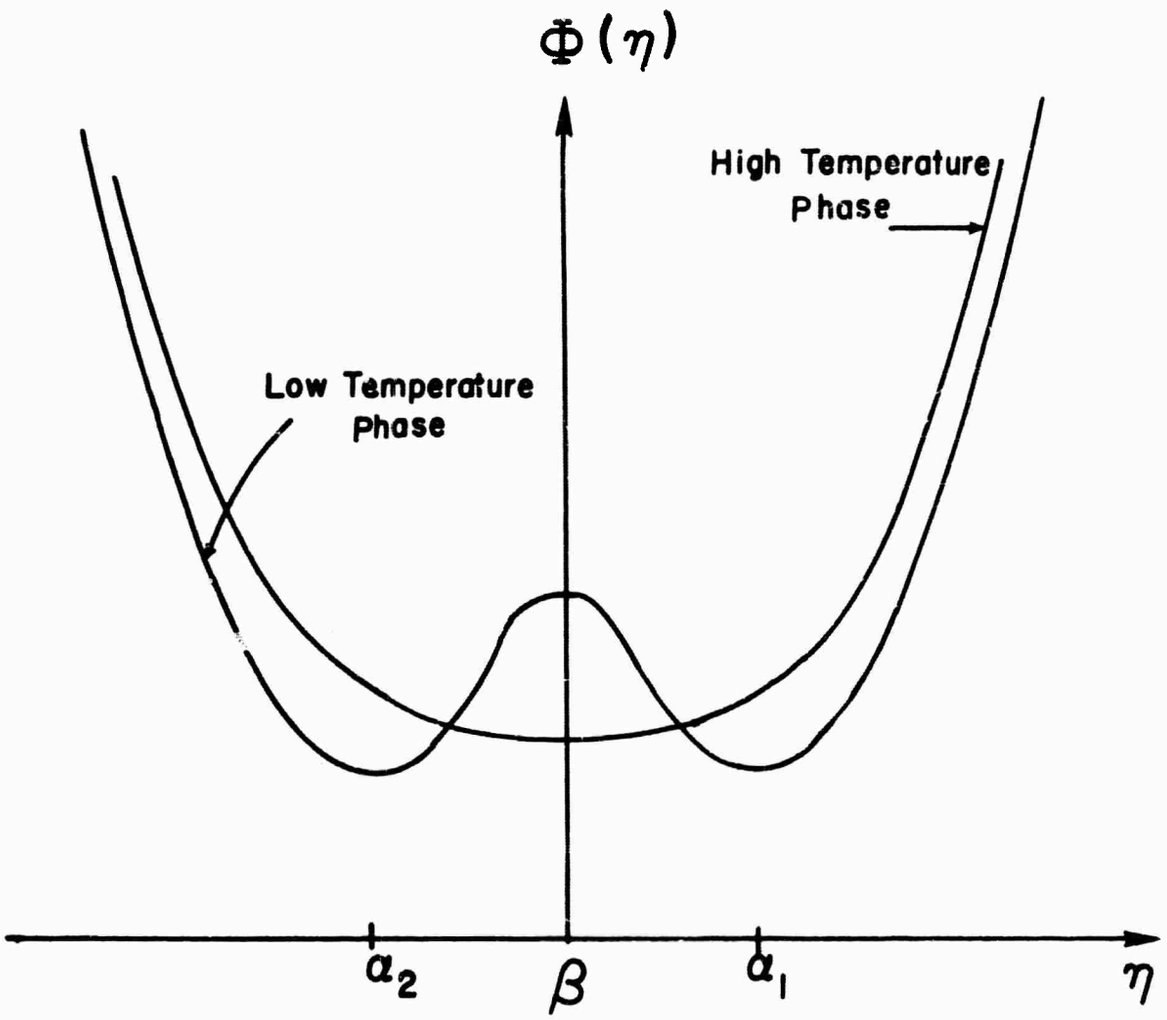

Fig. I-6. Thermodynamic potential, $\Phi(\eta)$ vs the order parameter, η, for the low temperature phase, $T << T_t$, and the high temperature phase, $T >> T_t$.

second order transition. The first derivatives of Φ are continuous, but the second derivatives (e.g. specific heat) contain singularities or discontinuities. The barrier height will decrease as $T \to T_t^-$; and at T_t the well has a flat bottom. The mean value of the order parameter at this temperature is zero, but the fluctuations about the mean can be very large. Above T_t there is a single well with a minimum at $\eta=0$.

If $b<0$ we have a first order transition and the first derivatives of Φ (e.g. volume and entropy) have discontinuities. As the temperature is increased, a third well appears at $\eta=0$ at a temperature below T_t. This allows a metastable state of the high temperature phase to coexist with the stable low temperature phase. At T_t there are three equal minima. As T is increased further, the central well becomes deeper and the high temperature phase can exist only as a metastable state. Finally, when T is sufficiently large, only one central minimum exists. The fact that in a first order phase transition near the transition temperature, both phases can exist simultaneously in the crystal leads to a possible temperature hysteresis in the observed properties. This is one of the distinctions between first and second order transitions.

Since the coefficients of the expansion of $\Phi(\eta)$ are functions of stress and temperature, there may exist a particular value of the stress and temperature such that both a and b equal zero. On a stress vs temperature plot, this point is called the Curie critical point. It is the point where a line of first order phase transitions meets the line of second order phase transitions (19). The curves $\Phi(\eta)$ vs η for $b=0$ for different temperatures are similar to those for an ordinary second order

transition discussed above (b>0) except for b=0 the well is flatter at T_t since the lowest non-vanishing term for $\Phi(\eta)$ is proportional to η^6.

Ginzburg and Levanyuk (31) applied Landau's theory of second order phase transitions to the alpha-beta quartz transition. They applied the equilibrium conditions to eq. (I-6) and found the equilibrium values of the order parameter.

The linear temperature dependence of a was assumed:

$$a = a'(T - T_t) \qquad \text{(I-7)}$$

The equilibrium conditions yield values of η_o:

$$\eta_o = 0 \qquad T > T_t \qquad \text{(I-8a)}$$

$$\eta_o^{\pm} = \pm \left(\frac{-b + (b^2 - 2ac)^{\frac{1}{2}}}{c} \right) \qquad T < T_t \qquad \text{(I-8b)}$$

The solution (I-8a) $\eta_o=0$ is for $T>T_t$; and the solution (I-8b) $\eta_o \neq 0$ contains the two values of η_o associated with the different twins for $T<T_t$. At the transition temperature ($T=T_t$) the order parameter equals zero since a=0.

It is possible that singularities at the transition temperature in the derivatives of $\Phi(\eta)$ exist. Because of these singularities the function $\Phi(\eta)$ is not analytic at T_t and for this reason, the Landau theory breaks down very close to the critical point (32).

Ginzburg's treatment of the alpha-beta phase transition predicted an anomalous increase in the intensity of the scattered light at the transition temperature. As is well known, fluctuations in the dielectric constant, $\Delta\varepsilon$, scatter light. These fluctuations can be written as a

function of the fluctuations in the order parameter. (The dielectric constant is also a function of the strain (x) and entropy (S) whose mean square fluctuations are proportional to the Brillouin and Rayleigh scattered intensities, respectively):

$$\Delta\epsilon = \left(\frac{\partial\epsilon}{\partial\eta^2}\right)_{X,S} \Delta(\eta^2) \qquad \text{(I-9)}$$

Ginzburg's selection of η^2 instead of η is an essential factor in his argument (31). With the choice of η^2 we will show that opalescence will be observed only at the Curie critical point.

Continuing with Ginzburg's argument, we have near the transition temperature in the lower temperature phase

$$\Delta\epsilon = \left(\frac{\partial\epsilon}{\partial\eta^2}\right)_{X,S} 2\eta_o\Delta\eta \qquad \text{(I-10)}$$

The intensity of the scattered light is proportional to the mean square fluctuations of the dielectric constant:

$$I \sim \overline{(\Delta\epsilon^2)} = \left(\frac{\partial\epsilon}{\partial\eta^2}\right)^2_{X,S} 4\eta_o{}^2\overline{(\Delta\eta)^2} \qquad \text{(I-11)}$$

From thermodynamic fluctuation theory, the mean square fluctuation of a quantity is (19)

$$\overline{(\Delta\eta)^2} = \frac{kT}{\left(\frac{\partial^2\Phi}{\partial\eta^2}\right)_{X,S}} \qquad \text{(I-12)}$$

where k is the Boltzman constant and T is the absolute temperature. From the expansion (I-6), the mean square fluctuation of the order parameter for $T < T_t$ is:

$$\overline{(\Delta\eta)^2} = \frac{kT}{4(b^2-2ac)^{1/2}\,\eta_o^2} \qquad \text{(I-13)}$$

Thus the scattered light is proportional to:

$$I(T) \sim \frac{\left(\frac{\partial \epsilon}{\partial \eta^2}\right)^2_{X,S} T}{(b^2-2ac)^{1/2}} \qquad T < T_t \qquad \text{(I-14)}$$

and at T_t

$$I(T) \sim \left(\frac{\partial \epsilon}{\partial \eta^2}\right)^2_{X,S} \frac{T_t}{b} \qquad T = T_t \qquad \text{(I-15)}$$

If $b>0$, as in a second order phase transition far from the Curie critical point, $I(T_t)$ is finite. At the Curie critical point, $a=b=0$, and from (I-13) and (I-15) one would expect the fluctuations and the intensity of the scattered light to become infinite. This obviously cannot happen. To keep the intensity finite Ginzburg added another term to the free energy expansion (I-6): $d(\nabla\eta)^2$ which is a gradient term taking into account the correlations between fluctuations in adjacent volume elements. Performing the same type of calculations which led to Eq (I-14) and including the $d(\nabla\eta)^2$ term in $\Phi(\eta)$ we obtain a new expression for the intensity of the scattered light (31):

$$I(T) \sim \frac{\left(\frac{\partial \epsilon}{\partial \eta^2}\right)^2 T}{\sqrt{b^2-2ac} + \frac{dcq^2}{2[\sqrt{b^2-2ac} - b]}} \qquad \text{(I-16)}$$

where q is the wave vector of the fourier component of the fluctuation giving rise to the scattered light. This expression shows that the

$$\overline{(\Delta\eta)^2} = \frac{kT}{4(b^2-2ac)^{-1/2}\,\eta_o^2} \qquad \text{(I-13)}$$

Thus the scattered light is proportional to:

$$I(T) \sim \frac{\left(\frac{\partial\varepsilon}{\partial\eta^2}\right)^2_{X,S} T}{(b^2-2ac)^{1/2}} \qquad T < T_t \qquad \text{(I-14)}$$

and at T_t

$$I(T) \sim \left(\frac{\partial\varepsilon}{\partial\eta^2}\right)^2_{X,S} \frac{T_t}{b} \qquad T = T_t \qquad \text{(I-15)}$$

If b>0, as in a second order phase transition far from the Curie critical point, $I(T_t)$ is finite. At the Curie critical point, a=b=0, and from (I-13) and (I-15) one would expect the fluctuations and the intensity of the scattered light to become infinite. This obviously cannot happen. To keep the intensity finite Ginzburg added another term to the free energy expansion (I-6): $d(\nabla\eta)^2$ which is a gradient term taking into account the correlations between fluctuations in adjacent volume elements. Performing the same type of calculations which led to Eq (I-14) and including the $d(\nabla\eta)^2$ term in $\Phi(\eta)$ we obtain a new expression for the intensity of the scattered light (31):

$$I(T) \sim \frac{\left(\frac{\partial\varepsilon}{\partial\eta^2}\right)^2 T}{\sqrt{b^2-2ac} + \frac{dcq^2}{2[\sqrt{b^2-2ac} - b]}} \qquad \text{(I-16)}$$

where q is the wave vector of the fourier component of the fluctuation giving rise to the scattered light. This expression shows that the

intensity remains finite at the Curie point when the term in d is retained. Moreover, the above equations show that at the Curie point $I(T_t) = 0$. However, I(T) has a sharp maximum just below the transition temperature (31).

Ginzburg was able to calculate the scattered intensity very near the transition temperature compared to the scattered intensity at room temperature.

If we neglect the correlation effects, the intensity of the scattered light for a second order phase transition very near the Curie critical point ($b \to 0$) is given by (I-15). In terms of the Rayleigh ratio (scattering cross section per solid angle per unit volume)(I-15) becomes (33):

$$R(T_t) = \frac{\pi^2}{\lambda_o^4} kT_t \left(\frac{\partial \epsilon}{\partial \eta}\right)^2 \frac{1}{b} \text{ cm}^{-1} \qquad \text{(I-17)}$$

where λ_o is the wavelength of light.

Ginzburg put this equation in terms of measurable quantities:

$$\left(\frac{\partial \epsilon}{\partial \eta^2}\right)^2 = \left(\frac{\epsilon_\alpha - \epsilon_\beta}{\eta_o^2}\right)^2 = \frac{4n^2 \Delta n^2}{\eta_o^4} \qquad \text{(I-18)}$$

where n is the index of refraction and Δn is the difference between the index of refraction in the alpha and the beta phase.

To find η_o^4 we assume that, in eq. I-8b, c is small; thus

$$\eta_o^2 = \frac{-a}{b} = + \frac{a'(T_t - T)}{b} .$$

Squaring both sides we have:

$$\eta_o^4 = \frac{a'^2 (T_t - T)^2}{b^2} \qquad (I-19)$$

From the jump in the specific heat for a second order phase transition (19):

$$\Delta c_p = \frac{a'^2 T_t}{b} \qquad (I-20)$$

solving for $(a')^2$

$$a'^2 = \frac{\Delta c_p b}{T_t} \qquad (I-21)$$

and substituting into (I-19)

$$\eta_o^4 = \frac{\Delta c_p (T_t - T)^2}{b T_t} . \qquad (I-22)$$

Thus from (I-18)

$$\left(\frac{\partial \epsilon}{\partial \eta^2}\right) = \frac{4n^2 \Delta n^2 T_t b}{\Delta c_p (T_t - T)^2} \qquad (I-23)$$

and putting (I-23) into (I-17) we have the Rayleigh ratio for the light scattered by quartz near the transition temperature:

$$R(T_t) = \frac{\pi^2}{\lambda_o^4} k \frac{4n^2 \Delta n^2 T_t^2}{c_p (T_t - T)^2} \quad cm^{-1} \qquad (I-24)$$

Ginzburg substituted the following measured quantities (31) into eq. (I-24)

$$\begin{aligned} n &= 1.56 \\ \Delta n &= 1.2 \times 10^{-3} \text{ for } T_t - T = .1C^\circ \\ \Delta c_p &= 4.2 \times 10^7 \text{ ergs/°C cm}^3 \\ T_t &= 846°K \end{aligned} \qquad (I-25)$$

and found:

$$R(573°C) = \frac{\pi^2}{\lambda^4} k\ 239 \times 10^{-7}\ cm^{-1} \qquad (I\text{-}26)$$

This calculation depends critically upon the measurement of the index of refraction vs temperature. Since the numerical values chosen for Δn and $T_t - T$ were taken from an unpublished experiment, it is difficult to critically examine these values. It should be pointed out that the temperature interval chosen, $T_t - T$, is very important since it occurs as the square of $T_t - T$. A value of $T_t - T = 1$ instead of equal to .1 would decrease eq. (I-26) by two orders of magnitude.

In calculating the room temperature intensity, Ginzburg assumed isotropy and used Einstein's relation for light scattered by isothermal density fluctuations (34). Ginzburg's value for the Rayleigh ratio at 20°C using the values in ref. (31) is:

$$R(20°C) = \frac{\pi^2}{\lambda^4} k\ (155 \times 10^{-11})\ cm^{-1} \qquad (I\text{-}27)$$

If quartz is correctly treated as a solid, the Rayleigh ratio at 20°C for light incident along the y directions and observed along the -x direction, with z perpendicular to the scattering plane is (33):

$$R(20°C) = \frac{\pi^2}{\lambda^4} k\ (99 \times 10^{-11})\ cm^{-1} \qquad (I\text{-}28)$$

If we take the ratio of (I-26) to (I-27) (the Rayleigh ratio of quartz treated as an isotropic substance), we find the relative increase in scattered intensity very near the transition temperature:

$$\frac{I(573°C)}{I\ (20°C)} = \frac{R(573°C)}{R\ (20°C)} = 1.5 \times 10^4 \qquad (I\text{-}29)$$

which is the value Ginzburg obtained.

If we take the ratio of (I-26) to (I-28) (the Rayleigh ratio of quartz correctly treated as a solid) we find the relative increase in scattered intensity very near the transition temperature:

$$\frac{I(573°C)}{I\ (20°C)} = \frac{R(573°C)}{R\ (20°C)} = 2.4 \times 10^4 \qquad \text{(I-30)}$$

Results (I-29) and (I-30) are not inconsistent with one another considering the errors on the quantities used to find these ratios.

Thus, if quartz undergoes a second order phase transition, the Landau theory predicts that the scattered intensity very near the transition temperature would be $\sim 10^4$ greater than the scattered intensity at room temperature.

Concurrently with Ginzburg's calculations, an experiment was performed which measured the relative changes in the light scattered by quartz as a function of temperature. Yakovlev et al (35) illuminated a piece of quartz with a mercury arc source and measured the scattered light with a photomultiplier tube. They found that the relative increase in scattered intensity was:

$$\frac{I(573°C)}{I\ (20°C)} = 1.4 \times 10^4$$

Yakovlev photographed the scattering column at the transition temperature. The scattering column had the appearance of a fog zone within the crystal, not unlike that observed in a liquid vapor system undergoing a phase transition near its critical point. The increase in light scattering at the quartz transition was termed opalescence, analogous to the observations in a liquid-vapor transition.

Thus, it appeared that quartz underwent a second order phase transition near the Curie critical point and at the transition temperature the quartz crystal opalesced.

Ginzburg also emphasized the dynamical origin of the "opalescence." Taking as the order parameter $\eta \equiv \gamma$, the fluctuations in η will then correspond to relative displacements of crystal sublattices so that η is identified with one of the zone center optical phonons. On the basis of available temperature-dependent spectroscopic information (21) Ginzburg identified η with the totally symmetric A_1 optic vibration, whose room temperature frequency is 207 cm^{-1}. Ginzburg proposed that as the temperature is raised toward the transition temperature, T_t, the frequency of this mode should decrease steadily toward zero. The Stokes and anti-Stokes components of the Raman spectrum would approach each other, finally merging into a single quasi-elastic peak which would continue to narrow and grow more intense due to the diverging fluctuations.

It was this interpretation by Ginzburg which was the impetus for our experiments. By spectral resolution of the scattered light we had hoped to find the key to the observed opalescence and answer the challenge posed by Ginzburg (31), "But why are there no experimental researches on the spectrum of the scattered light near second order phase transition points?"

CHAPTER II

RAMAN SCATTERING IN CRYSTALLINE QUARTZ

In this chapter we discuss the Raman scattering experiments performed on quartz from helium temperatures up to 600°C. After a brief review of the general theory of the Raman scattering process, the Raman selection rules for quartz will be discussed. Next, the early Raman scattering experiments performed on quartz will be reviewed. Following a description of our experimental apparatus, we present the results of our temperature dependent Raman scattering experiments. The chapter concludes with a discussion of these results.

A. CLASSICAL THEORY OF THE RAMAN EFFECT

The complete description of the Raman scattering process requires a quantum mechanical theory (36, 37). However, to obtain the frequency relations in the Raman effect we can treat the optical field and the crystal classically (38).

Because of momentum conservation, in the first order Raman effect only the modes at the center of the Brillouin zone (i.e. $q \approx 0$) are studied. Since, in normal vibrations with $q=0$ the atoms in all unit cells vibrate in phase, it is sufficient to consider only the motion of the atoms in one unit cell.

We consider a unit cell with n atoms, with a polarizability α, and with each atom connected to its nearest neighbor by a spring which represents the electron cloud separating them. A plane monochromatic

wave, $E_o^{\alpha}\cos\omega_o t$, is incident on the system and induces a dipole moment because of the interaction of the electron cloud with the incident electric field. Allowing for the tensor properties of the system, the induced dipole moment in the i (x, y, or z) direction resulting from the field polarized in the j direction is

$$P_i = \alpha_{ij}E_j \qquad \text{(II-1)}$$

The displacement of the atoms in a unit cell from the equilibrium position, $\{X-X_o\}$, can be written as a linear combination of the normal coordinates R_k:

$$\{X-X_o\} = \sum_k R_k \cos\Omega_k t \qquad \text{(II-2)}$$

where Ω_k is the frequency of one of the 3n-3 optic modes of vibration. Expanding the polarizability about the equilibrium position $\{X_o\}$,

$$\alpha_{ij} = \alpha_{ij}\{X_o\} + \sum_k \left(\frac{\partial\alpha_{ij}}{\partial R_k}\right)_{R_k=0}(R_k) \qquad \text{(II-3)}$$

and substituting (II-2) and (II-3) into (II-1), the induced dipole moment has the form:

$$P_i = \alpha_{ij}\{X_o\}\,E_j^o\cos\omega_o t + \sum_k\left(\frac{\partial\alpha_{ij}}{\partial R_k}\right)_{R_k=0}\frac{R_k E_j^o}{2}\left[\cos(\omega_o+\Omega_k)t + \cos(\omega_o-\Omega_k)t\right] \qquad \text{(II-4)}$$

The intensity of the scattered light is proportional to P_i^2. The first term in eq. (II-4) gives the light scattered at the incident frequency, and the second term gives two components of the scattered light for each normal vibration at frequencies:

$$\omega_s = \omega_o - \Omega_k$$

$$\omega_{as} = \omega_o + \Omega_k$$

called the Stokes and anti-Stokes components, respectively. From a quantum mechanical point of view, the Stokes radiation results from the creation of a phonon and the anti-Stokes radiation results from annihilation of a phonon.

1. Selection rules

The vibrational modes of the lattice can be studied in the Raman effect only if they couple to the incident field. Considering only the frequency shifted scattered light, we rewrite eq. (II-4)

$$P_i = \sum_k \alpha_{ij}^{k} E_j^{k} \qquad \text{(II-5)}$$

where

$$\alpha_{ij}^{k} = \frac{1}{2} \left(\frac{\partial \alpha_{ij}}{\partial R_k}\right)_{R_k=0} R_k$$

and

$$E_j^{k} = E_j^{o} [\cos (\omega_o + \Omega_k) t + \cos (\omega_o - \Omega_k) t]$$

From symmetry considerations we can determine which modes may be Raman active, i.e., $\alpha_{ij}^{k} \neq 0$ and which modes will be Raman inactive, i.e., $\alpha_{ij}^{k} \equiv 0$ (14).

The factor $\left(\frac{\partial \alpha_{ij}}{\partial R_k}\right)_{R_k=0}$ is evaluated at the equilibrium position of the atoms and, therefore, is a numerical quantity which is a property of the unit cell in its equilibrium configuration and is invariant under all symmetry operations of the group. Thus, under the operations of the

group the factor $\left(\frac{\partial \alpha_{ij}}{\partial R_k}\right)_{R_k=0} R_k$ transforms in the same way as the normal coordinate R_k and the quantity will be non zero only if R_k transforms in the same way as one of the polarizability components. Since the polarizability is a second rank tensor, the normal vibrations which have the same transformation properties, i.e., the same irreducible representations, as a second rank tensor will be Raman active. A second rank tensor transforms under the symmetry elements of the group in the same manner as the bilinear forms of the basis vectors x, y, and z (i.e., x^2, y^2, z^2, xy, xz, yz). Since the character tables (Table I-1) list the transformation properties of the various bilinear forms, we can immediately determine which species are Raman active.

If we represent the bilinear forms as a symmetric 3x3 matrix

$$\begin{bmatrix} x^2 & xy & xz \\ xy & y^2 & yz \\ xz & yz & z^2 \end{bmatrix}$$

we determine which Raman active species will be observed for a given scattering geometry and a given polarization of the incident and scattered light. These tensors, called the Raman or polarizability tensors, have been tabulated for the Raman active species of the 32 crystal point groups (37).

Table II-1 gives the polarizability tensors for alpha and beta quartz. Below each matrix is listed the corresponding irreducible representation of the normal vibration. An (x) or (y) occurring in brackets after an irreducible representation indicates that the vibration is also infra-red active and the polarization of the mode has the direction indicated. From this table we see that by coupling to any off

Table II-1

Polarizability Tensors for Alpha and Beta Quartz

$D_3(32)$

Alpha Quartz

$$\begin{bmatrix} a & . & . \\ . & a & . \\ . & . & b \end{bmatrix} \qquad \begin{bmatrix} c & -c & -d \\ -c & -c & d \\ -d & d & . \end{bmatrix}$$

A_1 $\qquad$ $E(x,y)$

$D_6(622)$

Beta Quartz

$$\begin{bmatrix} a & . & . \\ . & a & . \\ . & . & b \end{bmatrix} \qquad \begin{bmatrix} . & . & -c \\ . & . & c \\ -c & c & . \end{bmatrix} \qquad \begin{bmatrix} d & d & . \\ d & -d & . \\ . & . & . \end{bmatrix}$$

A_1 $\qquad$ $E_1(x,y)$ $\qquad$ E_2

diagonal component only $E(E_1+E_2)$ modes will be observed in alpha (beta) quartz. By coupling to the zz component, only the A_1 modes will be observed in alpha and beta quartz.

B. PAST EXPERIMENTS

It was in quartz that Raman scattering in solids was first discovered (39). In 1928 Landsburg and Mandel'shtam, while searching for a "fine structure of the Rayleigh line" in quartz, observed lines whose frequency shifts were so large that they could not be termed fine structure. They were subsequently explained as Raman lines (referred to as "Combination Lines" in the Russian literature) arising from normal vibrations in a similar manner as the Raman lines observed in liquids by C. V. Raman.

Subsequently, Krishnan in 1928 (40), Rasetti in 1932 (41) and several others, mostly in Russia and India, have investigated the Raman effect in quartz.

The group theory of alpha quartz shows that there should be 12 first order Raman lines, eight of which are doubly degenerate. At room temperature as many as 41 distinct lines have been observed (42), the majority of which were interpreted as second order Raman lines. While there was accord in the assignment of the four A_1 lines, there was wide disagreement in the assignment of the other observed lines.

The first study of the temperature dependence of the Raman spectra of quartz was performed in 1940 by Raman and Nedungadi who studied the spectra from liquid air temperatures up to 530°C (43). They observed that "the 220 cm^{-1} line behaves in an exceptional way; spreading out

greatly towards the exciting line and becoming a weak diffuse band as the transition is approached." They inferred that the resulting deformations of the atomic arrangements associated with this particular mode of vibration are responsible for the changes in the properties of the crystal.

Subsequent Raman studies in 1947 and 1948 by Narayanaswamy, who investigated quartz from room temperature into the beta phase, revealed that of all the fundamental vibrations of quartz, only the 207 cm^{-1} line had an anomalous temperature dependence, its frequency shifting toward zero frequency and its width broadening considerably as the transition temperature was approached (23). Narayanaswamy reported no lines in the beta phase corresponding to the 207 cm^{-1} line in the alpha phase. It was on the basis of Narayanaswamy's experiments that Ginzburg proposed that the 207 cm^{-1} mode was the vibration associated with the order parameter.

The most reliable pre-laser Raman study on alpha quartz was performed in 1962 by Zubov and Osipova, who used a Mercury arc source and photoelectric recording (44). Twelve lines were observed and the four A_1 modes were correctly identified. However, their assignments for the fundamental frequencies of the E vibrations disagree with the later experiments.

The first Raman study of alpha quartz using a laser as the exciting source was reported by Scott and Porto (45), who measured the frequencies of the A_1 and E modes and gave polarization assignments to the E modes.

C. APPARATUS

When one studies the spectra published in the literature cited above, the existence of some lines is immediately questioned. Compared to present

day Raman apparatus, the equipment used decades ago was quite crude and one is impressed by the perseverence of the pioneers in light scattering. The exciting source was usually a mercury arc. The scattered light was analyzed by a single grating or prism spectrometer, and the detection was photographic which required days of exposure time to obtain a spectrum. The frequency shifts were measured from a microphotometer tracing of the exposed and developed plate. Extraneous scattered light in the spectrograph, ghosts and other emission lines of the exciting source consistently complicated the spectra and increased the problems of data reduction.

The present day Raman scattering apparatus consists of a laser as the exciting source, a tandem spectrograph to reduce the extraneous scattered light inside the spectrograph, a photomultiplier tube to detect the scattered light, and a photon counting system to analyze the signal. With this system a spectrum is recorded in minutes, polarization studies can easily be made, and extraneous scattered light inside the spectrograph is reduced.

The apparatus used for our Raman experiments is shown in Fig. II-1. The early work was performed with a He-Ne gas laser (Spectra-Physics Model 125) with an output of 80 mW at 6328 A. Most of the experiments, however, were performed with an Argon Ion laser (Spectra-Physics Model 140) whose peak power at 4880 A was 800 mW. The laser light was focused into the sample. Two mirrors were used to rotate the image of the scattering column by 90° so that the image was parallel to the slits of the spectrometer. The scattered light was then focused onto the slits of a Spex (Model 1400) 3/4 meter tandem grating monochrometer. The slit

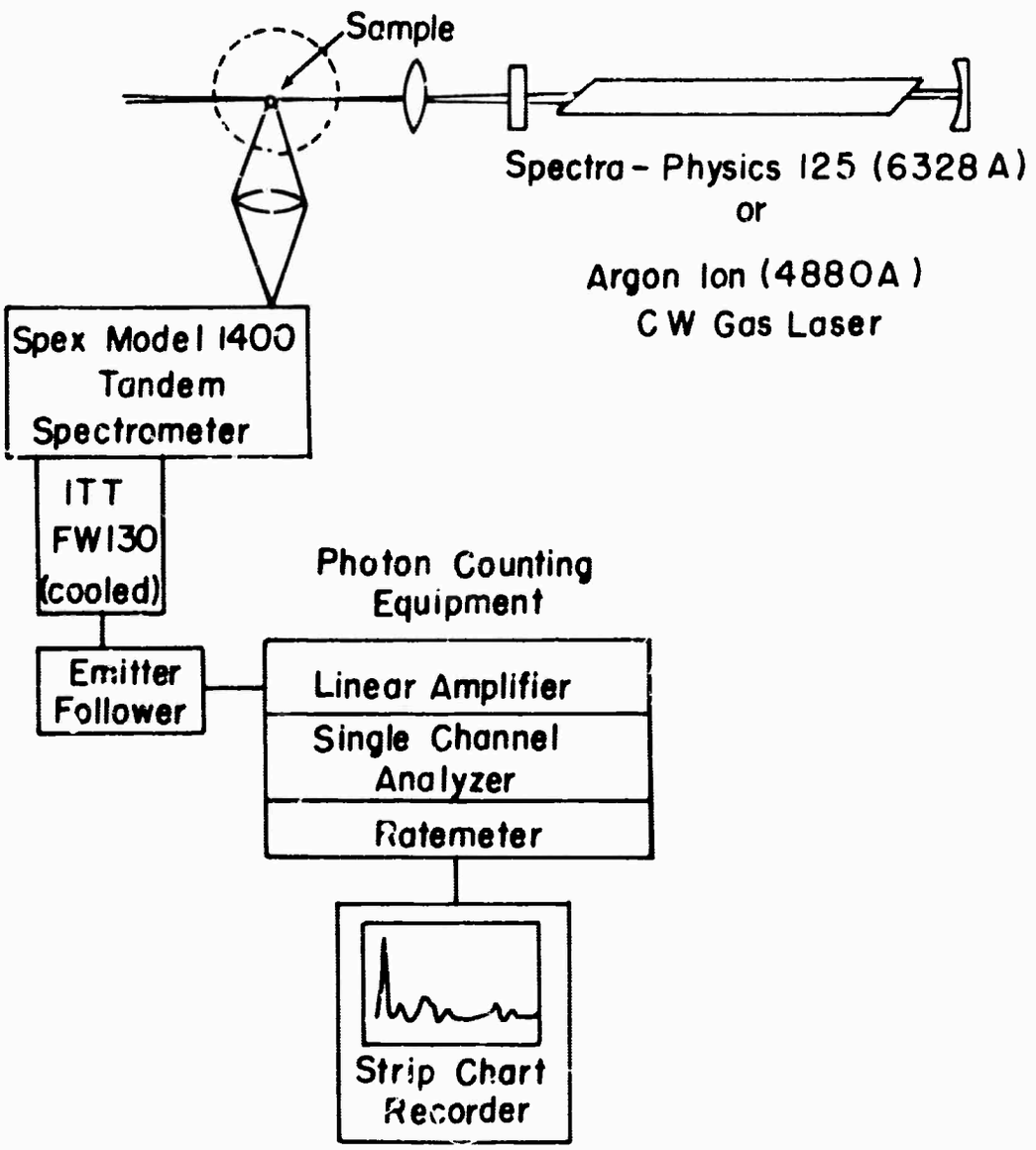

Fig. II-1. Apparatus used in Raman scattering experiments.

widths used were 250 and 100 microns, which gave a resolution of 7.5 cm^{-1} and 3.0 cm^{-1}, respectively.

The photomultiplier tube was an ITT Startracker (Model FW130) with a rectangular (18 mm x 2 mm) S-20 photocathode surface. The small photocathode results in a very low dark current, so that very weak signals may be detected. The room temperature dark count rate of 250 cts/sec. was reduced to 3-5 cts/sec. by cooling the tube.

The photomultiplier tube was followed by an emitter-follower, an amplifier (Sturrup-Model 1415) and a single channel analyzer (Sturrup-Model 1430) which discriminated against the pulses that did not originate at the photocathode. The uniform output pulses of the analyzer were counted and integrated by a ratemeter (Hammer-Model NR-10) and the signal was recorded on a strip-chart recorder (Leeds and Northrup Speedomax W).

The features in the spectrum are measured in terms of wavelength, converted to wavenumbers and then subtracted from the wavenumber of the exciting line to give the Raman shifts in cm^{-1}. For sharp lines, the error in the measured shifts is ± 2 cm^{-1}. For broader lines, and those close to the Rayleigh line, where the instrumental Rayleigh wings distort the line shape, the error is increased due to the uncertainty in the location of the line center.

A specially constructed, temperature regulated oven was used to study quartz from room temperature up to 650°C; its construction and performance are described in Appendix B. For low temperature work, a commercial Hofman Dewar was used to study quartz at liquid nitrogen temperatures (77°K) and close to liquid helium temperatures (20°K).

Two natural quartz and two synthetic quartz samples were studied, the former being Brazilian quartz and supplied by Karl Lambrecht-Crystal Optics and a private collector; and the latter were supplied by Western Electric Co. and Sawyer Research Corp. All samples were cut and polished with faces perpendicular to the XYZ axes and were approximately cubic in shape with each edge about 12 mm. in length.

The crystal orientation for the Raman experiments was with the light incident along X, scattered along Y, and Z perpendicular to the scattering plane. By proper polarization of the incident and scattered light we were able to select, separately, the A_1 and the E (in beta quartz $E_1 + E_2$) modes. For incident and scattered light polarized perpendicular to the scattering plane (denoted VV or in the notation of Damen, Porto and Tell (46) x(zz)y), we couple the light to the zz component of the polarizability tensor (Table II-1) and only the A_1 modes are observed. For vertically polarized incident light and horizontally polarized scattered light (VH or x(zx)y), or horizontally polarized incident light and unanalyzed scattered light (HT or x(yz+yx)y) we couple the light to the off diagonal components of the polarizability tensors and only the E modes (in beta quartz E_1+E_2) are excited.

D. EXPERIMENTAL RESULTS

Figure II-2 shows the room temperature A_1 and E spectra for alpha quartz which are in agreement with the first laser Raman spectra of quartz observed by Scott and Porto (45). The measured frequencies are our values, and the polarization assignments are those of Scott and Porto. The important observations are the appearance of 5 lines in the A_1 spectrum

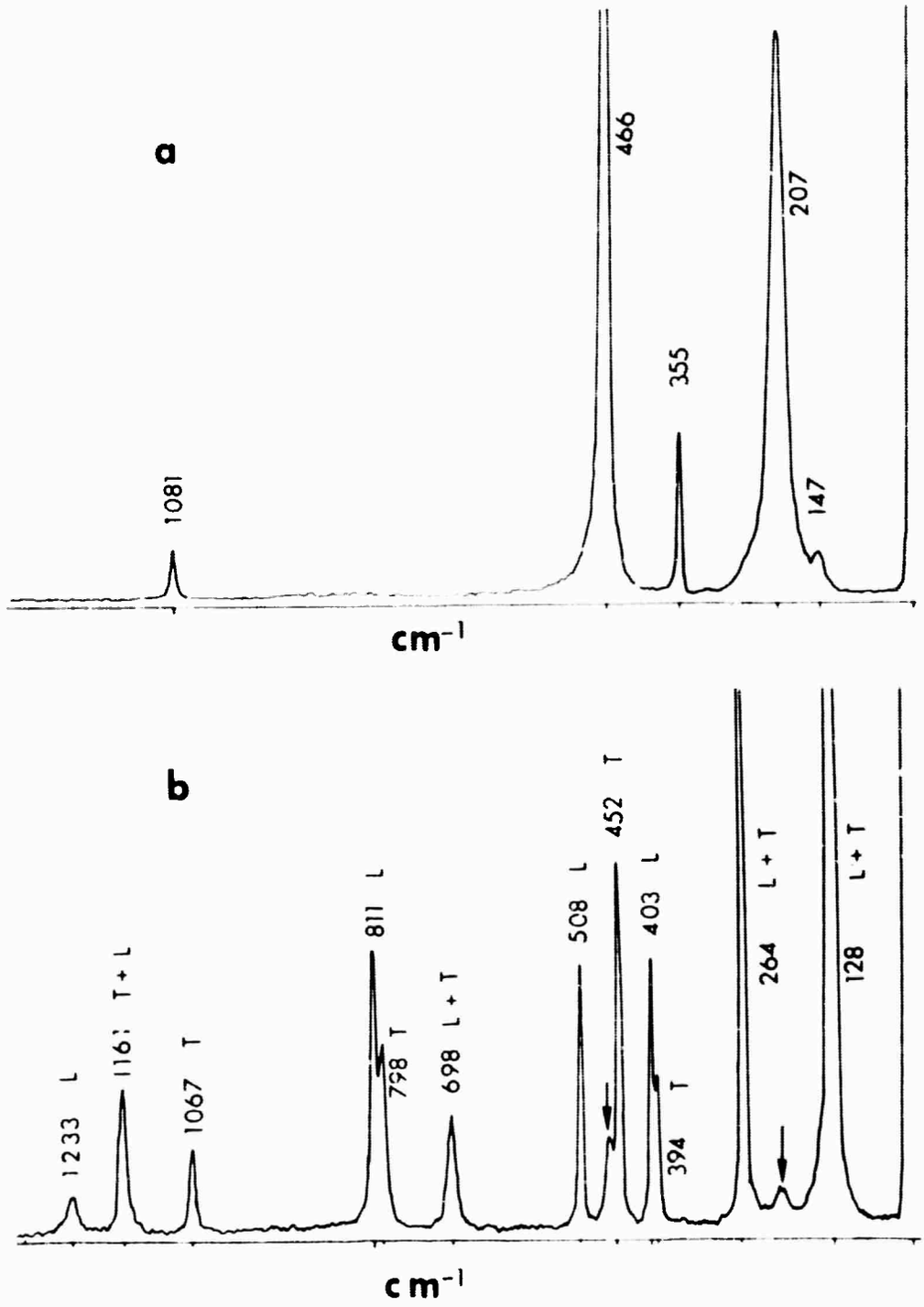

Fig. II-2. Room temperature Raman spectra of alpha quartz with measured values of frequencies in cm^{-1}, and Scott and Porto's (ref. 45) polarization assignments (L=longitudinal, T=transverse). (a) The x(zz)y spectrum showing the A_1 modes. (b) The x(yx+yz)y spectrum showing the E modes. The arrows indicate intense A_1 modes being transmitted due to non-ideal polarizers and imperfect alignment.

instead of the 4 predicted by group theory. In the observed E spectrum there are 12 lines instead of the 8 predicted by group theory. The origin of the extra lines in the E spectrum has been satisfactorily explained as due to a lifting of the degeneracies by long range electrostatic interaction. These observations will be discussed more fully in the next section.

On cooling the crystal to -250°C the Raman shifts changed very little from the room temperature values. Figure II-3 shows the A_1 spectra from 60 to 200 cm^{-1} at three different temperatures: -250°C, -194°C and -40°C. The sharp low frequency line is the 128 cm^{-1} E line which is transmitted due to imperfect alignment and non ideal polarizers. (The spectral features will be named according to their room temperature frequencies.) Note that the intensity of the 147 cm^{-1} line decreases quite rapidly as the temperature is decreased with little change in frequency or linewidth.

Figure II-4 shows the A_1 spectrum at five different temperatures above room temperature (the top trace is in the beta phase). The most striking result is the rapid increase in the intensity of the weak 147 cm^{-1} line and its corresponding decrease in frequency as the sample approaches the transition temperature. The 147 cm^{-1} line is not present in the beta phase. The 207 cm^{-1} line is seen to broaden and shift toward lower frequencies, as reported by Narayanaswamy, but its frequency does not reach zero and it is still present in the beta phase as a broad band centered at 162 cm^{-1}. The temperature dependence of the frequency of the 147 and 207 cm^{-1} lines is plotted in Fig. II-5. (We see that synthetic quartz has the same frequency vs temperature behavior as natural quartz.)

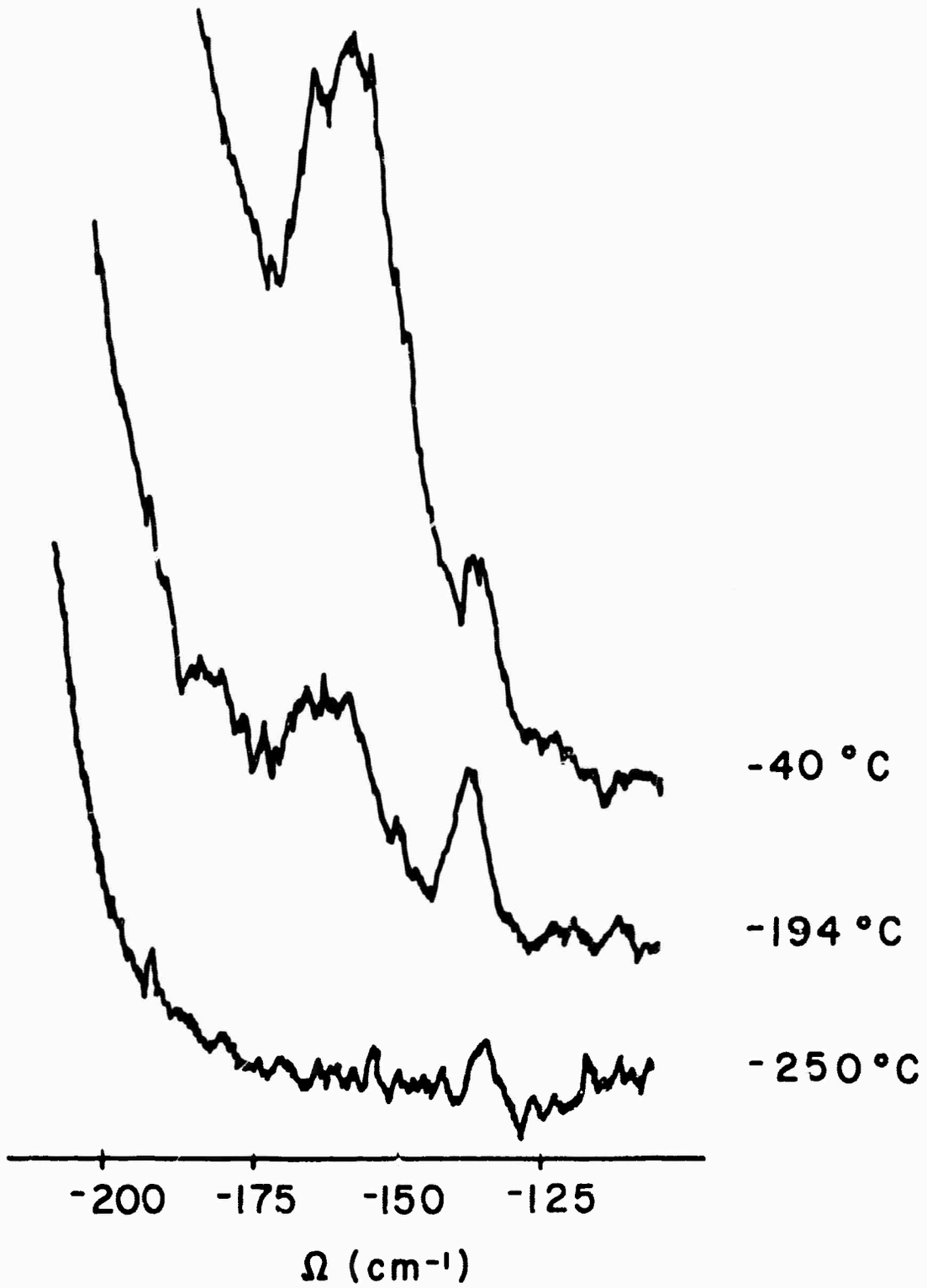

Fig. II-3. The 100 to 200 cm^{-1} portion of the x(zz)y Raman spectrum showing the temperature dependence of the 147 cm^{-1} feature.

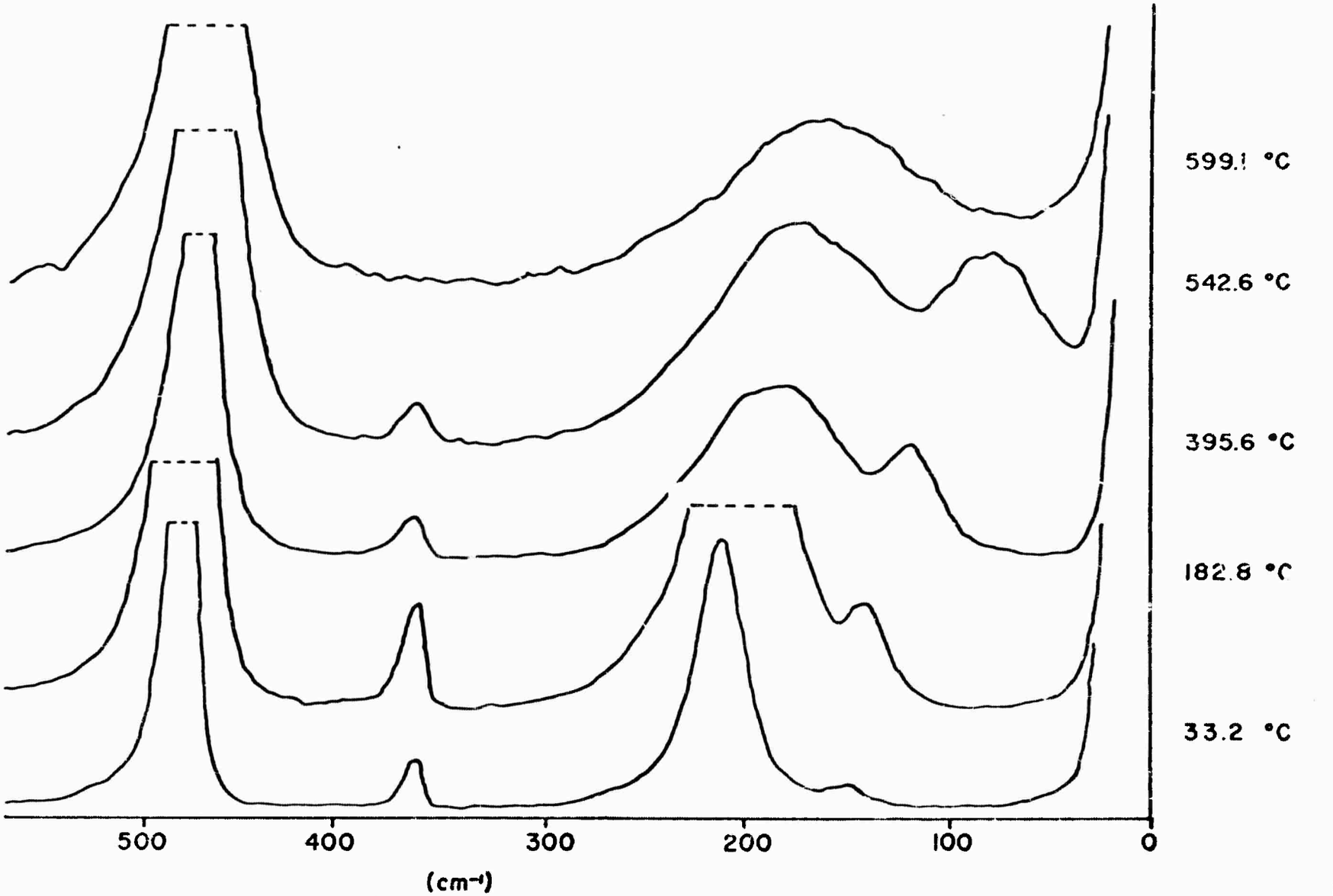

Fig. II-4. The 0 to 550 cm^{-1} portion of x(zz)y Raman spectra at different temperatures showing four of the five totally symmetric A_1 lines of quartz. The upper spectrum is for beta quartz. The gain of the lowest temperature curve is one-half that of the other curves.

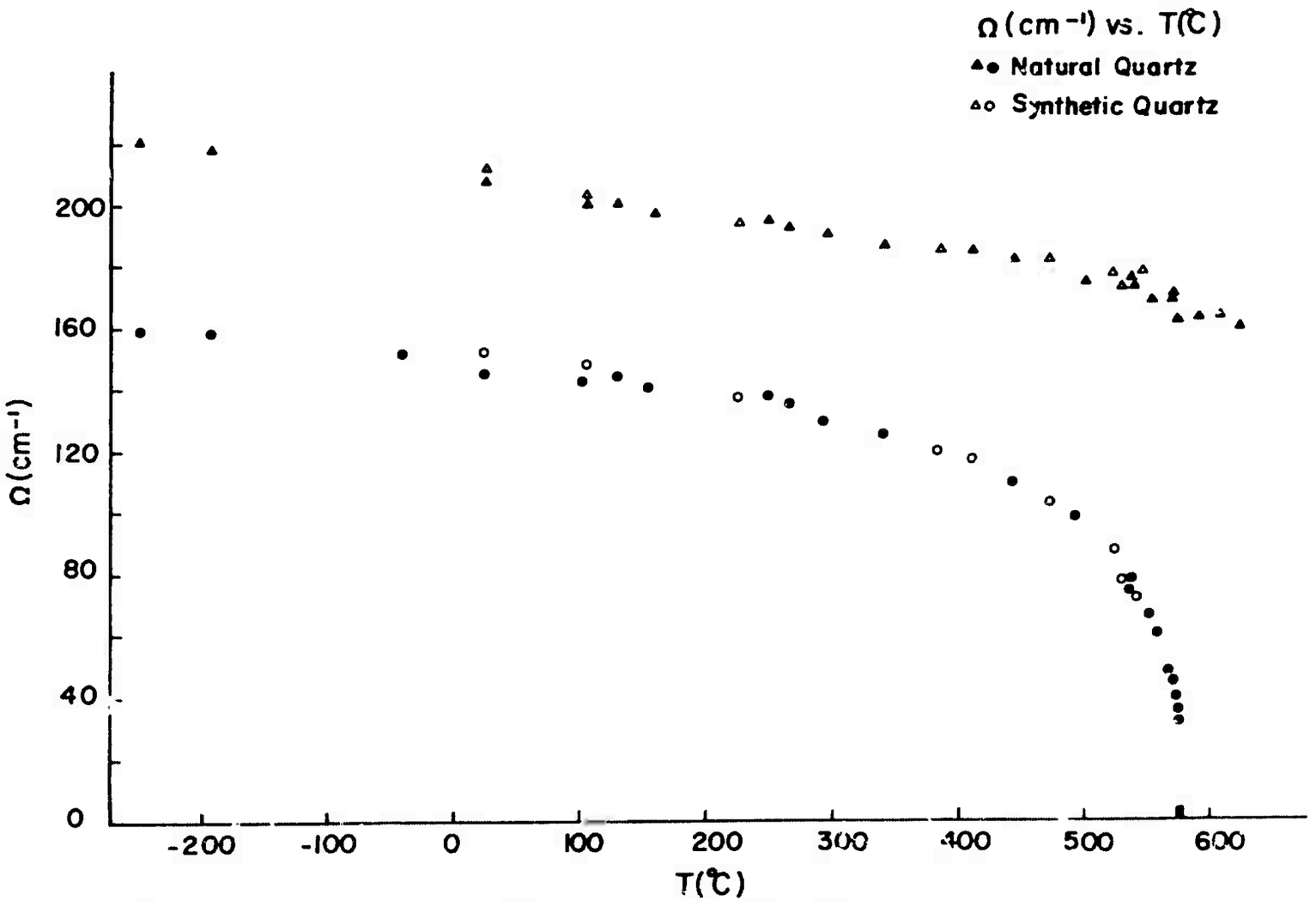

Fig. II-5. Ω (cm^{-1}) vs T (°C). Triangles - 207 cm^{-1} line; circles - 147 cm^{-1} line. Solid symbols - natural quartz, open symbols - synthetic quartz.

It is seen that the frequency of the 147 cm^{-1} line does not go to zero continuously, but decreases to a value of 30 cm^{-1} and then suddenly disappears from our spectra. On cooling, the line reappears at a temperature 1°C lower than that at which it disappeared on heating.

The frequencies of the other A_1 lines change very little with temperature, Fig. II-6. The 466 cm^{-1} line, which is very intense at room temperature, broadens somewhat with increasing temperature, but persists through the transition having shifted to 459 cm^{-1} in the beta phase. This has been observed in earlier experiments. The 355 cm^{-1} and 1081 cm^{-1} lines, which become B_1 Raman inactive modes in the beta phase, decrease in intensity with increasing temperature and are not present in the beta phase. Fig. II-7 is a plot of the intensity of the 355 cm^{-1} line vs temperature.

A plot of the measured linewidths of the 147 cm^{-1}, the 207 cm^{-1}, and the 467 cm^{-1} lines is shown in Fig. II-8. The 147 cm^{-1} and 207 cm^{-1} lines are already broad at room temperature and continue to broaden as the temperature is raised. There are large errors in these measurements especially at temperatures above 200°C where the determination of the zero intensity level is not possible due to the large amount of second order scattering being excited, and overlapping spectral lines.

Summarizing the observations on the A_1 lines, there appear to be five A_1 modes in the alpha phase (Fig. II-2, II-3, and II-4) and two modes in the beta phase (Fig. II-4). However, group theory predicts that there should only be four A_1 modes in the alpha phase, and at the transition three of the four A_1 modes become Raman inactive B_1 modes, while only one of the four will be present in the beta phase as a Raman active A_1 mode (Table I-3).

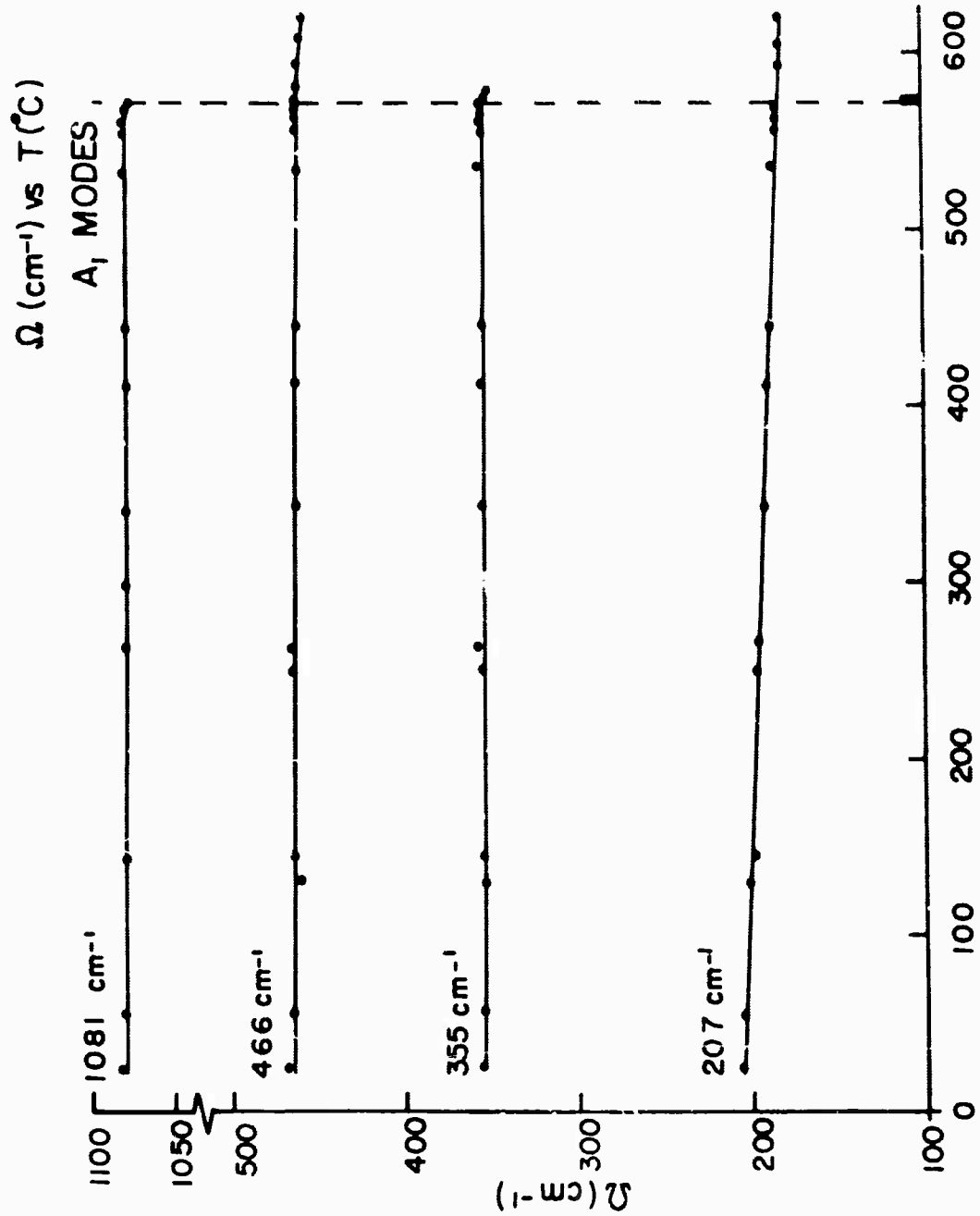

Fig. II-6. Ω (cm^{-1}) vs T (°C) for the 207 cm^{-1}, 355 cm^{-1}, 466 cm^{-1} and 1081 cm^{-1} A_1 lines.

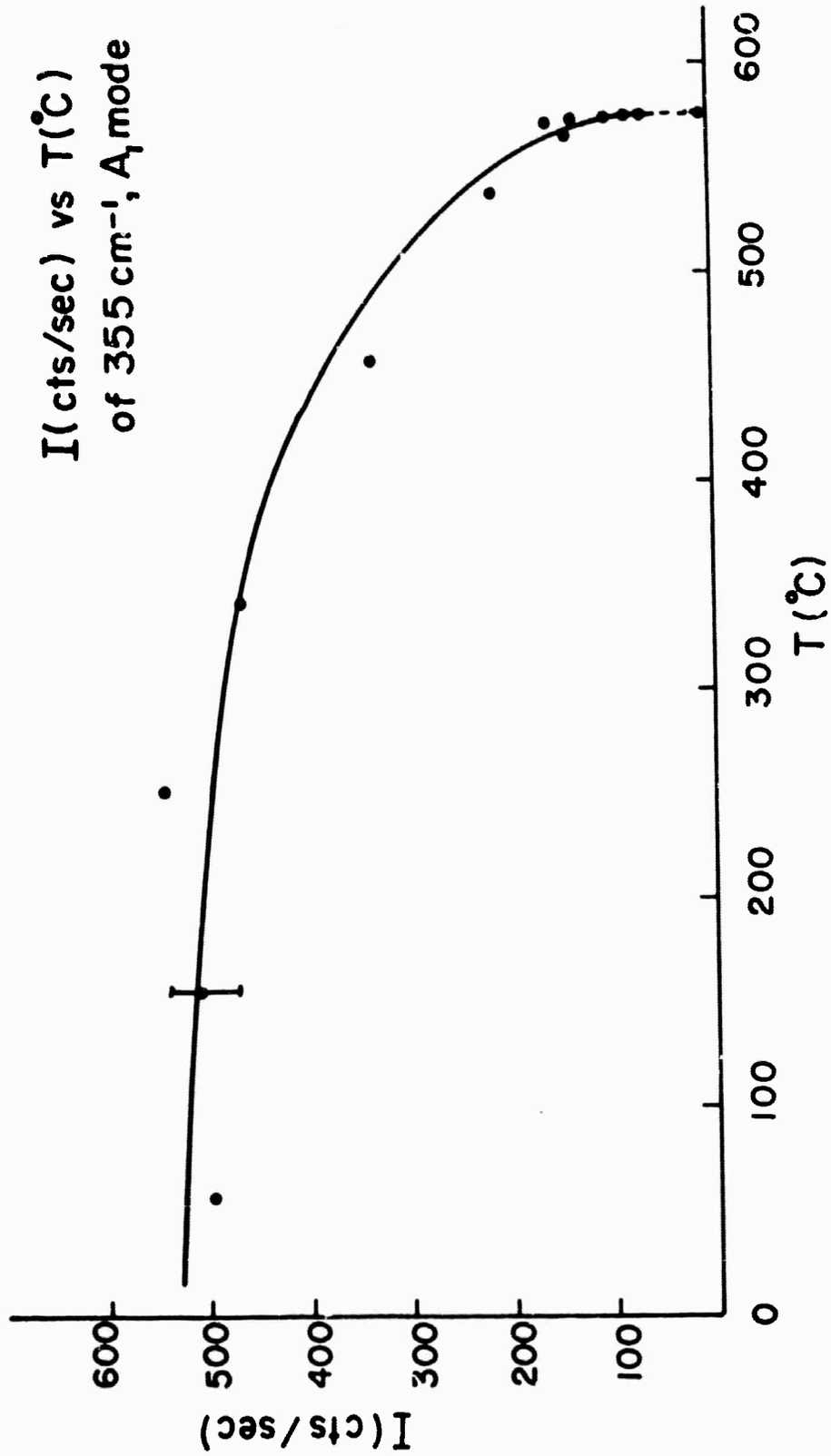

Fig. II-7. I (cts/sec.) vs T (°C) for the 355 cm^{-1} , A_1 vibration.

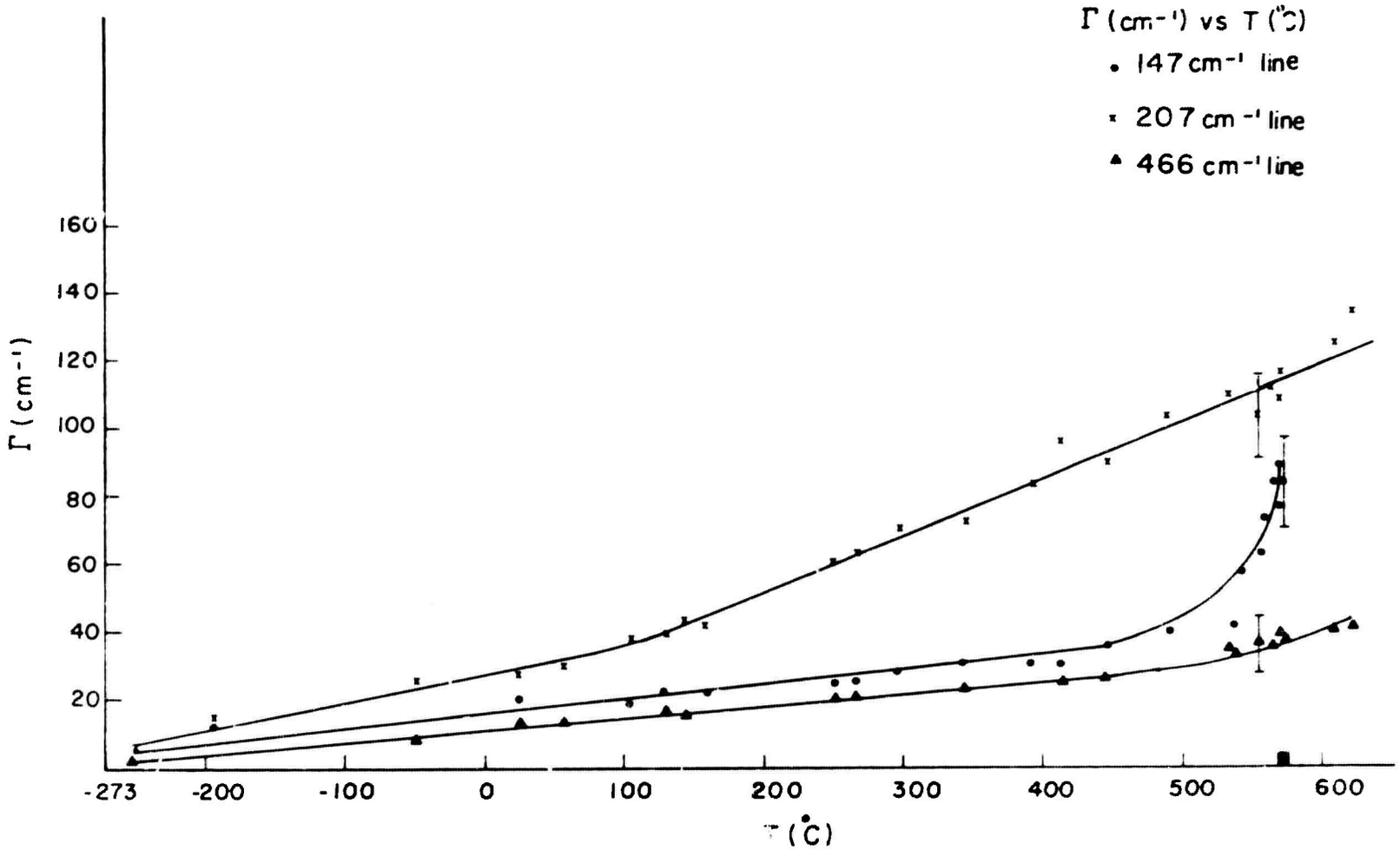

Fig. II-8. The linewidth, Γ (cm^{-1}), vs T (°C) for the 147 cm^{-1}, 207 cm^{-1} and 466 cm^{-1} lines.

The E modes show little temperature dependence. The lowest frequency E mode which has the strongest temperature dependence of the E modes shifts from its room temperature frequency of 128 cm^{-1} to 96 cm^{-1}. There has been wide interest in this mode since it is the lowest frequency transverse optical vibration. Attempts have been made to observe polaritons associated with this mode (47, 48). Also, this is the first infrared active vibration in a crystal to be observed in stimulated Raman scattering (49). Table II-2 correlates the E lines observed at room temperature with those observed in the beta phase. In the beta phase the E_1+E_2 lines have broadened and some splittings which were observed at room temperature are no longer seen at high temperatures.

E. DISCUSSION

1. E Spectrum

In the E spectrum of alpha quartz (Fig. II-1) there are 12 observed lines instead of the 8 doubly degenerate lines predicted by group theory. The explanation of the additional lines is that the E modes are also infra-red active so that there is a dipole moment associated with these vibrations which gives rise to a long range electric field which lifts some of the long wavelength phonon degeneracies.

The lifting of the degeneracies is closely related to the LST relation derived for a single optic vibration in ionic crystals (50). Loudon predicted a lifting of a degeneracy for uniaxial crystals (37), and Scott and Porto applied the theory to quartz (45). Born and Huang discuss the macroscopic equations governing the lattice modes in a solid (51):

Table II-2

Frequencies of E Modes in Alpha Quartz and

E_1+E_2 Modes in Beta Quartz

Alpha Quartz E Modes		Beta Quartz E_1+E_2 Modes
-25°C	525°C	585°C
128 (L+T) cm^{-1}	110 cm^{-1}	96 cm^{-1}
264 (L+T)	252	249
394 (T) 403 (L)	398	399
452 (T) 508 (L)	440 502	414 494
698 (T+L)	686	684
798 (T) 811 (L)	785 797	792
1067 (T) 1233 (L)	1063 1224	1067 1228
1161 (T+L)	1165	1149

$$\ddot{\vec{R}}_k = -\Omega_k^2 \vec{R}_k + Z_k \vec{E} \qquad \text{(II-6)}$$

$$\vec{P} = \sum_{k=1}^{m} Z_k \vec{R}_k + \alpha_\infty \vec{E} \qquad \text{(II-7)}$$

where $\vec{R}_k$ is proportional to the relative displacements of the atoms in the k^{th} vibrational mode; Z_k is the effective charge density for the k^{th} mode; $\vec{P}$ is the electric polarization, α_∞ is the electronic polarizability and $\vec{E}$ is the macroscopic field defined in Maxwell's equations. Ω_k^2 is proportional to the restoring force for the k^{th} mode which includes, in addition to the short range interatomic forces, the Lorentz field contribution to the effective field at an atom (5). The sum is over the m infrared active vibrational modes.

Letting $\vec{E}$, $\vec{P}$ and $\vec{R}_k$ all be plane waves proportional to $e^{i(\omega t - \bar{q}\cdot\bar{r})}$ we can solve (II-6) for R_k

$$\vec{R}_k = \frac{Z_k}{\Omega_k^2 - \omega^2} \vec{E} \qquad \text{(II-8)}$$

and substituting into eq. (II-7)

$$\vec{P} = \left[\alpha_\infty + \sum_{k=1}^{m} \frac{Z_k^2}{\Omega_k^2 - \omega^2} \right] \vec{E} \qquad \text{(II-9)}$$

From the definition of the electric displacement

$$\bar{D} = \varepsilon(\omega)\bar{E} = \bar{E} + 4\pi\bar{P} \qquad \text{(II-10)}$$

and substituting eq. (II-9) into eq. (II-10)

$$\varepsilon(\omega) = 1 + 4\pi\alpha_\infty + 4\pi \sum_{k=1}^{m} \frac{Z_k^2}{\Omega_k^2 - \omega^2}$$

$$\varepsilon(\omega) = \varepsilon(\infty) + \sum_k \frac{S_k \Omega_k^2}{\Omega_k^2 - \omega^2} \qquad \text{(II-11)}$$

where we defined the high frequency dielectric constant:

$$\varepsilon(\infty) = 1 + 4\pi\alpha_\infty \qquad \text{(II-12)}$$

and the mode strength for an infrared oscillation:

$$S_k = \frac{4\pi Z_k^2}{\Omega_k^2} \qquad \text{(II-13)}$$

The S_k determine the value of the static dielectric constant:

$$\varepsilon(o) = \varepsilon(\infty) + \sum_k S_k \qquad \text{(II-11')}$$

If we restrict ourselves to lattice waves having a phase velocity much less than the velocity of light in the crystal we can neglect any retardation effects and Maxwell's equation for the macroscopic field are:

$$\nabla\cdot\bar{D} = \nabla\cdot(\bar{E} + 4\pi\bar{P}) = 0 \qquad \text{(II-14)}$$

$$\nabla\times\bar{E} = 0. \qquad \text{(II-15)}$$

From eq. (II-14)

$$\nabla\cdot\bar{E} = -4\pi\nabla\cdot P \qquad \text{(II-16)}$$

and substituting eq. (II-7) into eq. (II-16) and using eq. (II-12)

$$\nabla\cdot\bar{E} = \frac{-4\pi}{\varepsilon(\infty)} \sum_{k=1}^{m} Z_k \nabla\cdot\bar{R}_k \qquad \text{(II-17)}$$

With eqs. (II-6) and (II-7) we can solve for the macroscopic field, $\vec{E}$. We split R_k into its transverse and longitudinal components, $\vec{R}_k = \vec{R}_{kL} + \vec{R}_{kT}$ and treat each case separately.

CASE I: If $\vec{R}_k$ is transverse, $\vec{R}_k = \vec{R}_{kT}$ and

$$\nabla \cdot \vec{R}_k = 0$$

$$\nabla \times \vec{R}_k \neq 0$$

From eq. (II-7) we see $\nabla \cdot \vec{E} = 0$; and from Maxwell's equation (II-15), $\nabla \times \vec{E} = 0$. Thus in a transverse optic (TO) mode, $\vec{E} = 0$. In the equation of motion (eq. II-6) the second term on the right is zero and the frequency of the transverse modes are the Ω_k's of eq. (II-6):

$$\Omega_{kT}^2 = \Omega_k^2$$

From eq. (II-7) we see that there is a polarization even though $\vec{E} = 0$. Since $\vec{P} = \left(\frac{\epsilon-1}{4\pi}\right) \vec{E}$ (eq. II-14) in order for $\vec{P} \neq 0$ as $E \to 0$, ϵ has to approach ∞. Thus, in terms of the dielectric constant, the frequencies of the TO phonons are the poles of $\epsilon(\omega)$ (eq. II-11).

CASE II: If $\vec{R}_k$ is longitudinal, $\vec{R}_k = \vec{R}_{kL}$, and

$$\nabla \times R_k = 0$$

$$\nabla \cdot R_k \neq 0$$

From the latter equation and eq. (II-17):

$$\vec{E} = \frac{4\pi}{\epsilon(\infty)} \sum_{k=1}^{m} Z_k \vec{R}_k \qquad \text{(II-18)}$$

Putting this into eq. (II-6):

$$\ddot{\vec{R}}_k = -\Omega_k^2 \vec{R}_k - \frac{1}{\varepsilon(\infty)} 4\pi Z_k \sum_{k'}^{m} Z_{k'} \cdot \vec{R}_{k'} \qquad \text{(II-19)}$$

Removing the k^{th} term from the sum and rewriting,

$$\ddot{\vec{R}}_k = -[\Omega_k^2 + \frac{4\pi}{\varepsilon(\infty)} Z_k^2]\vec{R}_k - \frac{4\pi}{\varepsilon(\infty)} Z_k \sum_{k' \neq k}^{m} Z_{k'} \cdot \vec{R}_{k'} \qquad \text{(II-20)}$$

From eq. (II-20) we see that the $\vec{R}_k$'s are no longer dynamically independent and that the frequency of the k^{th} longitudinal optic (LO) phonon differs from the frequency of the TO phonon.

If we consider the special case where there is only one mode there is no sum in eq. II-20, and

$$\ddot{\vec{R}}_k = -\left[\Omega_{kT}^2 + \frac{4\pi Z_k^2}{\varepsilon(\infty)}\right] \vec{R}_k \qquad \text{(II-21)}$$

The frequency of the k^{th} LO mode is:

$$\Omega_{kL}^2 = \Omega_{kT}^2 + \frac{4\pi Z_k^2}{\varepsilon(\infty)} \qquad \text{(II-22)}$$

Since all the factors are positive in the second term on the right, we see that the frequency of the LO phonon is greater than the frequency of the TO phonon.

From the definition of the strength of the mode (eq. II-13), eq. (II-22) becomes:

$$\Omega_{kL} = \Omega_{kT}^2 \left[1 + \frac{S_k}{\varepsilon(\infty)}\right] \qquad \text{(II-23)}$$

and from eq. (II-11')

$$\frac{\Omega_{kL}}{\Omega_{kT}^2} = \frac{\varepsilon(o)}{\varepsilon(\infty)} \qquad \text{(II-24)}$$

which is the LST relation for a single optic mode (50).

Returning to the general case with m vibrational modes, from eq. (II-18), $\vec{E}$ is non zero and eq. (II-16) implies:

$$\vec{E} = -4\pi\vec{P} \qquad \text{(II-25)}$$

and thus $\vec{D} = 0$ for an LO phonon. From the definition of the frequency dependent dielectric constant (eq. II-10) we see that for the LO phonon, $\varepsilon(\omega) = 0$. Thus the frequencies of the LO phonons are the zero's of the dielectric constant. From eq. (II-11):

$$0 = \varepsilon(\infty) + \sum_{k'} \frac{S_{k'}\Omega_{k'}^2}{\Omega_{k'T}^2 - \Omega_{kL}^2} \qquad \text{(II-26)}$$

If the TO modes are well separated from one another, so that in eq. (II-26), $|\Omega_{k'T}^2 - \Omega_{kL}^2| >> 1$ for $k' \neq k$, only the k^{th} term will contribute significantly to the sum and eq. (II-26) becomes the LST relation, eq.(II-24). If this approximation cannot be made, the sum in eq.(II-26) has to be performed and one finds a more complicated expression for the LST relation (52,53):

$$\prod_{k=1}^{m} \frac{\Omega_{kL}^2}{\Omega_{kT}^2} = \frac{\varepsilon(o)}{\varepsilon(\infty)} \qquad \text{(II-27)}$$

In summary, we have shown that the long range electrostatic interaction will remove the degeneracies of the E vibrations and that the frequencies of the longitudinal modes (the zero's of the dielectric constant) are greater than the frequencies of the corresponding transverse modes (the poles of the dielectric constant).

Scott and Porto (47) calculated the frequencies of the LO phonons for the E vibrations by using eq.(II-26), their measured values of Ω_{kT}^2 and the

mode strengths, S_k, from Spitzer and Kleinman (54). Their measured LO frequencies agreed, within experimental error, with our measured values.

In Fig. II-2 and Table II-2 we see that the splitting of the 128, 265, 697 and 1172 cm^{-1} lines is not resolved. The reason for this can be seen in eq. (II-23), where it is shown that the frequency difference between the LO and TO phonons is proportional to the infrared strength of the vibrations. The strengths of the 128, 265, 697 and 1172 cm^{-1} vibrations is small compared to the other infrared active vibrations (54). Attempts to resolve the LO-TO splitting of the 128 cm^{-1} line were made at low temperatures but with no success (55). However, the splitting did manifest itself as an observed broadening.

2. A_1 Spectrum

Another striking feature in the Raman spectrum of quartz is the appearance of 5 lines of A_1 symmetry in the alpha phase instead of the 4 A_1 lines predicted by group theory. In addition to this apparent disagreement with group theory below the transition temperature, there appears to be a contradiction with group theory above the transition temperature where two lines are present in the A_1 spectrum of the beta phase and group theory predicts only one.

The number of vibrations of each species is calculated by group theory on the basis of the space symmetry of the solid and the position of the atoms in the unit cell. The symmetry of alpha quartz has been well established for decades (1, 2) and the symmetry of beta quartz also seems beyond dispute (1, 2). Thus, since it is unlikely that the symmetry determination of the different phases of quartz is incorrect, another explanation for the discrepancy between the group theory and experiments is sought.

Originally (56) the 147 cm^{-1} was thought to be the result of a second order Raman scattering process. However, this explanation seemed unlikely because the striking temperature dependence of the frequency of the 147 cm^{-1} line (Figs. II-4 and II-5) indicated that it plays a fundamental role in the phase transition. The second order assignment would not, in any case, resolve the difficulty in the beta phase arising from the persistence of both the 466 and 207 cm^{-1} lines. An ad hoc model which explained the basic temperature dependent results was proposed by Shapiro, O'Shea and Cummins (22):

As we have seen, the silicon ions in the beta phase are located at hexagonal sites with the oxygens halfway between neighboring silicons. In the alpha phase the silicons are displaced in one of two directions along a twofold symmetry axis and the oxygens also move to one side of their beta phase sites. All the ions move in double minimum potentials centered around their beta phase sites. The double wells are strongly asymmetric due to the cooperative interaction in the (ordered) alpha phase so that all the ions tend to be on the same side of their double well. The two possible arrangements, depending on which side of the well has the lower energy, constitute the electrical or Dauphiné twins of quartz (20).

Although it is usually assumed that in an untwinned crystal all unit cells have the same configuration, any one cell has a finite probability of being in the unfavorable (higher potential minimum) configuration which is proportional to the appropriate Boltzmann factor. Thus, assuming the quadratic terms of the local potential to be different at the two sites, the strong normal oscillation at 207 cm^{-1} would be accompanied by a weaker satellite at a different frequency. As the temperature is

increased the energy difference between the two configurations decreases and the intensity of the satellite line would increase, approaching that of the parent line. If, in addition, the height of the barrier decreases faster than the energy difference between the two minima, it would be the satellite whose frequency would decrease steadily towards 0 as the transition is approached.

In order to explain the persistence of the "forbidden" A_1 mode in the beta phase, one might ascribe a dissymmetry to the local-potential minimum. Extensive x-ray measurements show that a double-minimum configuration with random occupation (appropriate to an order-disorder transition) in the beta phase is highly unlikely (20). Nonetheless, a small residual dissymmetry cannot be ruled out and could account for the extra A_1 mode observed in the beta phase.

Another model recently proposed by Scott (57) explains the unusual temperature dependence and selection rules exhibited by the 147 cm^{-1} and 207 cm^{-1} Raman features as due to the coupling between one and two phonon excitations. The 207 cm^{-1} line is essentially a zone center A_1 optic vibration while the feature at 147 cm^{-1} is a second order Raman line which is the result of the creation of two zone edge acoustic phonons with equal and opposite wavevectors. The arguments given by Scott for the second order nature of the 147 cm^{-1} line are the appearance of his spectra at low temperature and the peak at 70±5 cm^{-1} observed in neutron scattering experiments on polycrystalline quartz.

As the temperature is raised, the two excitations become mixed due to the coupling produced by the anharmonicity. Around 330°C the excitations are thoroughly mixed and the observed spectral features can no longer be described as one or two phonon processes. As $T \rightarrow T_t$, the

excitations again become distinct, and the low frequency component has become the one-phonon mode and the higher frequency line is the two phonon excitation. Thus apart from the complications produced by the mixing, the earlier assertion that the frequency of the 207 cm^{-1} mode approaches zero as the transition temperature is approached is apparently correct. Above T_t the observed feature at 165 cm^{-1} is essentially second order ($q \neq 0$) and hence does not violate group theory whose calculations are for $q = 0$. The soft optic mode is expected to harden for $T \rightarrow T_t$, but it is a Raman and infrared inactive B_1 vibration. Early attempts to detect it by neutron scattering experiments have been unsuccessful (58). However, recent neutron diffraction experiments have detected the soft mode in the beta phase (59).

Fig. II-9 is a log-log plot of the measured frequency of the 207 cm^{-1} and the 147 cm^{-1} lines vs $\Delta T = T_t - T$ where T_t is taken as 846°K (=573°C). The dotted lines show the temperature behavior of the soft, zone center Raman line and the second order Raman line in the harmonic approximation, i.e., if there were no anharmonic coupling. The uncoupled behavior of the soft phonon was deduced from the fact that at very low temperatures, $T_t - T = 826$°K, and at high temperatures, $T_t - T = 1$°K, the coupling between the zone center and the zone edge phonons is small. At the low temperature, the higher frequency line (220 cm^{-1}) is the $q = 0$ zone center optic phonon and the lower frequency line (160 cm^{-1}) is the second order Raman line resulting from the creation of the two acoustic phonons with opposite momenta. At the high temperatures, the higher frequency line is the second order Raman line and the lower frequency line is the soft optic phonon. The slope of the line connecting the frequency of the soft phonon at low temperatures with the value at the high temperature gives the temperature behavior of the frequency of the uncoupled soft phonon:

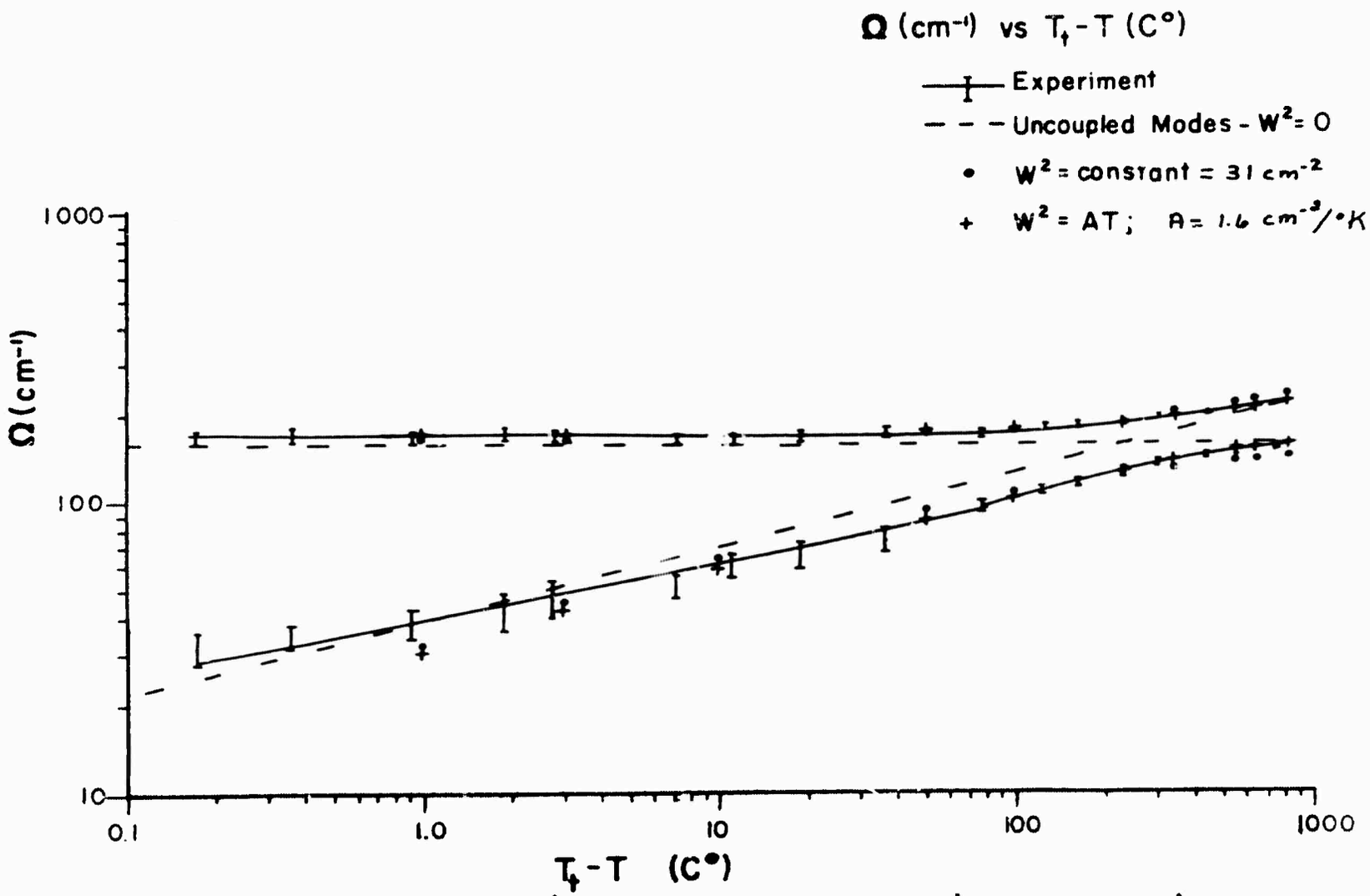

Fig. II-9. Log-log plot of $\Omega(cm^{-1})$ vs T_t-T (C°) for the 207 cm^{-1} and the 147 cm^{-1} lines. The dashed line represents solutions of eq. (II-24) with $\Omega = 41\ |T-T_t|^{1/2}$ cm^{-1}, $\Omega_a = 160$ cm^{-1} and $W^2 = 0$.

$$\Omega = A|T - T_t|^{\gamma}$$

where $A = 41 \pm 5\ cm^{-1}/(°K)^{\gamma}$

$\gamma = .25 \pm .05$

The frequency of the uncoupled second order Raman line is assumed to be temperature independent and is taken as the value at $T_t - T = 326°K$: 160 cm^{-1}.

Comparison of the observed frequencies with the uncoupled frequencies shows the characteristic level repulsion behavior predicted in other temperature dependent systems with coupled modes such as $BaTiO_3$ (60) and KDP (61).

We can derive a relation to fit the observed data. In Chapter I we discussed the harmonic approximation of a crystal system and showed that in the harmonic approximation the total Hamiltonian can be written as the sum of individual simple harmonic oscillator Hamiltonians. Considering only the soft mode and the two acoustic modes, the partial Hamiltonian, H can be written as

$$H = H_o + H_a' + H_a'' + W$$

where H_o is the Hamiltonian for the uncoupled zone center optic mode, H_a' and H_a'' are the Hamiltonians for the two uncoupled zone edge acoustic phonons with equal and opposite momenta, and W is the anharmonic contribution which couples the soft mode with the two zone edge phonons and enables energy to be transferred between the zone center and the zone edge phonons. The Hamiltonian, H, depends on temperature since H_o is temperature dependent and W may also have a temperature dependence, although H_a' and H_a'' are assumed to be temperature independent.

If the normal coordinate of the coupled system, Q, is a linear combination of the uncoupled coordinates, Q_o, Q_a' and Q_a'', we write (in matrix form)

$$Q = \begin{bmatrix} Q_o \\ Q_a' \\ Q_a'' \end{bmatrix} \qquad \text{(II-28)}$$

where Q_o, Q_a' and Q_a'' are the eigenvectors of the uncoupled Schrodinger equations:

$$H_o Q_o = \Omega_o Q_o \qquad \text{a}$$

$$H_a' Q_a' = \Omega_a' Q_a' \qquad \text{b (II-29)}$$

$$H_a'' Q_a'' = \Omega_a'' Q_a'' \qquad \text{c}$$

and Ω_o, Ω_a' and Ω_a'' are the normal frequencies of the optic and the two acoustic phonons at a given temperature. If we utilize the assumption that the two acoustic phonons are equal, but with opposite momenta, we can write:

$$(Q_a'')^* = Q_a'$$

This implies that $H_a' = H_a''$ and $\Omega_a' = \Omega_a''$.

If we write

$$Q_a = Q_a' + Q_a''$$

$$H_a = 2H_a'$$

$$\Omega_a = 2\Omega_a''$$

Eq. II-29 b and c can be combined:

$$H_a Q_a = \Omega_a Q_a \qquad \text{(II-30)}$$

The Schrodinger equation for the coupled system is:

$$\underline{\underline{H}}\,\underline{Q} = \Omega\underline{Q}$$

with $H = H_o + H_a + W$, or

$$\begin{bmatrix} H_o & W \\ W & H_a \end{bmatrix} \begin{bmatrix} Q_o \\ Q_a \end{bmatrix} = \Omega \begin{bmatrix} Q_o \\ Q_a \end{bmatrix} \qquad \text{(II-31)}$$

To find the eigenvalues of the coupled system we solve the secular equation:

$$|\underline{\underline{H}} - \Omega\underline{\underline{1}}|\,\underline{Q} = 0 \qquad \text{(II-32)}$$

and we obtain:

$$\Omega(\pm) = \frac{1}{2}\{\Omega_o + \Omega_a \pm [(\Omega_o - \Omega_a)^2 + 4W^2]^{1/2}\} \qquad \text{(II-33)}$$

where Ω_o is the frequency of the soft phonon line and Ω_a is the frequency of the second order Raman line in the uncoupled system.

In order to fit the observed data it is necessary to select the proper temperature dependence for the anharmonic coupling parameter W^2. Scott let W^2 be proportional to the experimental linewidth of the more intense line of the two spectral features.

We tried various forms for W^2 in order to obtain a good fit with the experimental curve. In Fig. II-9 the circles (•) represent a plot of eq. (II-33) vs temperature with a constant coupling parameter W^2 evaluated at the crossover point for the uncoupled modes ($\Omega_o = \Omega_a = 160\ cm^{-1}$). It is seen that the fit is quite good for small $T_t - T$, but for large $T_t - T$ (low temperatures) the calculated points lie beyond experimental error. Thus a constant W^2 is unacceptable.

Allowing W^2 to vary linearly with temperature yielded the best fit of eq. (II-33) with our experimental data (the crosses (+) in Fig. II-9). The use of a linear temperature dependence for the anharmonic coupling parameter is consistent with recent calculations of the many body Green's function of an anharmonic crystal (62, 63). In this formalism the harmonic frequency Ω_H is replaced by a renormalized frequency Ω,

$$\Omega^2 = \Omega_H^2 + 2\Omega_H D \qquad \text{(II-34)}$$

where D is the contribution of the self energy of the phonon to the frequency. Detailed expressions for the self energy factor D have been evaluated in the lowest order by Maradudin and Fein (62). D is a complex frequency and can be written as

$$D = \Delta - i\Gamma \qquad \text{(II-35)}$$

where Δ is the frequency shift due to the anharmonicity and Γ is the reciprocal lifetime of the phonon state.

The temperature dependence of D is due to the occupation number $n = \left[e^{\frac{\hbar\Omega_H}{kT}} - 1\right]^{-1}$, since the complete expression for eq. (II-35) shows D to be proportional to n (62, 63). In the high temperature limit, $kT \gg \hbar\Omega_H$, and thus

$$D \sim n \sim \frac{T}{\Omega_H} .$$

The self energy contribution to the harmonic frequency, D, includes the anharmonic terms of the total Hamiltonian. If we identify the quantity $2\Omega_H D$ in eq. (II-34) with W^2 of eq. (II-33), we see that

$$W^2 \sim \Omega_H D \sim \Omega_H n \sim \Omega_H \left(\frac{T}{\Omega_H} \right) \simeq T$$

Thus the coupling parameter, W^2 is proportional to T. This linear temperature approximation is the same as Scott used since the width of the spectral lines also appears to be a linear function of temperature far from T_t (Fig. II-8).

The above discussion, though lacking in rigor, does yield a convincing argument for a linear temperature dependence for the anharmonicity. This type of approach has been used by Cowley in the study of ferroelectricity and the phase transition in $SrTiO_3$ (64). In Cowley's theory the temperature dependence of the soft normal mode arises from the anharmonic interaction between the normal modes of the crystal. If, in eq. (II-34), the square of the harmonic frequency is negative and written as $-KT_t$, and the quantity $2\Omega_H D$ is written as KT, eq. (II-34) becomes

$$\Omega^2 = K(T - T_t)$$

which is just the temperature dependence of the soft mode of a ferroelectric crystal derived by Cochran, who considered the temperature dependence of the soft mode as arising from a change in the potential function with temperature (65).

Additional evidence that Scott (57) used to support the second order nature of the 147 cm^{-1} line is that his low temperature spectrum (100°K) shows several broad, asymmetric maxima in the 147 cm^{-1} region. We have observed the low temperature Raman scattering in the low frequency region of the A_1 spectrum (Fig. II-3) and our spectra differ

appreciably from Scott's. We see the strong 207 cm^{-1} line, the broad 147 cm^{-1} line and, also, a small part of the 128 cm^{-1} E line which is transmitted due to non-ideal polarizers. The several maxima Scott saw in the 147 cm^{-1} feature were not observed in our spectra. However, the second order nature of the 147 cm^{-1} excitation manifests itself in the T dependence of its intensity. In first order Raman scattering one phonon is created (Stokes line) and the intensity of the line is proportional to (n_1+1) $\left[n_1 = \left(e^{h\Omega_1/kT}-1\right)^{-1}\right.$ where Ω_1 is the frequency near the center of the Brillouin zone$\left.\right]$. In second order Raman scattering two phonons with equal frequency and opposite momenta are created (overtone Stokes line) and the intensity is proportional to $(n_2+1)^2$ $\left[n_2 = \left(e^{h\Omega_2/kT}-1\right)^{-1}\right.$ where Ω_2 is the frequency of one of the phonons involved$\left.\right]$ (37). In quartz, the second order Raman line is due to the creation of two zone edge acoustic phonons (57). A plot of (n_1+1) and $(n_2+1)^2$ vs temperature (Fig. II-10) shows that in the 150 cm^{-1} frequency region a second order Raman line ($2\Omega_2$ = 150 cm^{-1}) has a stronger temperature dependence than a first order Raman line (Ω_1 = 150 cm^{-1}). Our spectra show this qualitative behavior if we compare the intensity of the 128 cm^{-1} first order E line with the 147 cm^{-1} line in Fig. II-3.

Thus we conclude that the 147 cm^{-1} line is a second order Raman line and that the anharmonic coupling between the zone center and two zone edge phonons contributes to the anomalous temperature dependence of the frequency and intensity of the 147 cm^{-1} and the 207 cm^{-1} lines. The 207 cm^{-1} line is the "soft" mode, as predicted, but its nature is complicated by the coupling.

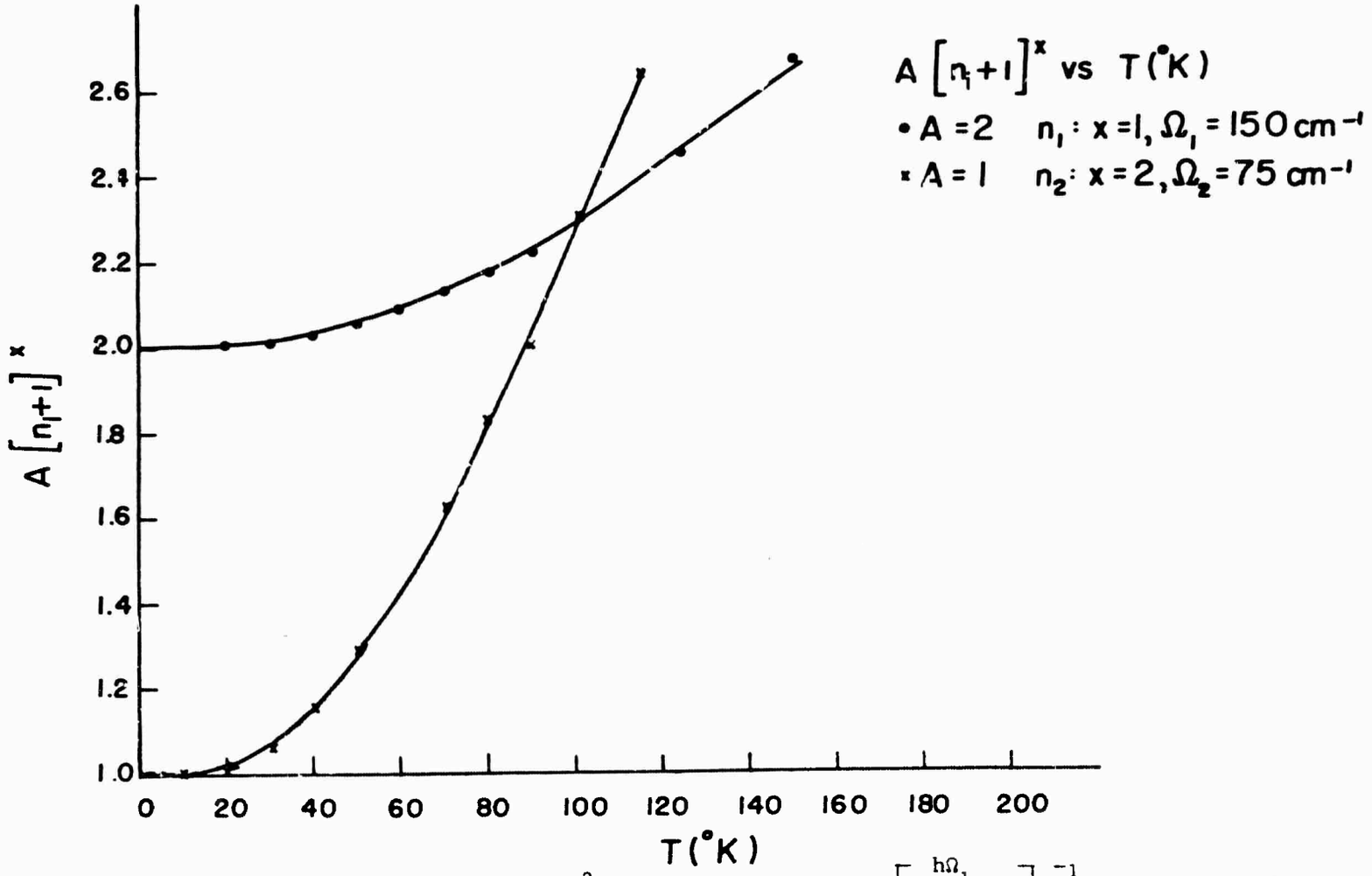

Fig. II-10: A plot of $[n_1+1]$ and $[n_2+1]^2$ vs T (°K) where $n_1 = \left[e^{\frac{h\Omega_1}{kT}} - 1\right]^{-1}$, $\Omega_1 = 150\ cm^{-1}$; $n_2 = \left[e^{\frac{h\Omega_2}{kT}} - 1\right]^{-1}$, $\Omega_2 = 75\ cm^{-1}$. The two functions were made equal at 90°K.

CHAPTER III

BRILLOUIN SCATTERING IN CRYSTALLINE QUARTZ

In this chapter we discuss the Brillouin scattering experiments performed on crystalline quartz from room temperature up to 600°C. We begin with a discussion of Brillouin scattering in solids and then discuss the elastic and photoelastic behavior of solids. Next we review the early Brillouin experiments performed on quartz. Following the description of the apparatus, the results of the present Brillouin experiments will be presented. The elastic constants calculated from the Brillouin shifts will be compared with the elastic constants measured by ultrasonic techniques.

A. THEORY

As discussed in Chapter I, fluctuations in the dielectric constant of a material cause light to be scattered. Since these fluctuations in the dielectric constant arise from the atomic motions of the system, we can expand the fluctuations in terms of the normal coordinates of the solid:

$$\Delta\epsilon_{ij} = \sum_{k=1}^{3n} \frac{\partial \epsilon_{ij}}{\partial R_k} R_k \qquad \text{(III-1)}$$

where the translational symmetry of the crystal has been used to reduce the sum to 3n terms (n is the number of atoms within a unit cell). The above sum can be broken up into two sums:

$$\Delta\varepsilon_{ij} = \sum_{k=1}^{3} \frac{\partial\varepsilon_{ij}}{\partial R_k^a} R_k^a + \sum_{k=4}^{3n} \frac{\partial\varepsilon_{ij}}{\partial R_k^o} R_k^o \qquad \text{(III-2)}$$

where the first sum corresponds to the 3 acoustic modes with a given momentum and the second sum corresponds to the 3n-3 optic modes of vibration.

In the preceding chapter we discussed the optic modes of vibration at $q \approx 0$ which were studied by Raman scattering. In this chapter we deal with light scattering from acoustic modes, which for $q \approx 10^5$ cm^{-1} are 100 times lower in frequency than the optic modes. The phenomenon of light scattering from acoustic modes is called Brillouin scattering after L. Brillouin who, in 1922, predicted that light should be inelastically scattered by sound waves in a transparent medium (66).

The theory of Brillouin scattering in solids has been adequately discussed in several papers (67, 68, 69, 70). We will not repeat any derivations but will draw upon the references for the necessary relationships.

In light scattering experiments, momentum conservation restricts $q \approx 10^5$ cm^{-1} near the center of the Brillouin zone. From the dispersion curve for the acoustic modes (Fig. I-3) we see that in this region, Ω_k^a is proportional to q. The proportionality constant is the velocity of sound in the medium:

$$\Omega_k^a = v_k q \qquad (k=1,2,3) \qquad \text{(III-3)}$$

From momentum conservation:

$$\vec{q} = \vec{k}_i - \vec{k}_s \qquad \text{(III-4)}$$

where k_i is the wavevector, in the solid, of the incident light and k_s is the wavevector, in the solid, of the scattered light. Thus the scattering geometry selects the direction of a particular q and, since the frequency of sound is much less than the frequency of light, $|k_i| \simeq |k_s|$, the magnitude of q is:

$$|q| \simeq 2|k_i| \sin\frac{\theta}{2}$$

$$\simeq \frac{4\pi n}{\lambda_o} \sin\frac{\theta}{2} \qquad \text{(III-5)}$$

where θ is the scattering angle, λ_o is the wavelength of light in vacuum and n is the index of refraction of the medium (birefringence has been neglected). Thus the frequencies of the phonons excited in light scattering experiments are

$$\Omega_k^a = v_k \frac{4\pi n}{\lambda_o} \sin\frac{\theta}{2} \qquad (k=1,2,3)$$

$$= 2\omega_o \frac{v_k}{c} n \sin\frac{\theta}{2} \qquad \text{(III-6)}$$

where ω_o is the frequency of the incident light. Fig. III-1 shows the scattering arrangement for light scattered at angle θ.

In a solid, for a given q, there exist three acoustic modes: one longitudinal (L) or quasi-longitudinal (QL), and two transverse (T) or quasi-transverse (QT). These three modes may all have distinct frequencies, or some may be degenerate. A Brillouin spectrum will, in general, contain three down-shifted, Stokes lines (phonons created) at frequencies:

$$\omega_k^s = \omega_o - \Omega_k^o = \omega_o\left[1 - \frac{2v_k}{c} n \sin\frac{\theta}{2}\right] \quad (k=1,2,3)$$

$$\text{(III-7)}$$

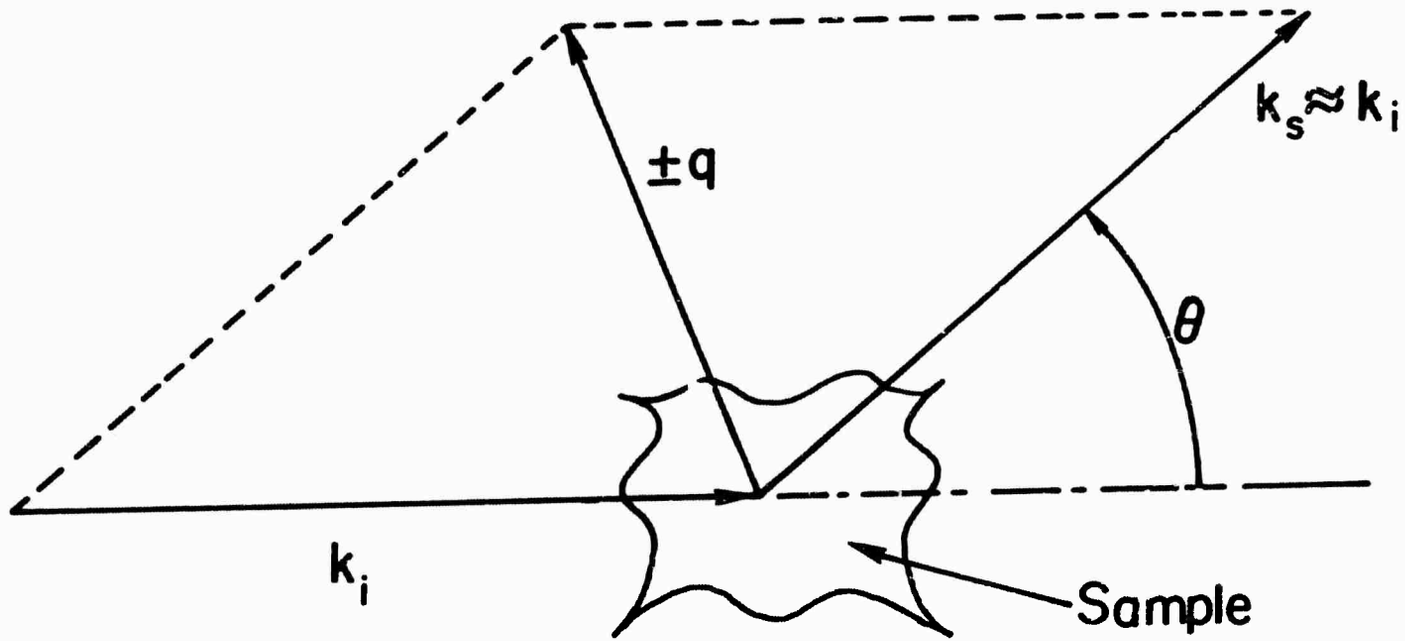

Fig. III-1. Scattering geometry for light scattering experiments. $\vec{k}_i$ is the wavevector of the incident beam and $\vec{k}_s$ is the wavevector of the scattered beam (both measured in the sample). $\vec{q} = \vec{k}_i - \vec{k}_s$ is the wavevector of the phonon. Since $|\vec{k}_i| \approx |\vec{k}_s|$, $|q| = 2 \sin \theta/2$.

and three upshifted, anti-Stokes lines (phonons annihilated) at frequencies:

$$\omega_k^{as} = \omega_o + \Omega_k^{a} = \omega_o[1 + \frac{2v_k}{c} n \sin \frac{\vartheta}{2}] \quad (k=1,2,3) \qquad \text{(III-8)}$$

A typical room temperature quartz Brillouin spectrum is shown in Fig. III-2. Here q is along the [110] direction of the quartz crystal. We see that none of the modes are degenerate and that the frequency shifts are less than 1 cm^{-1}.

In the Brillouin experiments, the frequency shifts, Ω_k^{a}, and the angle are measured; whence the sound velocity can be computed by eq.(III-6). The velocity of sound, in turn, is related to the elastic properties of the medium. Thus by means of Brillouin scattering we are able to study the behavior of the elastic properties of the solid at a higher frequency than conventional ultrasonic techniques ($\sim 10^{10}$ vs $\sim 10^{6}$ Hz.).

1. Elastic Properties of Solids

The properties of the long wavelength acoustic modes of a crystal can be derived by considering the crystal as an elastic continuum and applying the classical theory of elasticity (71, 72). The generalized Hooke's law relating the stress and strain tensors is:

$$X_{ij} = C_{ijkl} x_{kl} \qquad \text{(III-9)}$$

where X_{ij} is the stress, x_{kl} is the strain and C_{ijkl} are the elastic stiffness constants (summation over repeated indices is implied). There is an additional contribution to the stress from the piezoelectricity:

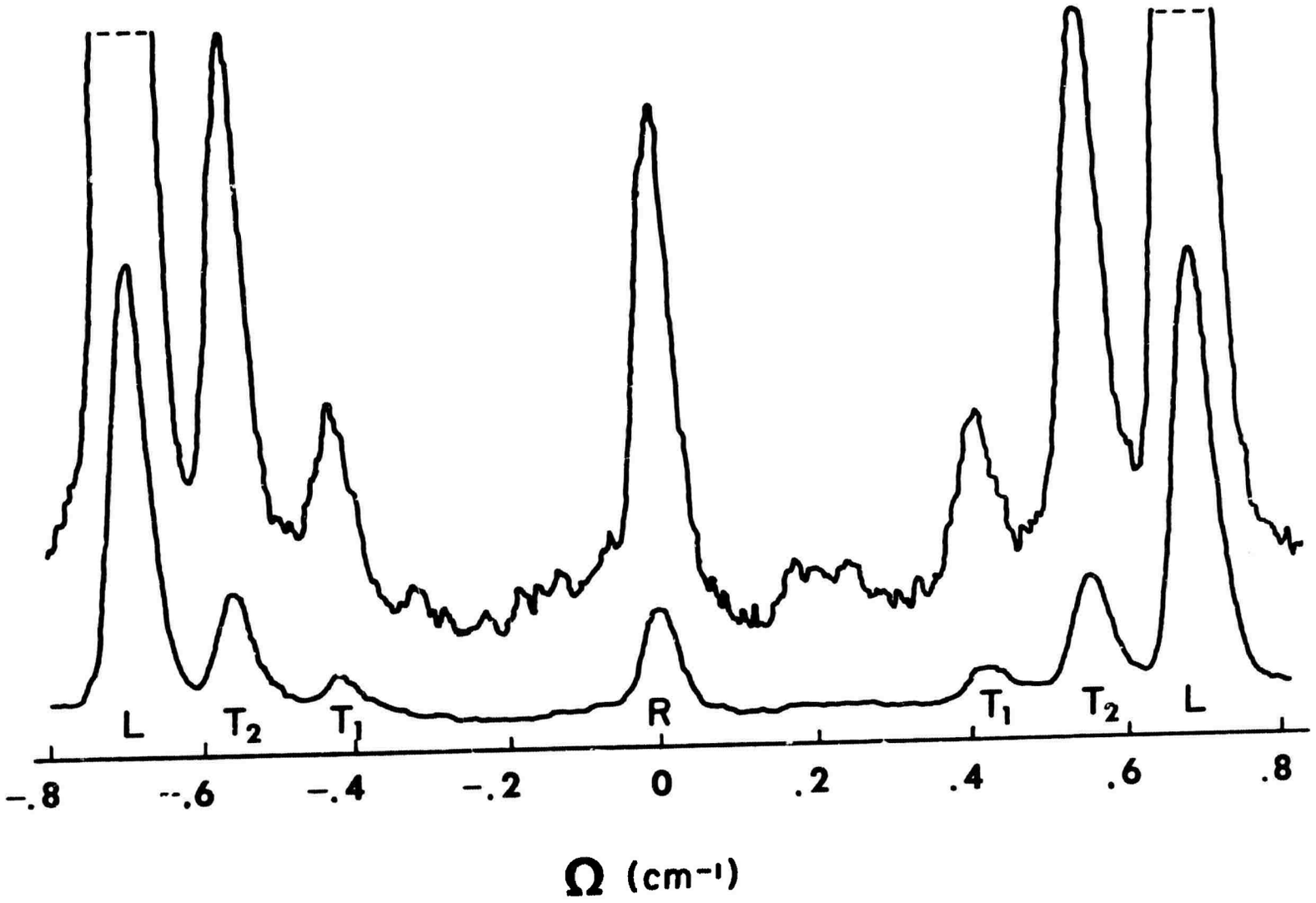

Fig. III-2. Brillouin scattering spectra of crystalline quartz at room temperature showing the Rayleigh peak (R), the longitudinal (L) and the two transverse (T_1, T_2) Brillouin peaks at two different gains. $\vec{q}$ is parallel to the [110] direction.

$-e_{ij}E_j$ (where e_{ij} is the piezoelectric coefficient) but in quartz this contributes < 1% to the velocites and is dropped in these calculations. If we utilize the symmetry properties of the elastic constants (9):

$$C_{ijkl} = C_{jikl} = C_{ijlk} = C_{klji}$$

and use the reduced notation (see Chapter I, p. 15 or Reference 9) we rewrite eq.(III-9) in the reduced notation:

$$X_m = C_{mn} x_n \qquad \text{(III-10)}$$

(the subscripts i,j,k,l take on values from 1 to 3; and the subscripts m,n,p,r take on values from 1 to 6). For each crystal system, the elastic constants C_{mn} are restricted by symmetry and some vanish identically. Appendix A gives the measured values of the elastic constants for alpha and beta quartz and displays them in matrix form.

The components of the symmetrized strain are related to the particle displacement $\vec{u}(\vec{r})$, by

$$x_{ij} = \frac{1}{2}\left(\frac{\partial u_i}{\partial r_j} + \frac{\partial u_j}{\partial r_i}\right) \qquad \text{(III-11)}$$

The equations of motion of an elastic body with a mean density ρ, are given by:

$$\rho \ddot{u}_j = \frac{\partial X_{ij}}{\partial r_i} \qquad \text{(III-12)}$$

and from the definition of the stress (eq. III-9), and using the unsymmetrized strain we have:

$$\rho \ddot{u}_j = C_{ijkl} \frac{\partial}{\partial r_i}\left(\frac{\partial u_k}{\partial r_l}\right) \qquad \text{(III-13)}$$

We look for plane wave solutions of the form,

$$\mu(\vec{r},t) = \vec{\mu} e^{(\bar{q}\cdot\bar{r} - \Omega t)} \qquad \text{(III-14)}$$

Substituting into the equation of motion (eq. III-12),

$$[C_{ijk\ell}\, q_i\, q_\ell - \rho\Omega^2\delta_{jk}]\, \vec{\mu}_k = 0 \qquad \text{(III-15)}$$

Letting $\hat{q}_k$ be the k^{th} component of the unit vector $\hat{q}$, and putting $\Omega^2/q^2 = v^2$, we have the following secular equation:

$$|C_{ijk\ell}\, \hat{q}_i\, \hat{q}_\ell - \rho v^2\delta_{jk}| = 0 \qquad \text{(III-16)}$$

For a particular value of q there are three real positive roots of eq. (III-16):

$$\rho v_j^2 = C_j^2 \qquad \text{(III-17)}$$

where C_j is proportional to a combination of elastic constants. Once the eigenvalues are found the direction cosines of the displacement vector (α,β,γ) can be calculated.

If the elastic constants are known, the velocities and the displacement direction cosines of different phonons can be computed. Conversely, if the velocities are measured, we can calculate the elastic constants. For quartz the elastic constants at room temperature have been measured by ultrasonic techniques. Table III-1a-b give for alpha and beta quartz the roots of eq.(III-16), the computed velocities and the particle displacement direction cosines (α,β,γ) for four values of q: [100], [010], [001], and [110] (73).

Table III-1a

Acoustic Modes of Alpha Quartz Calculated from Known Elastic Constants (79)

$\vec{q}$	$\rho v_j^2 (10^{10}$ dyne/cm^2)	$v_j (10^5$ cm/sec)	Direction Cosines of Particle Displacement (α β γ)	Polarization
[100]	86.87	5.725	(1 0 0)	L
	69.26	5.112	(0 -.523 -.852)	T_2
	28.81	3.297	(0 -.852 .523)	T_1
[010]	95.57	6.005	(0 -.901 .435)	QL
	49.48	4.321	(0 -.435 -.901)	QT_2
	39.89	3.880	(1 0 0)	T_1
[001]	105.74	6.317	(0 0 1)	L
	58.18	4.686	(1 0 0)	T_2
	58.18	4.686	(0 -1 0)	T_1
[110]	92.12	5.896	(-.716 -.585 -.381)	QL
	60.11	4.763	(-.085 .614 -.785)	QT_2
	32.65	3.511	(-.693 .530 .490)	QT_1

L = Longitudinal
QL = Quasi-longitudinal
T = Transverse
QT = Quasi-transverse

Table III-1b

Acoustic Modes of Beta Quartz (578°C) Calculated from Known Elastic Constants (92)

$\vec{q}$	$\rho v_j^2 (10^{10}$ dyne/cm^2)	$v_j (10^5$ cm/sec)	Direction Cosines of Particle Displacement (α β γ)	Polarization
[100]	90.00	5.979	(1 0 0)	L
	50.00	4.456	(0 1 0)	T_2
	36.50	3.807	(0 0 1)	T_1
[010]	90.00	5.979	(0 -1 0)	L
	50.00	4.456	(1 0 0)	T_2
	36.50	3.807	(0 0 1)	T_1
[001]	91.50	6.028	(0 0 1)	L
	36.50	3.807	(1 0 0)	T_2
	36.50	3.807	(0 -1 0)	T_1
[110]	90.00	5.979	(-.707 -.707 0)	L
	50.00	4.456	(-.707 .707 0)	T_2
	36.49	3.807	(0 0 1)	T_1

L = Longitudinal

T = Transverse

In Brillouin scattering the acoustic modes couple to the light through the modulation of the dielectric constant by the strain waves that are thermally excited in the crystal. This elasto-optic or photo-elastic phenomenon is called the Pockel's effect and is described mathematically by (9):

$$\Delta\epsilon_{ij} = -\epsilon_i \epsilon_j \; P_{ijk\ell} \; x_{k\ell} \qquad \text{(III-18)}$$

where ϵ_i is one of the three principal values of the dielectric tensor and the $P_{ijk\ell} = P_{jik\ell} = P_{ij\ell k}$ are the Pockel's (or elasto-optic or photo-elastic) coefficients. Since the intensity of the scattered light is proportional to the mean square of the fluctuations in the dielectric constant, the intensity of the scattered light will be proportional to the square of the Pockel's coefficients. For each crystal system, the Pockel's coefficients are restricted by symmetry and some vanish identically. These coefficients can be written in reduced notation and put in a 6 x 6 matrix form. In general, the matrices of the Pockel's coefficients are not symmetric, i.e., $p_{mn} \neq p_{nm}$ (9).

The symmetrized strain (eq. III-11) for a plane wave solution of eq. (III-13), is:

$$x_{k\ell} = \frac{1}{2} \{\hat{\mu}_k \hat{q}_\ell + \hat{\mu}_\ell \hat{q}_k\} \; |\vec{\mu}||\vec{q}| \; e^{i(\vec{q}\cdot\vec{r} - \Omega t)} \qquad \text{(III-19)}$$

from eq. (III-18), the fluctuations of the dielectric constant about the mean, using eq. (III-19) is:

$$\Delta\epsilon_{ij} = -\epsilon_i \epsilon_j \frac{1}{2}\{P_{ijk\ell}(\hat{\mu}_k \hat{q}_\ell + \hat{\mu}_\ell \hat{q}_k)\}|\vec{\mu}||\vec{q}| \; e^{i(\vec{q}\cdot\vec{r} - \Omega t)} \qquad \text{(III-20)}$$

Hence the intensity of the scattered light is proportional to

$$I \sim \overline{\Delta\epsilon_{ij}^2} = \frac{1}{4}\epsilon_i^2\epsilon_j^2\{P_{ijk\ell}(\hat{\mu}_k\hat{q}_\ell + \hat{\mu}_\ell\hat{q}_k)\}^2\overline{|\vec{\mu}\vec{q}|^2} \qquad \text{(III-21)}$$

where the mean square Fourier strain component $\overline{|\mu q|^2}$ is given by thermodynamic fluctuation theory (19):

$$\overline{|qu|^2} = \frac{kT}{V\rho v_\alpha^2}$$

If we write the intensity of the light scattered by mode α, in terms of the Rayleigh ratio (33) defined as the scattered intensity polarized in the $\hat{E}_j$ direction, per unit volume per unit solid angle per unit incident intensity polarized in the $\hat{E}_i$ direction ($\hat{E}_j$ and $\hat{E}_i$ are unit vectors), we have

$$R_{ij}^{\alpha} = \frac{\pi^2}{\lambda_o^4} kT[\hat{E}_j \cdot \vec{\vec{T}}^{\alpha} \cdot \hat{E}_i]^2 \qquad \text{(III-22)}$$

where

$$T^{\alpha} \equiv \epsilon_i\epsilon_j T_{ij}^{\alpha}$$

$$T_{ij}^{\alpha} \equiv P_{ijk\ell}\left(\frac{\hat{\mu}_k\cdot\hat{q}_\ell + \hat{\mu}_\ell\cdot\hat{q}_k}{2}\right) \qquad \text{(III-23)}$$

These T_{ij}^{α}'s determine the selection rules and once they are calculated we can determine which modes will be observed for a given q and a given choice of the polarization of the incident and scattered radiation. If the elastic problem is solved for a particular choice of q we can find the components of the strain. In six component forms the strain is (9):

$$\begin{bmatrix} x_1 \\ x_2 \\ x_3 \\ x_4 \\ x_5 \\ x_6 \end{bmatrix} \propto \begin{bmatrix} q_1\mu_1 \\ q_2\mu_2 \\ q_3\mu_3 \\ (q_2\mu_3 + q_3\mu_2) \\ (q_1\mu_3 + q_3\mu_1) \\ (q_1\mu_2 + q_2\mu_1) \end{bmatrix} \qquad \text{(III-24)}$$

For alpha quartz, symmetry D_3, certain Pockel's coefficients vanish. The components of T for any acoustic mode of alpha quartz using eq.(III-23) are

$$\begin{bmatrix} T_1 \\ T_2 \\ T_3 \\ T_4 \\ T_5 \\ T_6 \end{bmatrix} = \begin{bmatrix} P_{11} & P_{12} & P_{13} & P_{14} & 0 & 0 \\ P_{12} & P_{11} & P_{13} & P_{14} & 0 & 0 \\ P_{31} & P_{31} & P_{32} & 0 & 0 & 0 \\ P_{41} & P_{41} & 0 & P_{44} & 0 & 0 \\ 0 & 0 & 0 & 0 & P_{44} & P_{41} \\ 0 & 0 & 0 & 0 & P_{14} & P_{66} \end{bmatrix} \begin{bmatrix} q_1\mu_1 \\ q_2\mu_2 \\ q_3\mu_3 \\ (q_2\mu_3 + q_3\mu_2) \\ (q_1\mu_3 + q_3\mu_1) \\ (q_1\mu_2 + q_2\mu_1) \end{bmatrix} \qquad \text{(III-25)}$$

The calculation of the T matrix involves carrying out the matrix multiplication above. Table III-2 gives the T matrices, the velocities and direction cosines of the phonons propagating in the [100], [010], [001] and [110] directions. Also shown are the components of the T matrix studied for various choices of the polarization of the incident light and scattered light (V ≡ light polarized perpendicular to the scattering plane, H ≡ light polarized in the scattering plane).

If the Pockel's coefficients are known, from the T matrices we can predict the intensity of the Brillouin components. Conversely, from the intensity of the Brillouin components we can measure the Pockel's coefficients. The Pockel's coefficients for most crystals are not known (75). For alpha quartz, the Pockel's coefficients have been measured but the results are over 60 years old (76)! These values are given in Appendix A.

Table III-2a

$q = [100]$

$$T \begin{bmatrix} P_{11}\alpha & P_{14}\gamma + P_{66}\beta & P_{44}\gamma + P_{41}\beta \\ P_{14}\gamma + P_{66}\beta & T_{12}\alpha & P_{41}\alpha \\ P_{44}\gamma + P_{41}\beta & P_{41}\alpha & P_{31}\alpha \end{bmatrix}$$

	L	T_2	T_1
ρv^2	86.9×10^{10} dynes/cm^2	69.3×10^{10} dynes/cm^2	28.8×10^{10} dynes/cm^2
α	1	0	0
β	0	-.52	-.85
γ	0	-.85	.52

For $\vec{k}_i = \frac{1}{\sqrt{2}}[1\ 1\ 0]$ and $\vec{k}_s = \frac{1}{\sqrt{2}}[\bar{1}\ 1\ 0]$

or $\vec{k}_i = \frac{1}{\sqrt{2}}[\bar{1}\ \bar{1}\ 0]$ and $\vec{k}_s = \frac{1}{\sqrt{2}}[1\ \bar{1}\ 0]$

Polarization Choice	Observed Components
VV	T_{33}^2
VH	$(T_{31} - T_{32})^2$
HV	$(T_{13} - T_{32})^2$
HH	$(T_{11} - T_{12})^2$

Table III-2b

$q = [010]$

$$T: \begin{bmatrix} P_{12}\beta + P_{14}\gamma & P_{66}\alpha & P_{41}\alpha \\ P_{66}\alpha & P_{11}\beta - P_{14}\gamma & -P_{41}\beta + P_{44}\gamma \\ P_{41}\alpha & -P_{41}\beta + P_{44}\gamma & P_{31}\beta \end{bmatrix}$$

	L	T_2	T_1
ρv^2	95.57×10^{10} dynes/cm^2	49.48×10^{10} dynes/cm^2	39.89×10^{10} dynes/cm^2
α	0	0	1
β	-.90	-.43	0
γ	+.43	- .9	0

For $\vec{k}_i = \frac{1}{\sqrt{2}} [\bar{1}\ \dot{1}\ 0]$ and $\vec{k}_s = \frac{1}{\sqrt{2}} [\bar{1}\ \bar{1}\ 0]$

or $\vec{k}_i = \frac{1}{\sqrt{2}} [\dot{1}\ \bar{1}\ 0]$ and $\vec{k}_s = \frac{1}{\sqrt{2}} [\dot{1}\ \dot{1}\ 0]$

Polarization Choices	Observed Components
VV	T_{33}^2
VH	$(T_{31} - T_{32})^2$
HV	$(T_{31} + T_{32})^2$
HH	$(T_{11} - T_{22})^2$

Table III-2c

$q = [001]$

$$T: \begin{bmatrix} P_{13}\gamma + P_{14}\beta & P_{14}\alpha & P_{44}\alpha \\ P_{14}\alpha & P_{13}\gamma - P_{14}\beta & P_{44}\beta \\ P_{44}\alpha & P_{44}\beta & P_{33}\gamma \end{bmatrix}$$

	L	T_2	T_1
ρv^2	105.75×10^{10} dynes/cm^2	58.18×10^{10} dynes/cm^2	58.18×10^{10} dynes/cm^2
α	0	1	0
β	0	0	-1
γ	1	0	0

For $\vec{k}_i = \frac{1}{\sqrt{2}}[\overset{+}{1}\ 0\ \overset{+}{1}]$ and $\vec{k}_s = \frac{1}{\sqrt{2}}[\overset{+}{1}\ 0\ \overset{-}{1}]$

or $\vec{k}_i = \frac{1}{\sqrt{2}}[\overset{-}{1}\ 0\ \overset{-}{1}]$ and $\vec{k}_s = \frac{1}{\sqrt{2}}[\overset{-}{1}\ 0\ \overset{+}{1}]$

Polarization Choices	Observed Components
VV	T_{22}^2
VH	$(T_{21} + T_{23})^2$
HV	$(T_{21} - T_{23})^2$
HH	$(T_{11} - T_{33})^2$

Table III-2d

$$q = \frac{1}{\sqrt{2}}[110]$$

$$T: \begin{bmatrix} \alpha p_{11} + \beta p_{12} + \gamma p_{14} & \gamma p_{14} + (\alpha + \beta) p_{66} & \gamma p_{44} + (\alpha + \beta) p_{41} \\ \gamma p_{14} + (\alpha + \beta) p_{66} & \alpha p_{12} + \beta p_{11} - \gamma p_{14} & (\alpha - \beta) p_{41} + \gamma p_{44} \\ \gamma p_{44} + (\alpha + \beta) p_{41} & (a - \beta) p_{41} + \gamma p_{44} & (\alpha + \beta) p_{31} \end{bmatrix}$$

	L	T	T
ρv^2	92.12×10^{10} dynes/cm^2	60.11×10^{10} dynes/cm^2	32.65×10^{10} dynes/cm^2
α	-.72	-.09	-.60
β	-.59	-.61	+.53
γ	-.38	-.78	.49

For $\vec{k}_i = [100]$ and $\vec{k}_s = [\bar{1}00]$

or $\vec{k}_i = [\bar{1}00]$ and $\vec{k}_s = [100]$

Polarization Choices	Observed Components
VV	T_{33}^2
VH	T_{31}^2
HV	T_{23}^2
HH	T_{12}^2

B. PAST EXPERIMENTS

In 1930 E. Gross observed the Brillouin components in light scattered by crystalline quartz (77). This was the first observation of Brillouin scattering in a solid. Brillouin and Mandel'shtam had predicted that these satellite lines would arise from ". . . thermal elastic waves which propagate in the medium with the velocity of sound and produce periodical variations of the amplitude of the scattered light, thus giving rise to two new frequencies" (77).

Following the observations of Gross, investigators in India also observed the Brillouin components in crystalline quartz (78). Extensive theoretical and experimental work has been performed on quartz by Indian scientists starting in the 1930's and continuing into the present decade (79).

The first observation of the Brillouin spectrum of quartz using a laser source was reported in 1966 (80). In recent high resolution Brillouin experiments on quartz using a single frequency laser, the linewidths ($\propto$ absorption of sound) as well as the frequency shifts have been measured (81).

Brillouin scattering was not used as a technique to measure the elastic constants of solids until the 1950's (82). Elastic constants of solids had been measured by several methods: the static method (83), the resonance, or dynamic method (84), the ultrasonic method (85), and by means of light diffraction (86). Since quartz is widely used as a transducer, there are several reliable measurements of the elastic constants of alpha quartz at room temperature (74, 82-89). There have also been measurements of the temperature dependence of the elastic

constants of alpha quartz (1", 90-92) and measurements of the elastic constants of beta quartz (93, 94, 95), but these have been made with the lower frequencies associated with the conventional methods mentioned above. not light scattering.

C. APPARATUS

Since Brillouin shifts are generally only a fraction of a cm^{-1}, a high resolution spectrograph and a relatively narrow bandwidth exciting light source are required. The pre-laser Brillouin studies were performed with a high resolution prism or grating spectrograph using a single line of a Mercury arc as the exciting source.

The Brillouin apparatus used in the present experiments is basically the same as that used by Chiao and Stoicheff (96) and has been described in the literature (97). Fig.(III-3) shows the layout of the Brillouin apparatus. A Spectra Physics (Model 125) He-Ne laser with an output of 80 mw at 6328 Å serves as the exciting source. The polarization of the emitted light could be changed continuously by a Spectra Physics (Model 310) polarization rotator. Normally the incident light is polarized either perpendicular (V) or parallel (H) to the scattering plane. The beam is focused by a 50 cm focal length lens (L_p) into the quartz sample placed in the specially constructed oven (Appendix B). Light scattered at 90 ± 1° to the incident direction is collected and made parallel by a 23.5 cm focal length lens (L_c). A 6328 Å, narrow pass filter is placed after the lens to eliminate the blackbody background when working at elevated temperatures. At times it was necessary to select a certain polarization of the scattered light and this was done with a Polaroid HN-38 polarizer.

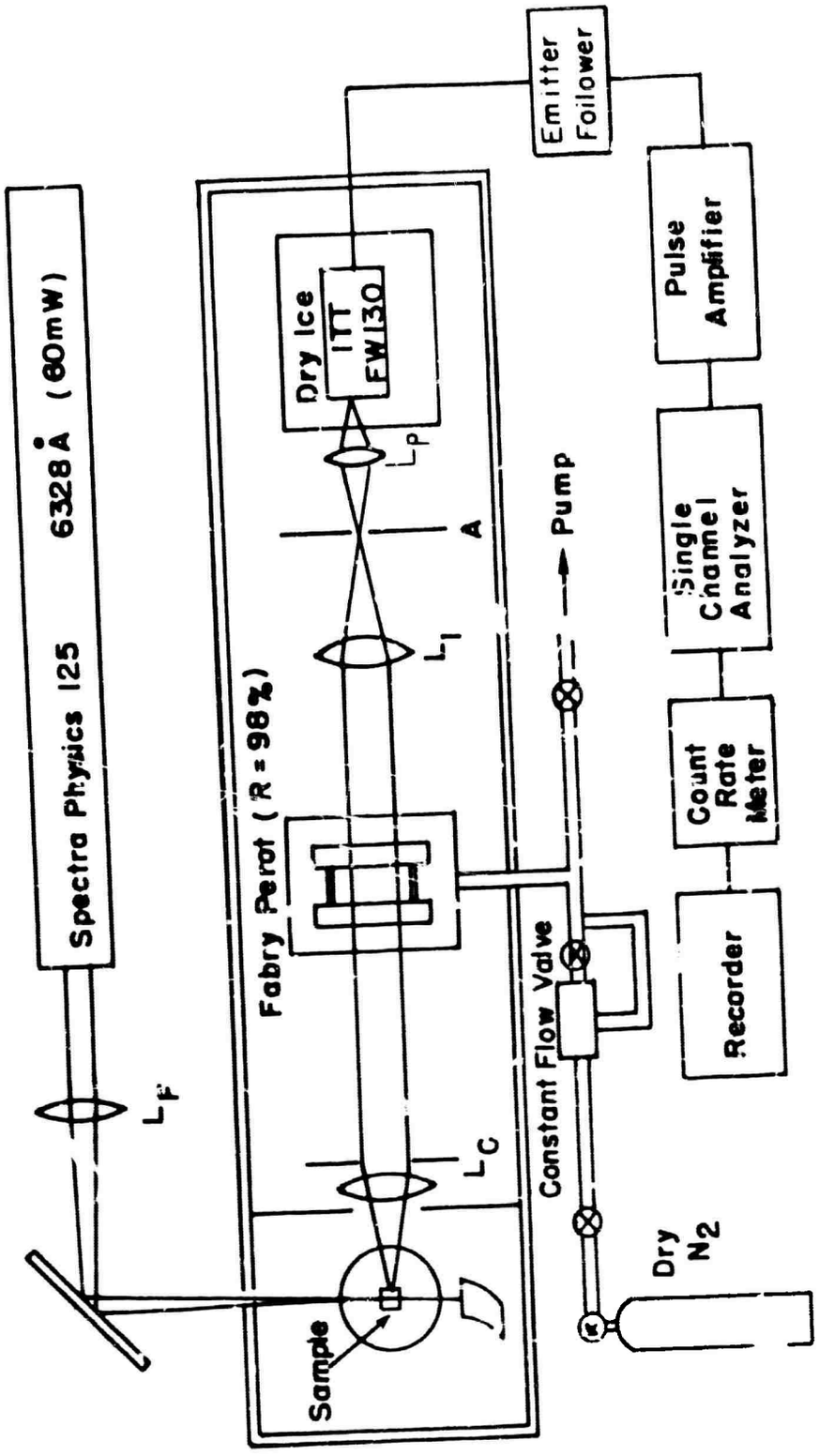

Fig. III-3. Apparatus used in Brillouin scattering experiments: L_F = 50 cm. f.l., L_C = 23.5 cm f.l., L_I = 36 cm. f.l., and L_P = 20 cm. f.l.

The scattered light was frequency analyzed by a pressure swept Fabry-Perot etalon (98). The etalon consists of a pair of Perkin-Elmer fused quartz, 2 inch diameter, $\lambda/100$ interferometer flats separated by an invar spacer. The flats were coated for a reflectance (R) = 98% at 6328 A. This gave a contrast of $\sim 10^4$. The etalon spacing was the same throughout the experiments, 0.3 cm ± 1% which yields a free spectral range (FSR) of 1.67 cm^{-1} = 50 GHz. The overall working finesse of the system, measured as the ratio of the FSR to the full width at half maximum of the Rayleigh peak, was between 25 and 35, which for a 0.3 cm spacer corresponds to a resolution of 2.0 to 1.4 GHz. This approached the maximum finesse obtainable with the laser whose linewidth was 1.5 GHz.

The pressure scan was linearized with a constant differential flow controller made by Moore Products Co. (Model 63-BU-L). The flow rate of the dry nitrogen gas was controlled by an Olin-Matheson (Model-4133) needle valve. The high pressure side of the controller was kept at 2 atmospheres by a regulator valve With this back pressure the flow rate was constant to ~1% over 2 orders.

An iris diaphragm, which followed the Fabry-Perot, served as the system aperture stop, determined the collection solid angle and the diameter of the plates used. Only the 2.5 cm central region of the Fabry-Perot plates was used.

A 36 cm. f.l. lens was used to focus the parallel light from the Fabry-Perot onto a 1.3 mm. pinhole which blocked all but the central fringe. A 20 cm. f.l. lens was used to focus the light passing through the pinhole onto the photocathode of a dry-ice cooled, ITT-FW130

photomultiplier tube. The PM tube had an effective photocathode diameter of 0.1 inch with an S-20 surface. With this small cathode the dark count rate was 75 cts/sec at room temperature and 0-2 cts/sec at the temperature of dry ice. The signal processing circuitry was the same as that used in the Raman scattering experiments: an emitter follower, linear amplifier, single channel analyzer, ratemeter and strip chart recorder.

The Brillouin frequency shifts were measured directly from the recorder charts. The centers of the peaks were determined by graphically dividing in half the width of the peaks near the half power level. The shift, in fraction of an FSR, was taken as the distance between the Stokes and anti-Stokes components of the m^{th} order spectrum divided by the sum of the m-1 to m anti-Stokes and m to m+1 Stokes component separation. Measuring in this way averages the component displacements on the trace in such a way that errors due to uniform changes of the scan rate are cancelled.

Three different samples of natural Brazilian quartz were used. The samples were approximately cubic in shape with each edge about 12 mm in length. Each sample was cut and polished with the crystallographic axes appropriately oriented so that the incident and scattered wavevectors were perpendicular to polished faces. In addition, a piece of synthetic quartz supplied by Sawyer Research Corporation was studied and the results were compared to the natural quartz. The samples of natural quartz were unusually clear and free from imperfections as evidenced by the small Rayleigh peak in the Brillouin spectrum shown in Fig. III-2.

D. RESULTS AND DISCUSSION

Table III-3 summarizes the results of alpha (25°C) and beta quartz (600°C) for the four phonon propagation directions studied. We show the polarization of the phonon as determined from the solution of the elastic problem, eq.(III-15) (L ≡ longitudinal, T_1 ≡ low frequency transverse, T_2 ≡ high frequency transverse). We also state whether the optical coupling was strong enough to allow observation of the light scattered by the particular phonon. ρv^2 is given in terms of the elastic constants. In the next two columns the numerical values of ρv^2 measured by light scattering are compared with the values calculated from published elastic constants. We immediately see that the agreement between the elastic constants measured by light scattering and the elastic constants measured by ultrasonics or other techniques is good. Since the frequency of sound measured in Brillouin scattering is at least 3 orders of magnitude greater than the frequencies used in ultrasonics, we can conclude that there is no appreciable dispersion of the elastic constants for quartz, for frequencies up to ~30 GHz.

There is disagreement in the literature on the sign of the elastic constant C_{14}. Several authors report $C_{14} > 0$ (88, 90, 92) and several others, including the IRE standards (3) select $C_{14} < 0$ (74, 84, 89). From measurements of velocities it is impossible to remove the ambiguity because only C_{14}^2 appears in the velocity equations (Table III-3). However by measurement of the intensity of the Brillouin peaks we can determine the sign of C_{14}(99).

We studied the light scattered by $[0\overset{\pm}{1}\overset{\pm}{1}]$ phonons. Since the positive directions of Y and Z are not known, there are four possible $\vec{q}$ directions

Table III-3a

Alpha Quartz (25°C)

Phonon Direction: $\vec{q}$	Polarization of Brillouin Components	Observed	ρv^2	ρv^2 (10^{10}dynes/cm^2) Light Scattering	ρv^2 (10^{10}dynes/cm^2) Ultrasonics (74)
[100]	L	Yes	C_{11}	87.10	86.87
	T_2	Yes	$\frac{1}{2}\{[C_{66}+C_{44}]+[(C_{66}-C_{44})^2-4C_{14}^2]^{1/2}\}$	68.10	69.28
	T_1	No	$\frac{1}{2}\{[C_{66}+C_{44}]-[(C_{66}-C_{44})^2-4C_{14}^2]^{1/2}\}$	-----	28.81
[010]	QL	Yes	$\frac{1}{2}\{C_{44}+C_{11}+[(C_{44}-C_{11})^2-4C_{14}^2]^{1/2}\}$	96.60	95.57
	QT_2	Yes	$\frac{1}{2}\{C_{44}+C_{11}-[(C_{44}-C_{11})^2-4C_{14}^2]^{1/2}\}$	50.14	49.48
	T_1	No	C_{66}	-----	39.89
[001]	L	Yes	C_{33}	105.80	105.74
	$T_2 = T_1$	Yes	C_{44}	57.93	58.18
[110]	QL	Yes	Admixtures of C_{11}, C_{12}, C_{14}, C_{33}, C_{44}	91.00	92.12
	QT_2	Yes		59.04	60.11
	QT_1	Yes		33.77	32.65

Table III-3b

Beta Quartz (600°C)

Phonon Direction: $\vec{q}$	Polarization of Brillouin Components	Observed	ρv^2	$\rho v^2 (10^{10}$dynes/cm^2) Light Scattering	$\rho v^2 (10^{10}$dynes/cm^2) Ultrasonics (ref.11)
[100]	L	Yes	C_{11}	119.8	121.5
	T_2	No	C_{66}	-----	51.6
	T_1	Yes	C_{44}	34.9	35.9
[010]	L	Yes	C_{11}	94.0[a]	90.0[b]
	T_2	No	C_{66}	----	51.0[b]
	T_1	Yes	C_{44}	34.3[a]	36.5[b]
[001]	L	Yes	C_{33}	106.9	110.6
	T_1=T_2	Yes	C_{44}	34.0	35.9
[110]	L	Yes	C_{11}	117.1	121.5
	T_2	No	C_{66}	----	51.6
	T_1	Yes	C_{44}	35.0	35.9

[a] Measurement at 575°C.

[b] Ref. 92 at 578°C.

with light incident along Y and scattered along Z: [011], [0$\bar{1}\bar{1}$], [0$\bar{1}$1], and [01$\bar{1}$]. If we solve the elastic problem for the four q vectors with $C_{14} > 0$ and $C_{14} < 0$, we obtain the following eigenvalues and direction cosines:

	$C_{14}>0$			$C_{14}<0$		
[011] = [0$\bar{1}\bar{1}$]	L	T_2 (A)	T_1	L	T_2 (B´)	T_1
$\rho v^2 (10^{10}$dynes/cm^2)	97.63	67.05	38.78	130.5	41.97	30.99
α	0	1	0	0	0	1
β	.52	0	-.86	.74	.67	0
γ	.86	0	.52	.67	-.74	0
[0$\bar{1}$1] = [01$\bar{1}$]		(B)			(A´)	
$\rho v^2 (10^{10}$dynes/cm^2)	130.5	41.97	30.99	97.63	67.05	38.78
α	0	0	1	0	1	0
β	-.74	-.67	0	-.52	0	.86
γ	.67	-.74	0	.86	0	.52

From the measurement of the frequency shifts we distinguish between cases A-A´ and cases B-B´. We note that the magnitude of the directions cosines for A and A´ are equal but have different signs. The same is noted for B and B´. The particular scattering geometry selected had horizontally polarized light (H) incident along Y and unanalyzed light scattered along Z (T). Thus in terms of the T matrix, we study the T_4 and the T_5 elements (eq. III-23). The ratio of the intensity of the longitudinal peak to the transverse peak is given by eq.(III-22):

$$\frac{I_L}{I_T} = \frac{\rho v_T^2}{\rho v_L^2} \frac{(T_4^2 + T_5^2)_L}{(T_4^2 + T_5^2)_T} \qquad \text{(III-26)}$$

Using the values of the Pockel's coefficients listed in the appendix and the calculated eigenvalues and direction cosines (Table III-1), we calculate the ratio in eq.(III-26):

(a) For cases A-A′ we calculate

A	$C_{14} > 0$	A′	$C_{14} < 0$
	$I_L < I_{T_2}$		$I_L > I_{T_2}$

and we observe

$$I_L < I_{T_2}$$

(b) For cases B-B′ we calculate

B	$C_{14} > 0$	B′	$C_{14} < 0$
	$I_L > I_{T_1}$		$I_L < I_{T_1}$

and we observe

$$I_L > I_{T_1}$$

Thus we conclude that $C_{14} > 0$. This result is in agreement with a similar calculation based on the phonons propagating along [100] (99).

The temperature dependence of the frequency of 8 acoustic modes, ([100]-L, [010]-L, [010]-T_2, [001]-L, [001]-T, [110]-L, [110]-T_2, [110]-T_1), was studied and the results are plotted in Figs. III-4 to III-8 . The temperature dependence of the frequencies of the modes studied all exhibit

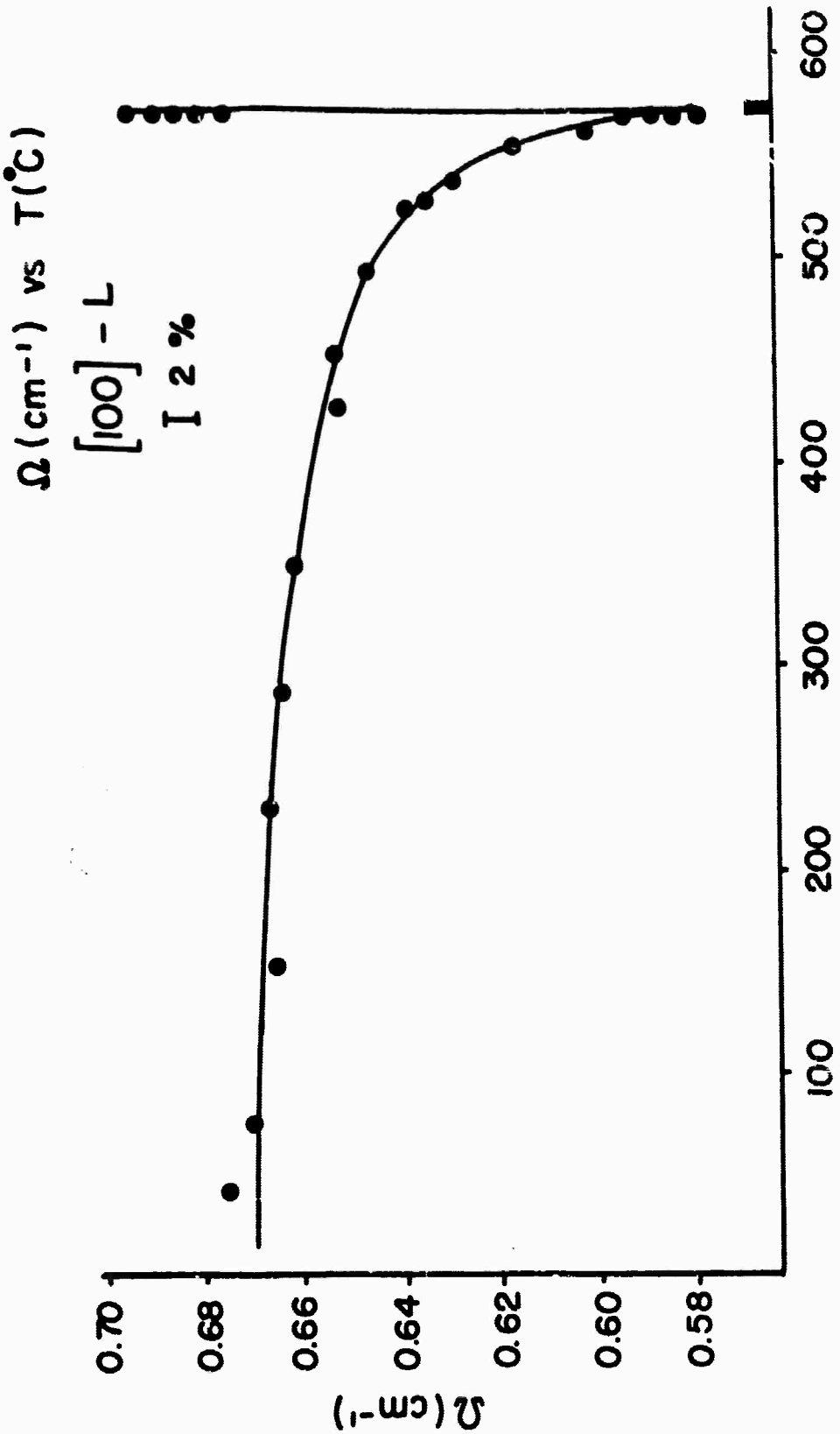

Fig. III-4. Measured frequency Ω (cm^{-1}) vs T (°C) of the [100]-L phonon.

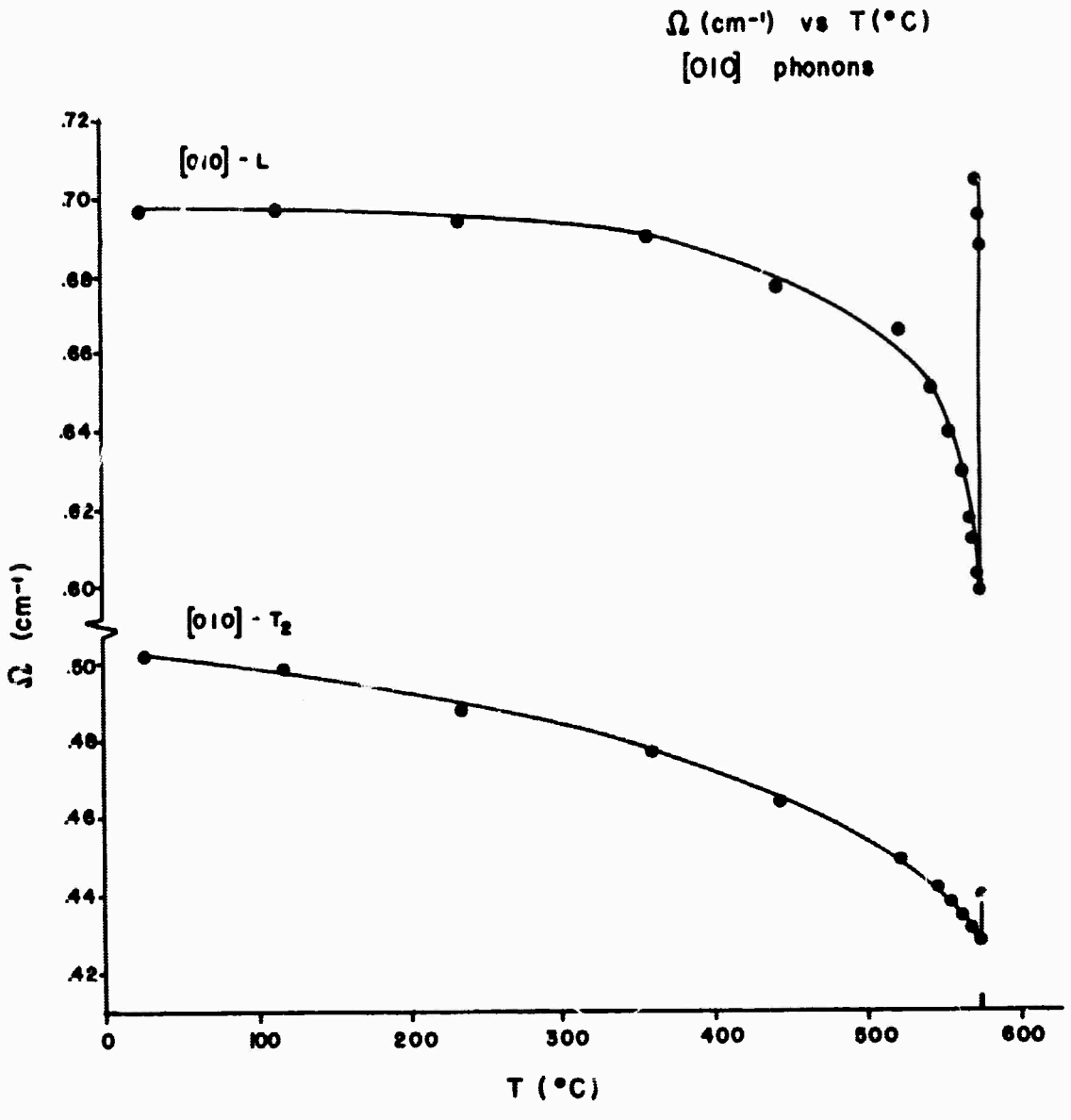

Fig. III-5. Measured frequency Ω (cm^{-1}) vs T (°C) of the [010]-L and [010]-T_2 phonons.

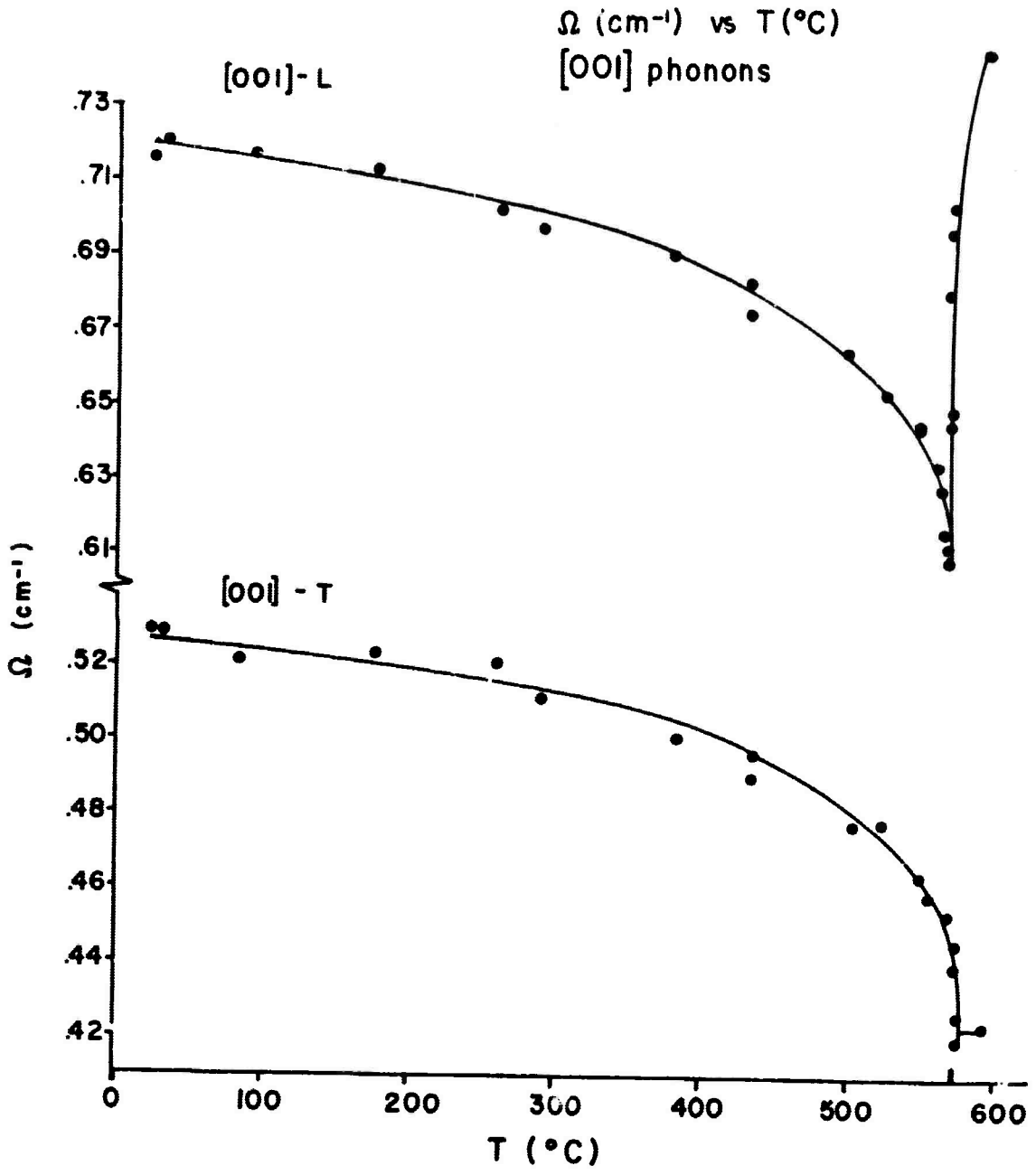

Fig. III-6. Measured frequency $\Omega(cm^{-1})$ vs T (°C) of the [001]-L and [001]-T phonons.

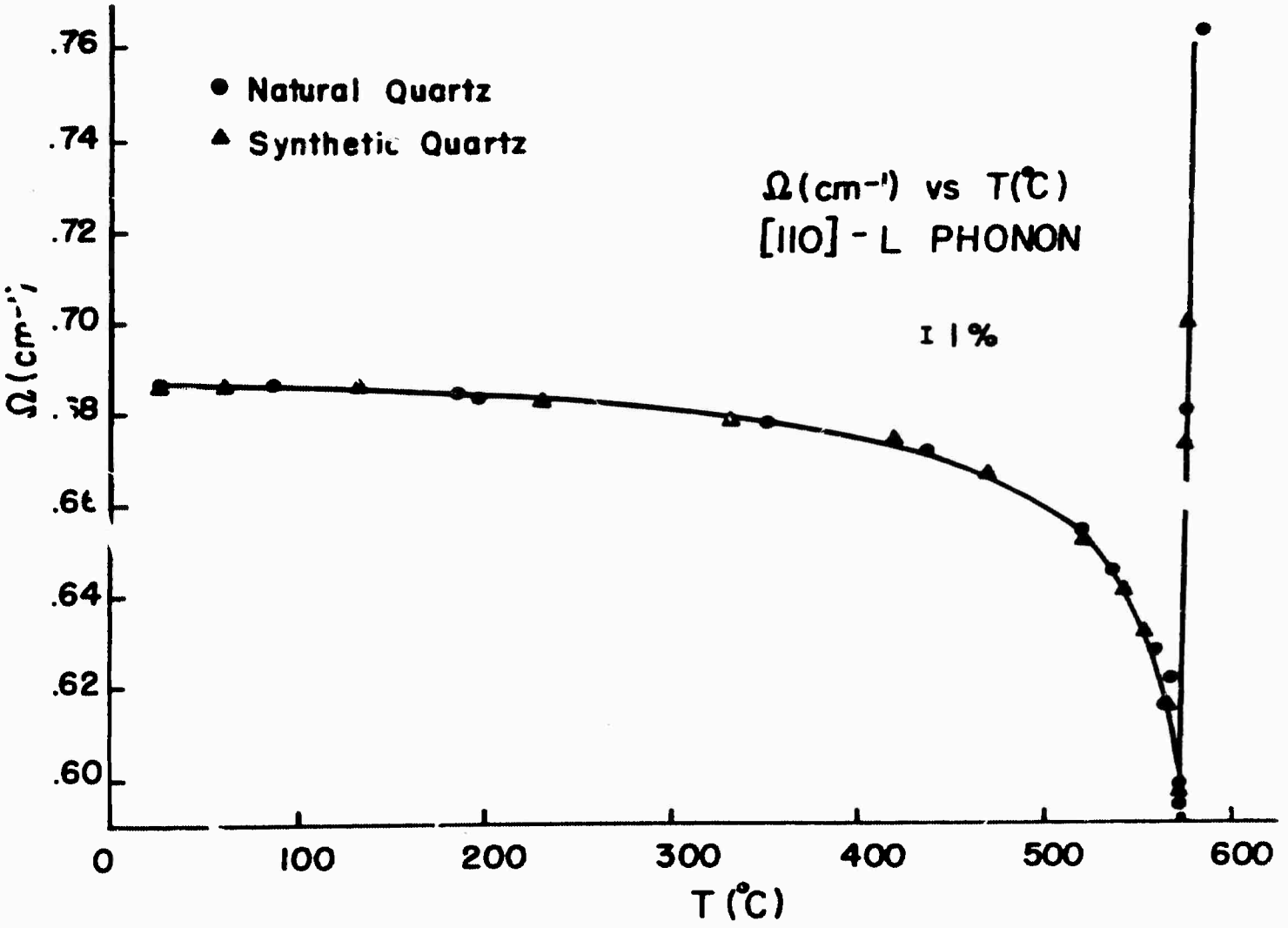

Fig. III-7. Measured frequency Ω (cm^{-1}) vs T (°C) of the [110]-L phonon for (●) natural quartz and (▲) synthetic quartz.

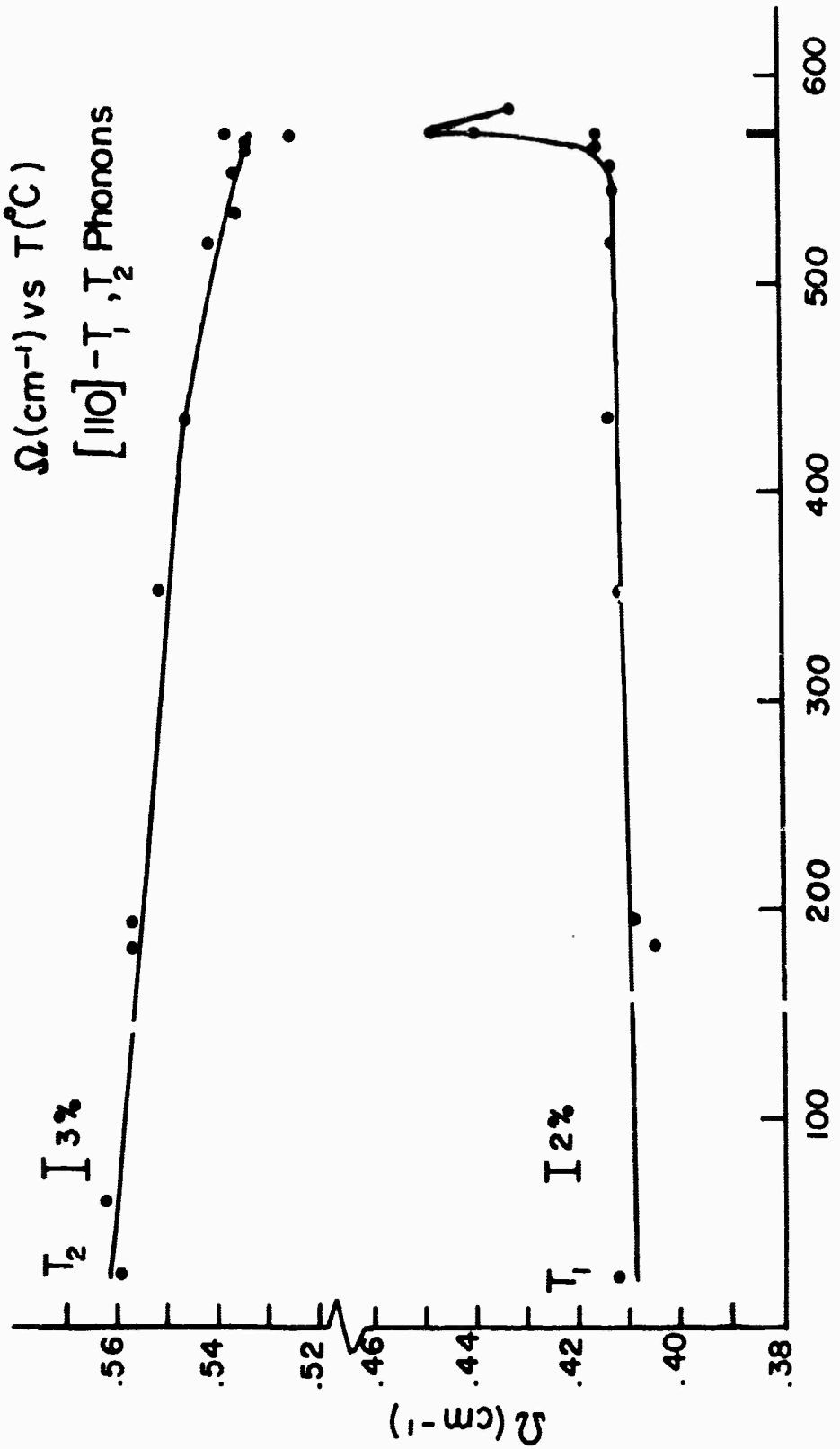

Fig. III-8 . Measured frequencies Ω (cm^{-1}) vs T (°C) for the [110]-T_1 and [110]-T_2 phonons.

similar behavior. As the temperature is increased from room temperature to the transition temperature the frequency decreases gradually to a value that is 10 to 20% of the value at room temperature. At the transition temperature the frequency reaches a minimum value and just above the transition temperature there is an abrupt increase ($\sim$15%). At the temperature corresponding to the minimum of the frequency, the intensity of the Rayleigh component increases to $\sim 10^4$ times its intensity just below the transition. The origin of this anomaly in the Rayleigh scattering will be discussed in the next chapter.

Fig III-7 is a plot of the temperature dependence of the frequency of the [110]-L mode for samples of natural quartz and synthetic quartz. We see very good agreement between the two samples.

Fig. III-9 is a plot of the temperature dependence of the intensity of the [100]-L Brillouin component. Eq. (III-22) predicts a linear temperature dependence of the intensity far from the transition temperature where V_L^2 is independent of temperature (Fig. III-4). This is observed in Fig. III-9. At the transition temperature where there is an abrupt increase in the velocity, there is a corresponding decrease in the intensity due to the $1/V_L^2$ factor in eq. (III-22). This also is observed in Fig. III-9.

From Table III-2 we note that we can measure the temperature dependence of the following elastic constants: C_{11}, C_{33}, C_{44} and C_{14}. Since the coupling to the [010]-T_1 mode is too weak to observe, we could not measure $C_{66} = \frac{1}{2}(C_{11} - C_{12})$. In none of the cases studied were we able to measure C_{13}. With C_{11} measured by the [100]-L phonon, we added and subtracted the frequencies of the [010]-L and [010]-T_2 to find C_{44}

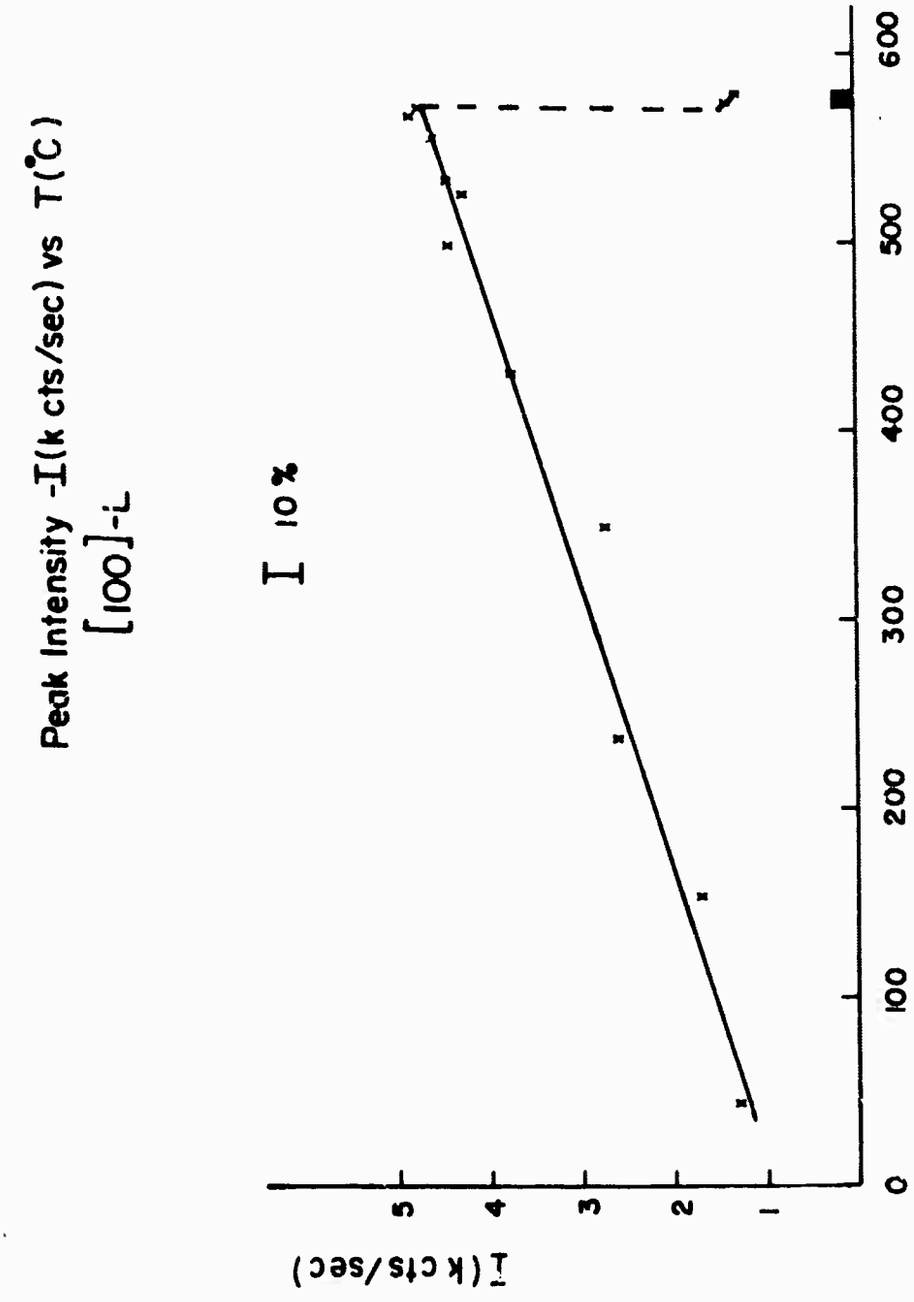

Fig. III-9. Peak intensity, I (k cts/sec) vs T (°C) of the [100]-L Brillouin component.

and C_{14}. Measurements of [010]-T gave us another method of determining C_{44}; the two measurements agreed. Fig. III-10 is a plot of the temperature dependence of the elastic constants C_{11}, C_{33}, C_{44} and C_{14} measured by light scattering. Also plotted, for comparison, are the temperature dependence of the elastic constants as measured by ultrasonic techniques (11, 90, 92, 94). We see that there is good agreement between the temperature dependence of the elastic constants measured by light scattering techniques and the temperature dependence of the elastic constants measured by conventional ultrasonic techniques and we can conclude that there is no appreciable frequency dispersion of the elastic constants up to $\sim$30 GHz.

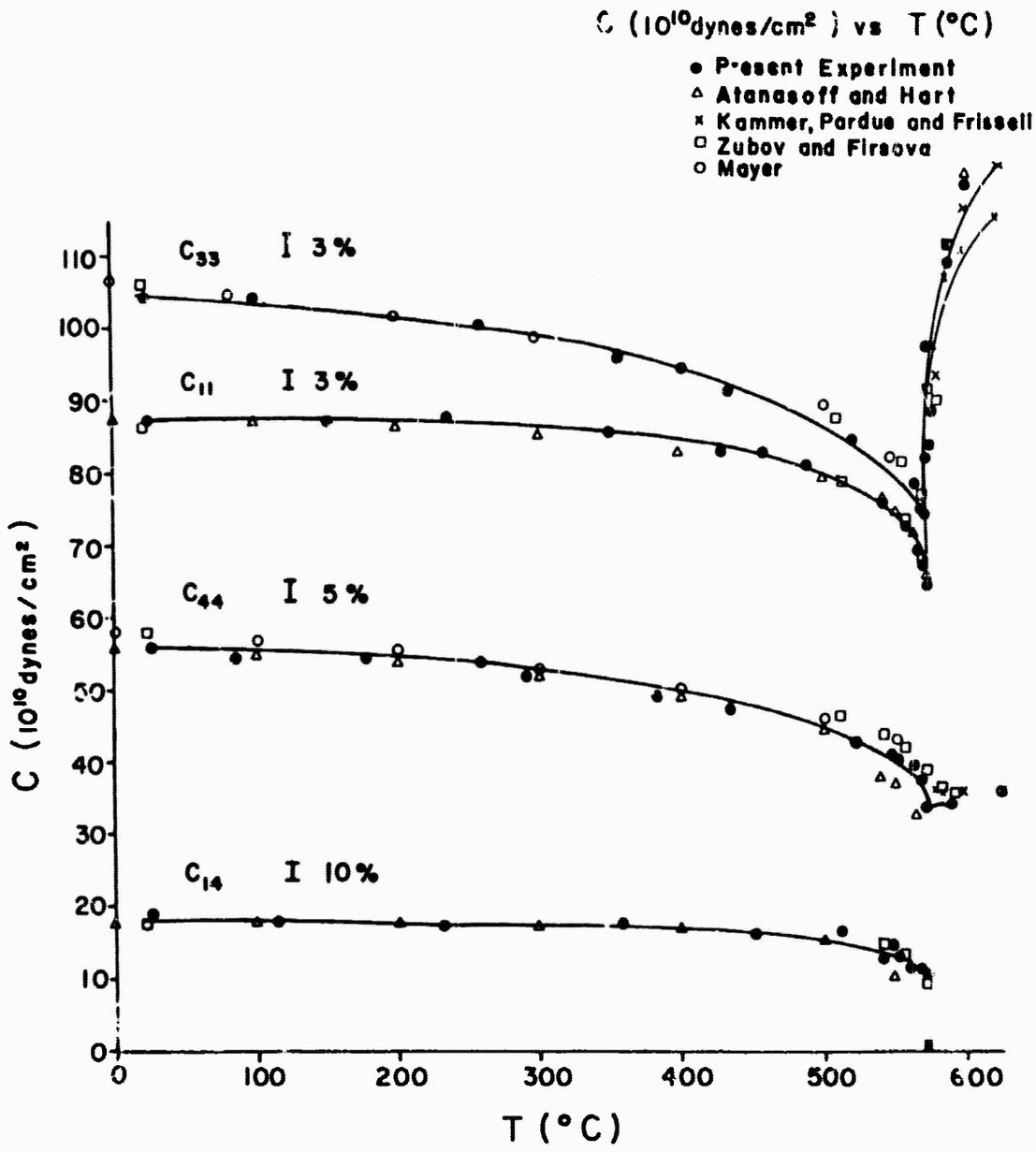

Fig. III-10. C_{33}, C_{11}, C_{44} and C_{14} (10^{10} dynes/cm^2) vs T (°C). Comparison is made with the elastic constants measured by ultrasonic techniques (11, 90, 92 and 94).

CHAPTER IV

THE ALPHA-BETA TRANSITION REGION

In Chapter I we reviewed the accepted theory of the quartz transition as proposed by Ginzburg (31). We repeated Ginzburg's calculation and predicted an increase in the scattered light at the transition temperature of $\sim 10^4$. We also discussed the experiment of Yakovlev et al., who observed that the scattering of Hg light by quartz increases by $\sim 10^4$ over the room temperature intensity and that under white light illumination the scattering volume appeared as a "fog zone" (35). This phenomenon was termed "critical opalescence" since it resembled the intense scattering (known as critical opalescence) observed in fluids near the critical point. It has been generally accepted that the large increase in scattering at the alpha-beta transition arises from the divergence of the fluctuations of the order parameter η. Ginzburg identified η with the totally symmetric A_1 optical mode whose room temperature frequency is 207 cm^{-1}. As the transition temperature is approached, the frequency of this mode would decrease toward zero while the fluctuations of η diverge.

In this chapter we investigate the Raman and Brillouin scattering in the transition region, 570°C to 576°C, and study the intense Rayleigh scattered light at the transition temperature (100).

A. RAMAN SCATTERING IN THE ALPHA-BETA TRANSITION REGION

In Chapter II we studied the Raman scattering by crystalline quartz from 20°K up to 873°K (=600°C). We showed that it is not the 207 cm^{-1} line, but a small A_1 satellite at 147 cm^{-1} at room temperature whose frequency approached zero as $T \to T_t$ from below. The probable origin of this complication was discussed in terms of anharmonic coupling between one and two phonon excitations (57). We showed that at room temperature the 207 cm^{-1} line is essentially a zone center A_1 optical vibration, while the feature at 147 cm^{-1} is a two phonon zone-edge excitation. As the temperature is raised the two excitations become mixed due to the anharmonic coupling and the observed features can no longer be described as one or two phonon processes. For temperatures near the transition temperature, the excitations again become distinct and the low frequency component has become the one phonon mode and the high frequency component is the two phonon excitation. Thus, in this section we restrict ourselves to temperatures close to the transition temperature so that the low frequency A_1 vibration (still called the 147 cm^{-1} line) is the "soft" zone center optic mode.

The results of the transition region study of the frequency of the 147 cm^{-1} line are shown in Fig. IV-1. We see that on heating the frequency decreases to a minimum of 30 cm^{-1} at the alpha to beta transition temperature, $T_{\alpha\beta}$ = 573.4°C, at which point the line disappears from our spectra. On cooling, the line reappears at the beta to alpha transition temperature, $T_{\beta\alpha}$ = 572.4°C, one degree below the temperature at which it disappears on heating. The soft component is quite broad (> 80 cm^{-1}; Fig. II-8) when it attains its minimum frequency of 30 cm^{-1}. The intense

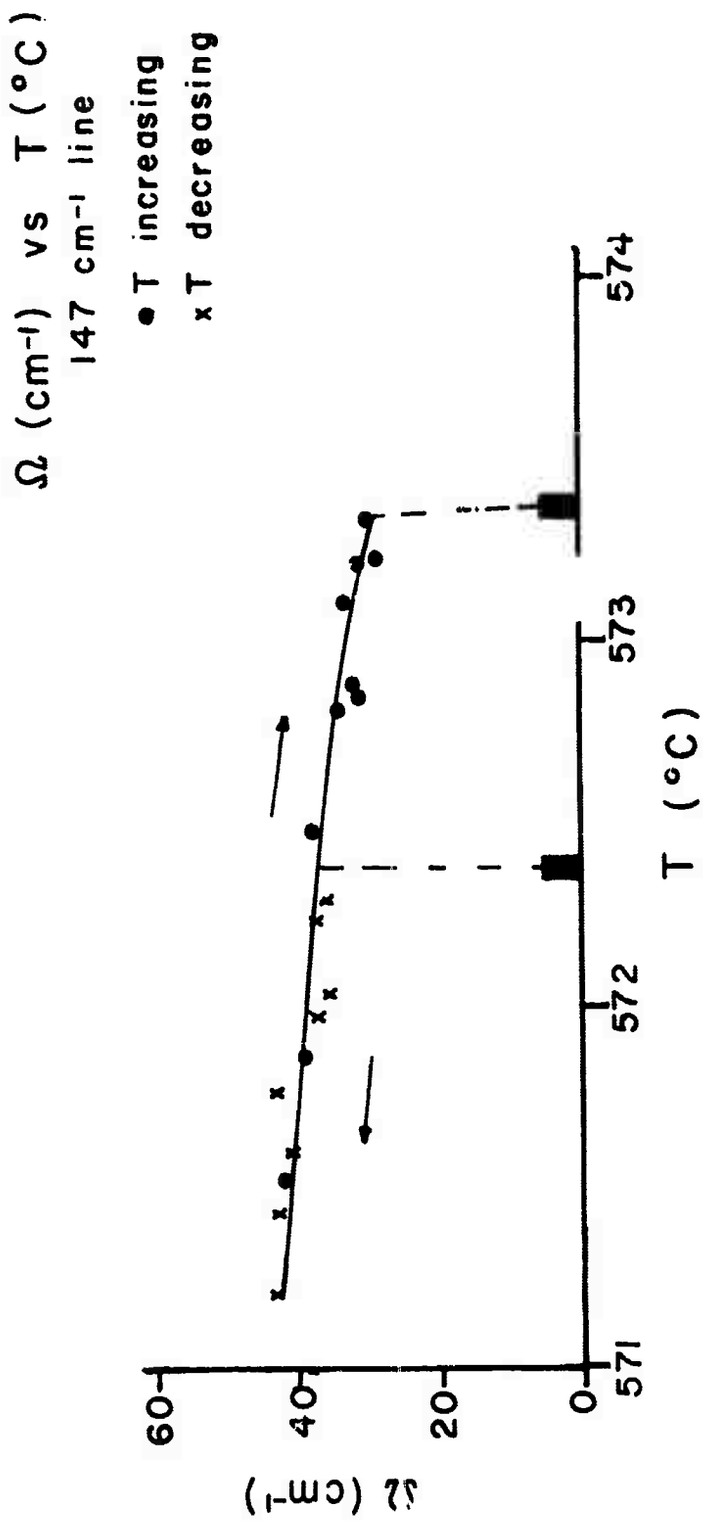

Fig. IV-1. Frequency Ω (cm^{-1}) vs T (°C) of the 147 cm^{-1} line in the transition temperature region. The arrows indicate the direction of the temperature change.

Rayleigh scattering suddenly appears with the disappearance (on heating) and the reappearance (on cooling) of the Raman components. The spectral width of the Rayleigh line was never resolved in this experiment (instrumental resolution: $\sim$2 cm^{-1}).

Thus the smooth collapse of the soft mode into an overdamped quasi-elastic component envisioned by Ginzburg[31] is not observed and the intense Rayleigh scattering cannot be considered as the overdamped remnant of the soft optic lattice vibration.

We also studied the intensity of the 355 cm^{-1} line as a function of temperature in the transition region. We recall (Table I-3) that the 355 cm^{-1} line is a Raman active A_1 vibration in alpha quartz which becomes a Raman inactive and infrared inactive E_1 vibration in beta quartz. Its frequency changes very little with increasing temperature (Fig. II-6) and its intensity decreases steadily toward zero as $T \rightarrow T_t$ (Fig. II-7). Fig. IV-2 is a plot of the intensity of the 355 cm^{-1} line in the transition region. It shows that the intensity of the 355 cm^{-1} line exhibits the same thermal hysteresis that was observed in the frequency of the "soft" mode (Fig. IV-1). What is striking is the persistence of the 355 cm^{-1} line through the fog zone and into the beta phase. On further heating of the crystal, this line gradually disappears. On cooling from the beta phase this spectral line appears before the beta to alpha transition occurs. When the fog zone appears and the crystal transforms to alpha quartz, there is an abrupt increase in the intensity of the 355 cm^{-1} line. The presence of this spectral feature in the beta phase where it is forbidden by group theory is probably due to strains present in the crystal as it undergoes its transition. These strains locally

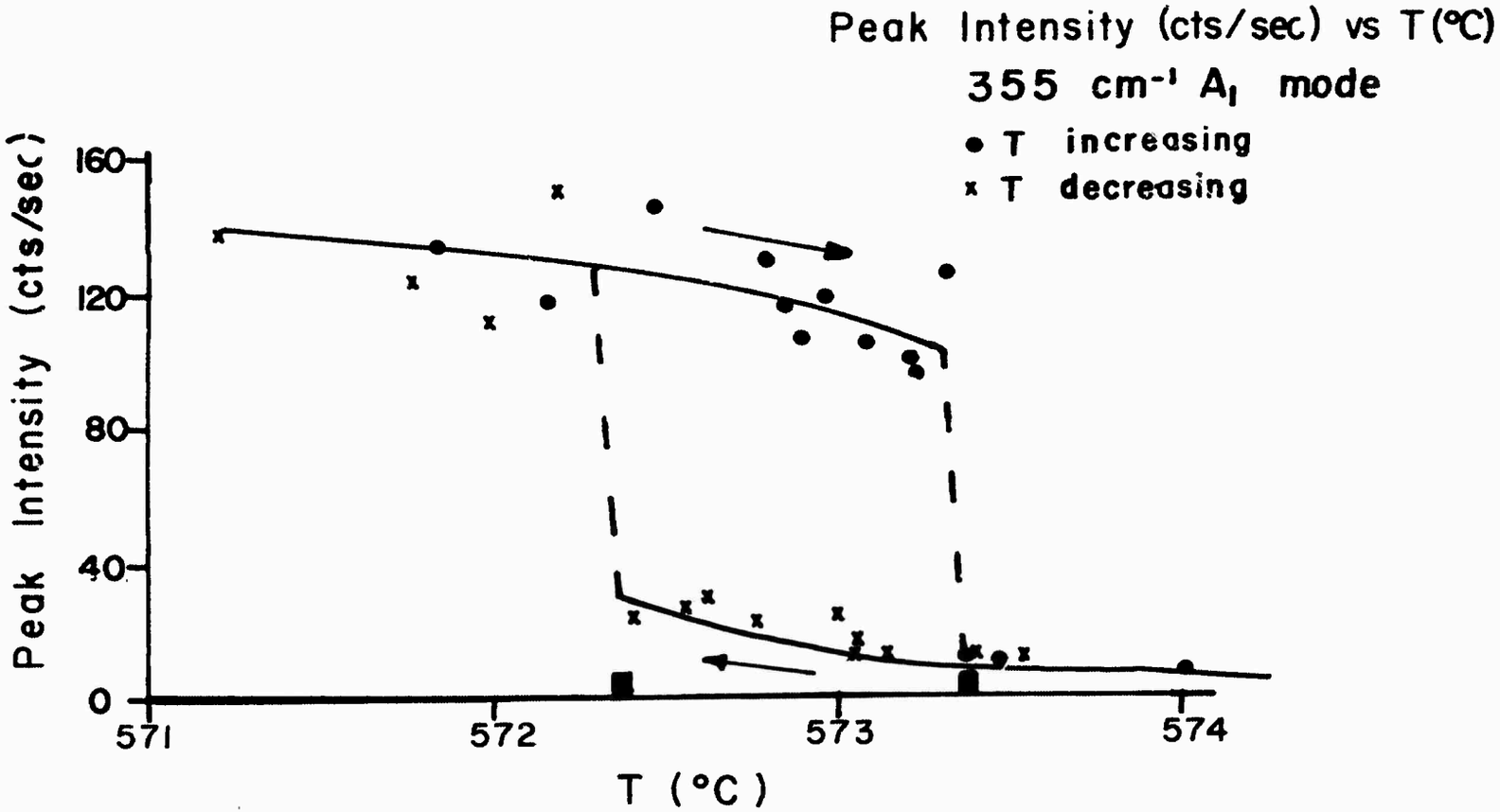

Fig. IV-2. Peak intensity (cts/sec) vs T (°C) of the 355 cm^{-1}, A_1 mode in the transition temperature region. The arrows indicate the direction of the temperature change.

break the symmetry and can allow a normally inactive Raman mode to become Raman active.

B. BRILLOUIN SCATTERING IN THE ALPHA-BETA TRANSITION REGION

In Chapter III we discussed the Brillouin scattering by crystalline quartz from room temperature up to 600°C. In this section we restrict ourselves to Brillouin measurements of phonons propagating in the [100], [010], [001] and [110] directions in the transition temperature region, 570°C - 576°C. The spectra of all phonons studied showed a distinct change at the transition temperatures. Fig. IV-3 shows the spectra of the [100] phonons for (a) alpha quartz just below the alpha to beta transition temperature ($T_{\alpha\beta}$ = 574.30 ± .03°C), and (b) beta quartz just above the transition temperature. Fig. IV-4 is a plot of the measured frequency shifts of the [100]-L phonon in the 571°C - 576°C temperature region. We see that on heating the frequency exhibits an abrupt increase at $T_{\alpha\beta}$ = 574.3°C as the alpha to beta transition occurs, and on cooling the frequency gradually decreases and at $T_{\beta\alpha}$ = 573.0°C the transition beta to alpha occurs. At these two temperatures, intense Rayleigh scattering is observed.

Figs. IV-5 and IV-6 show the behavior of the linewidth and the peak intensity of the [100]-L Brillouin peak in the transition temperature region. The temperatures where the abrupt changes occur in these properties are the same temperatures at which the fog zone appears. It is interesting to note that the cooling curves of the frequency shift and the linewidth strongly resemble, aside from the discontinuities, the relaxational process occurring in second order lambda type transition treated theoretically by

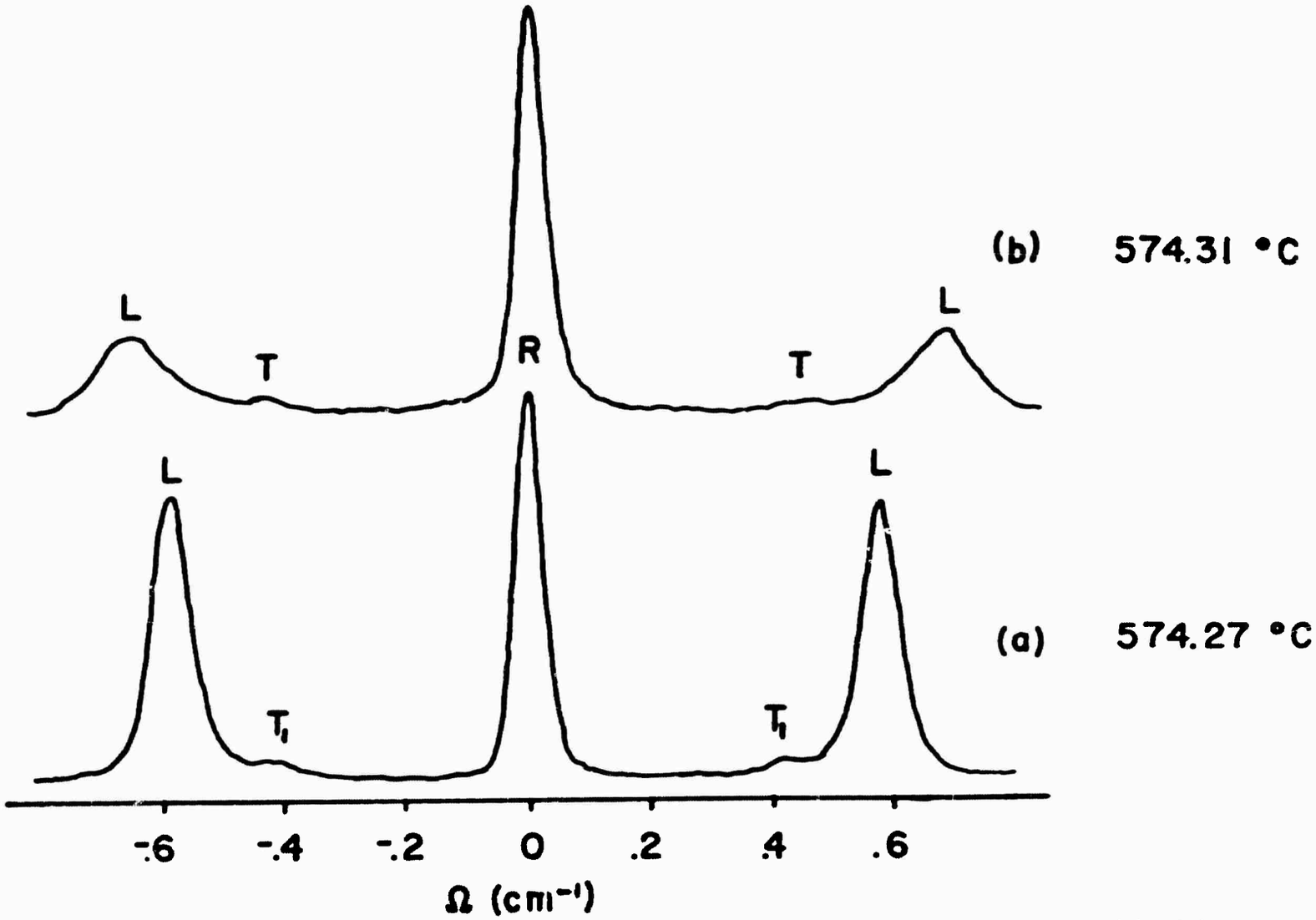

Fig. IV-3. Brillouin spectra for phonons propagating in the [100] direction for (a) alpha quartz and (b) beta quartz. $T_{\alpha\beta}$ = 574.03°C.

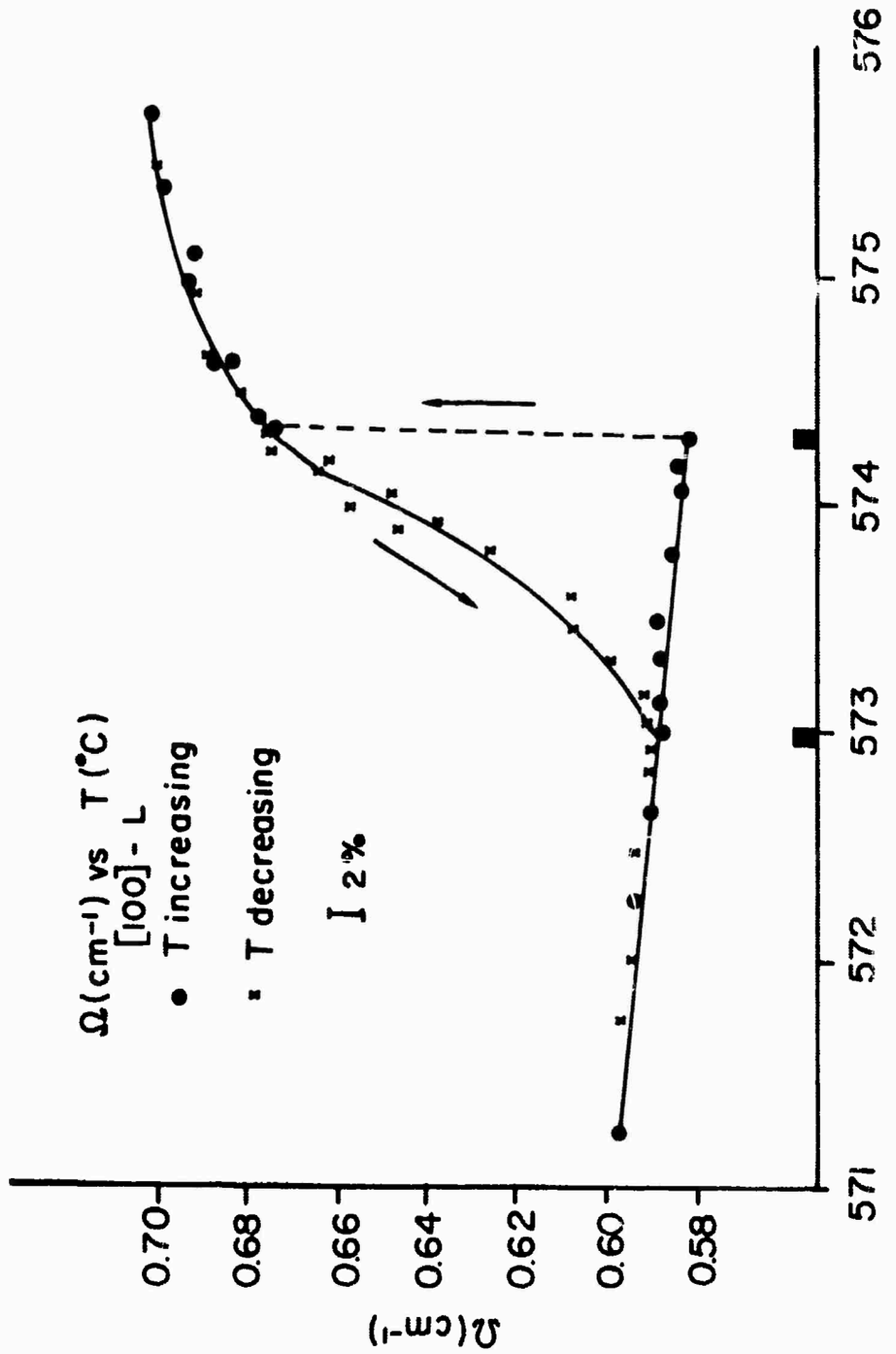

Fig. IV-4. Measured frequency Ω (cm^{-1}) vs T (°C) of the [100]-L phonon in the transition temperature region. Arrows indicate direction of the temperature change.

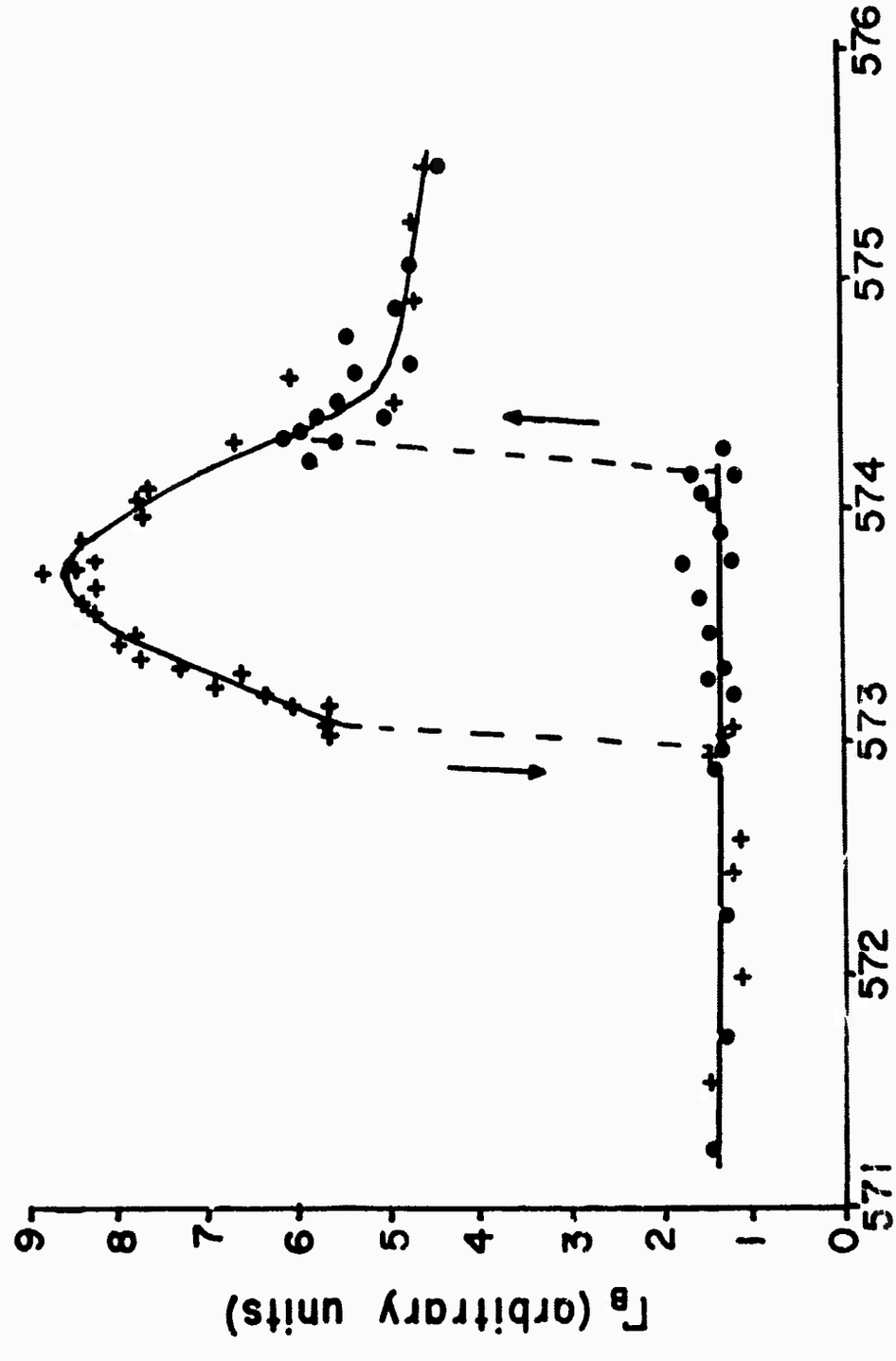

Fig. IV-5. The linewidth, Γ (in arbitrary units) vs T (°C) for the [100]-L phonon in the transition temperature region. The linewidth was measured by subtracting the full-width at half maximum of the Rayleigh peaks from the fullwidth at half maximum of the longitudinal Brillouin peak.

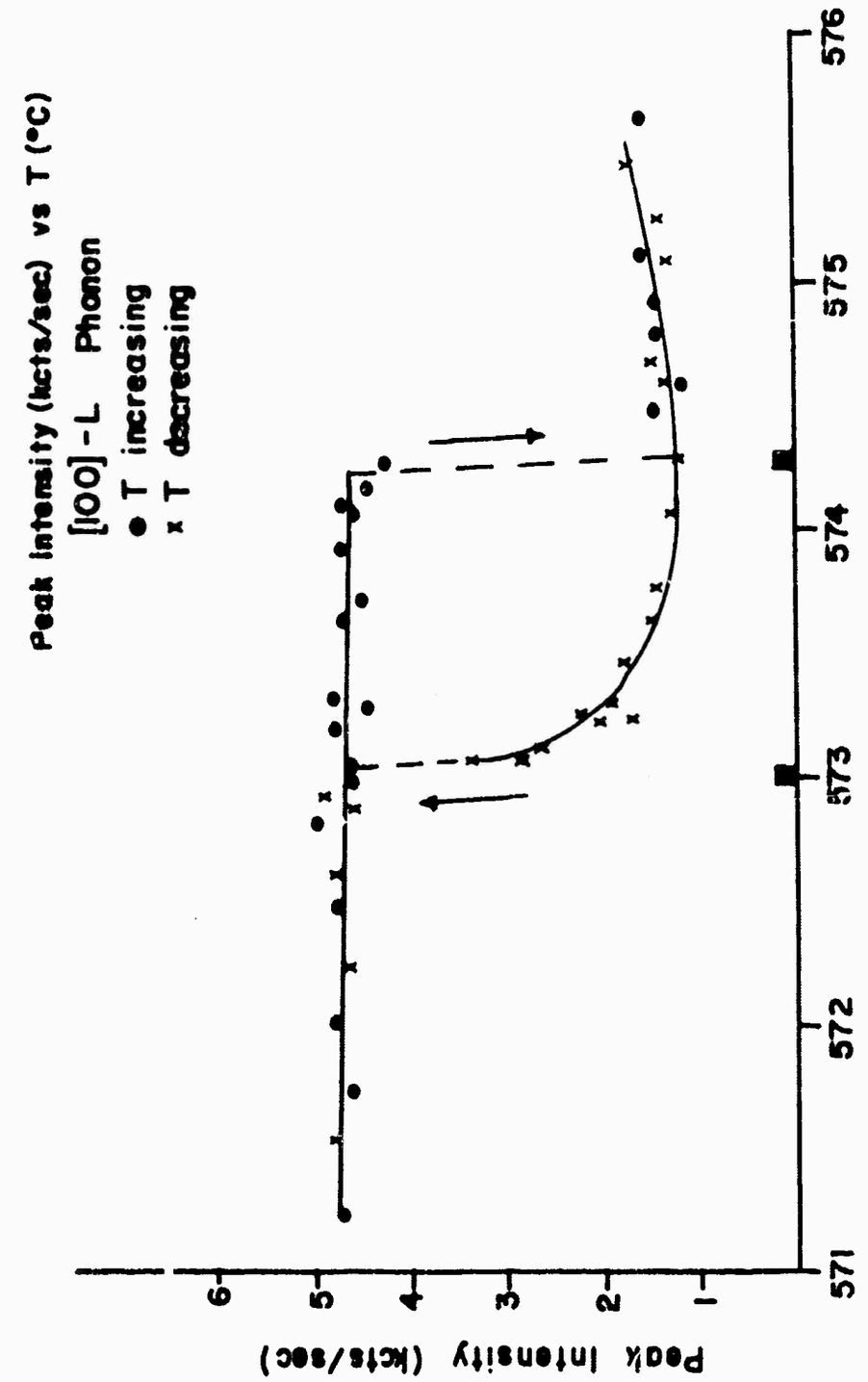

Fig. IV-6. Peak intensity (k cts/sec) vs T (°C) of the [100]-L phonon in the transition temperature region. The arrows indicate the direction of temperature change.

Landau and Khalatnikov (101) and observed in ferroelectric TGS in ultrasonic experiments (102) and in Brillouin experiments (103).

The measured Brillouin frequencies vs temperature in the transition region for the phonons: [010]-L, [010]-T, [001]-L, [001]-T and [110]-L in natural quartz are shown in Figs. IV-7 to IV-9. In all curves a thermal hysteresis is observed varying from 0.55 C° to 1.30 C°. The hysteresis loops of the longitudinally polarized phonons are approximately triangular in shape and for the transversely polarized phonons are approximately rectangular in shape. For the longitudinally polarized phonons there are large increases in the frequency on heating ($\sim$15%) while for the transversely polarized phonons the change in frequency is smaller ($\sim$5%).

In Figs. IV-10 to IV-12 we plot the calculated elastic constants, C_{11}, C_{33}, C_{44} and C_{14} in the transition region. There are no ultrasonic measurements this close to the transition temperature to compare with our results.

In all crystals, the fog zone was observed at the temperatures where the abrupt changes in the spectra occurred. The temperatures at which the fog zone appeared differ for the different phonons studied. This can be attributed to the fact that different crystals were used and the transition temperature can vary from crystal to crystal (± 0.4). Also there is a lack of temperature reproducibility after dismantling and reassembling the oven. Considering all the cases studied, the average transition temperatures are:

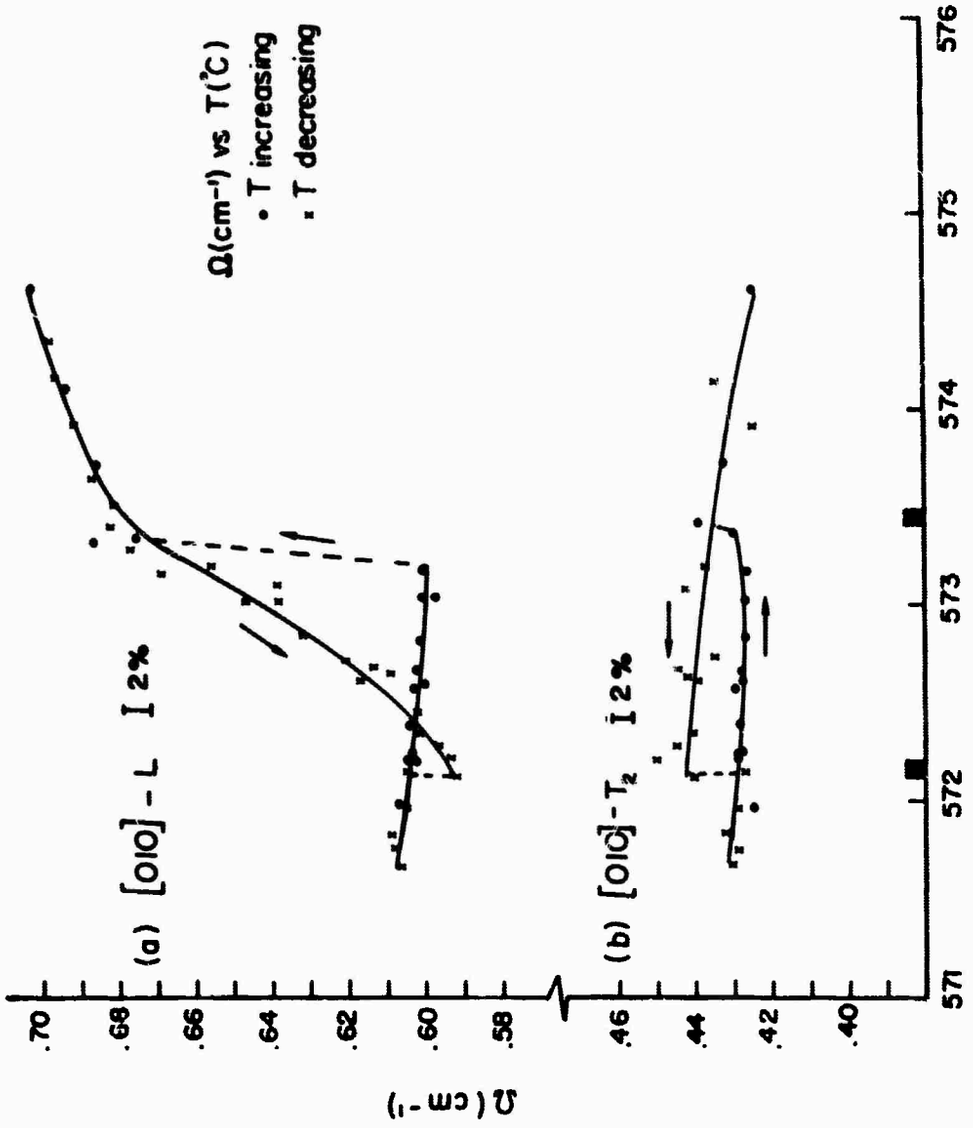

Fig. IV-7. Measured frequency Ω (cm^{-1}) vs T (°C) of the [010]-L and the [010]-T_2 phonons in the transition temperature region.

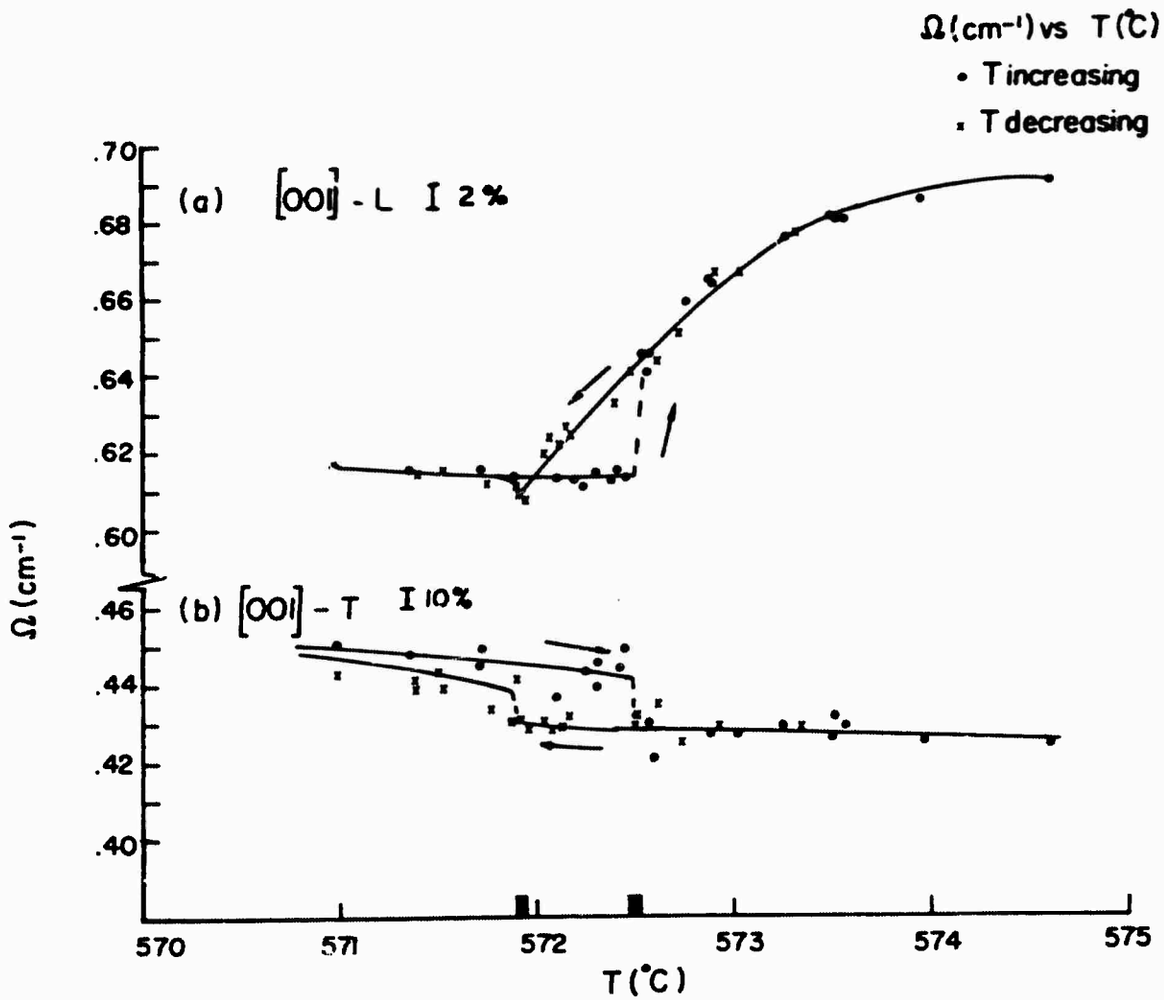

Fig. IV-8. Measured frequency Ω (cm^{-1}) vs T (°C) of the [001]-L and the [001]-T phonons in the transition temperature region.

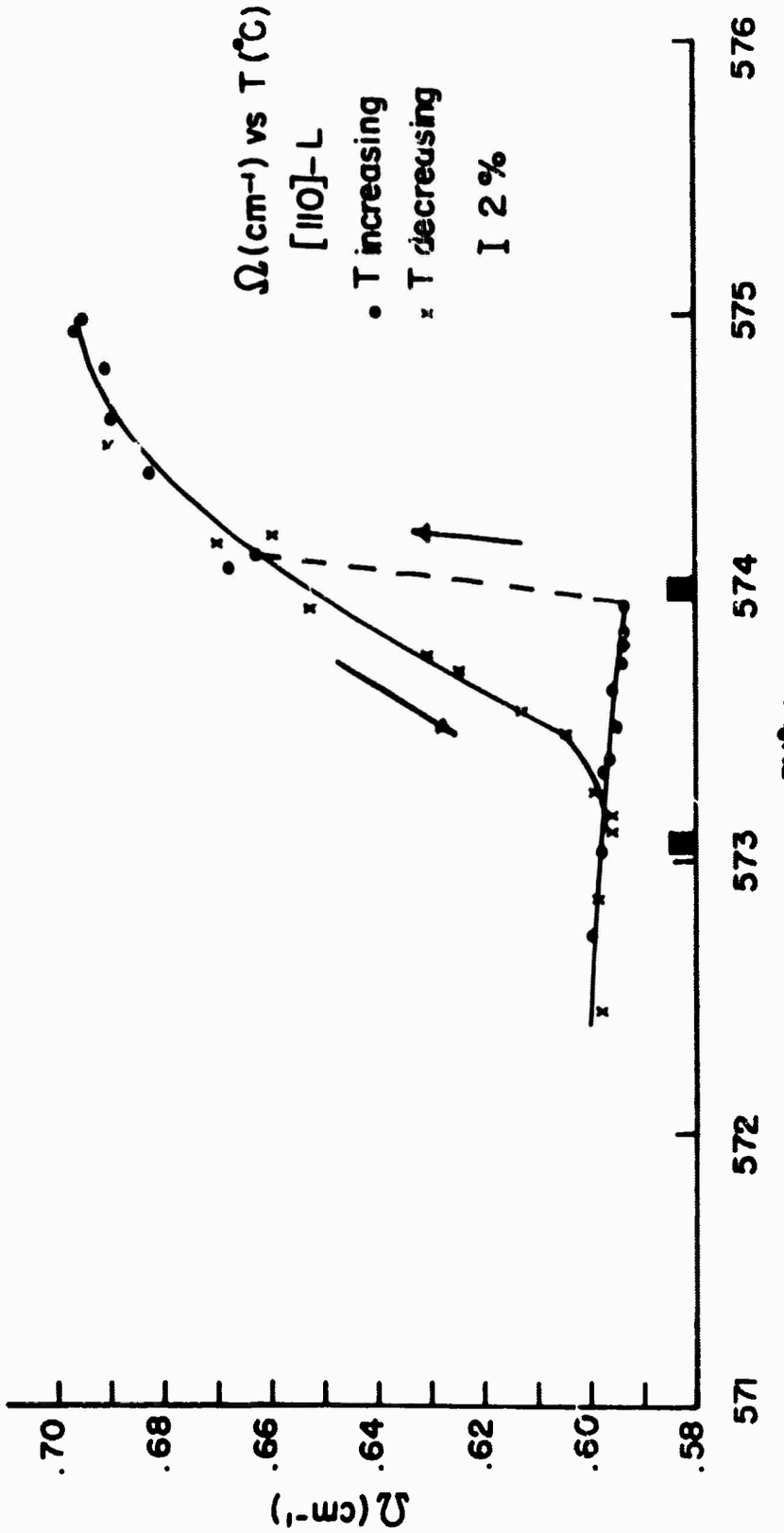

Fig. IV-9. Measured frequency Ω (cm^{-1}) vs T (°C) of the [110]-L phonon in the transition temperature region. The arrows indicate the direction of the temperature change.

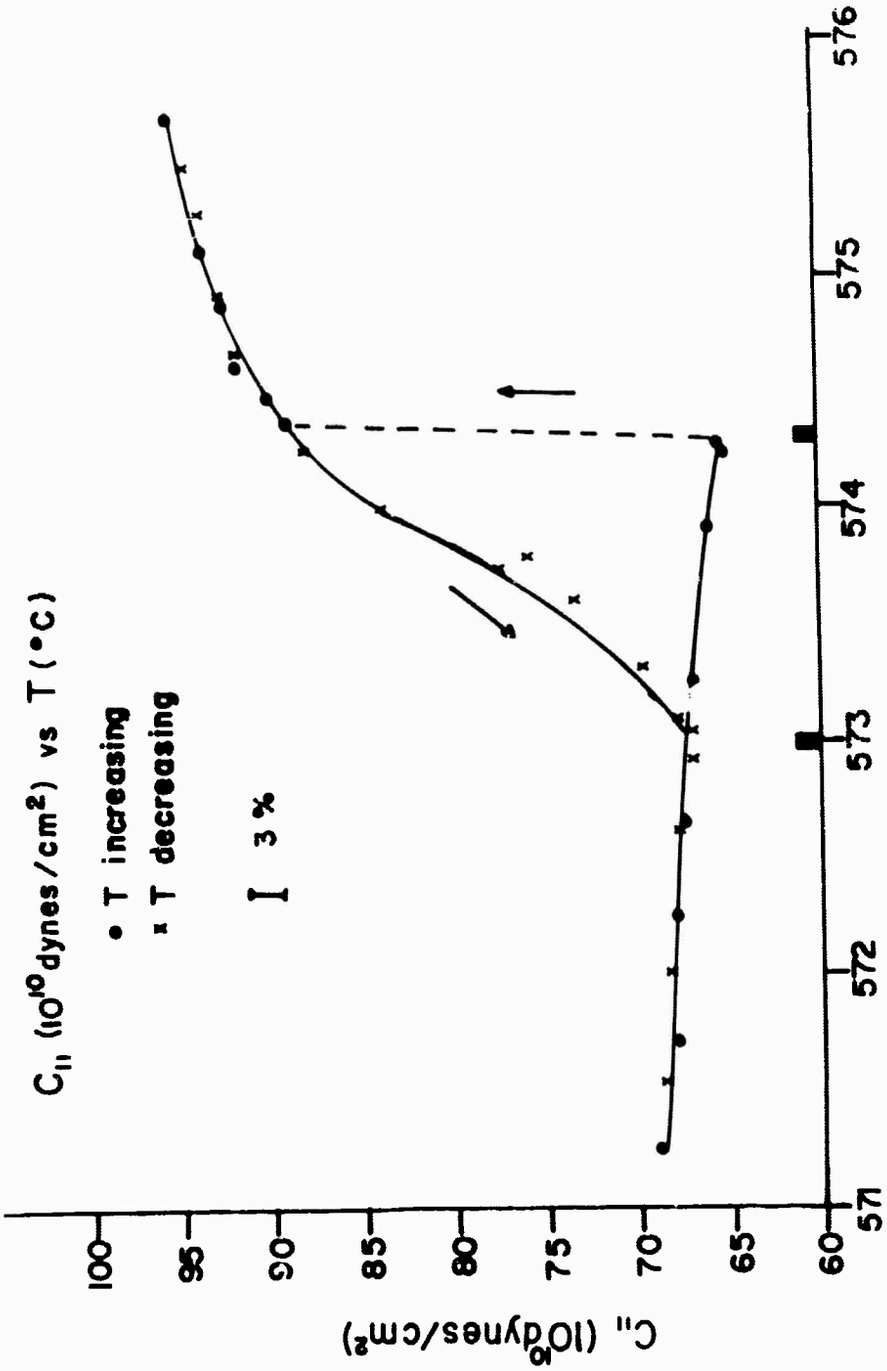

Fig. IV-10. C_{11} (10^{10} dynes/cm^2) vs T (°C) in the transition temperature region calculated from the measured temperature dependence of the [100]-L frequency. The arrows indicate the direction of the temperature change.

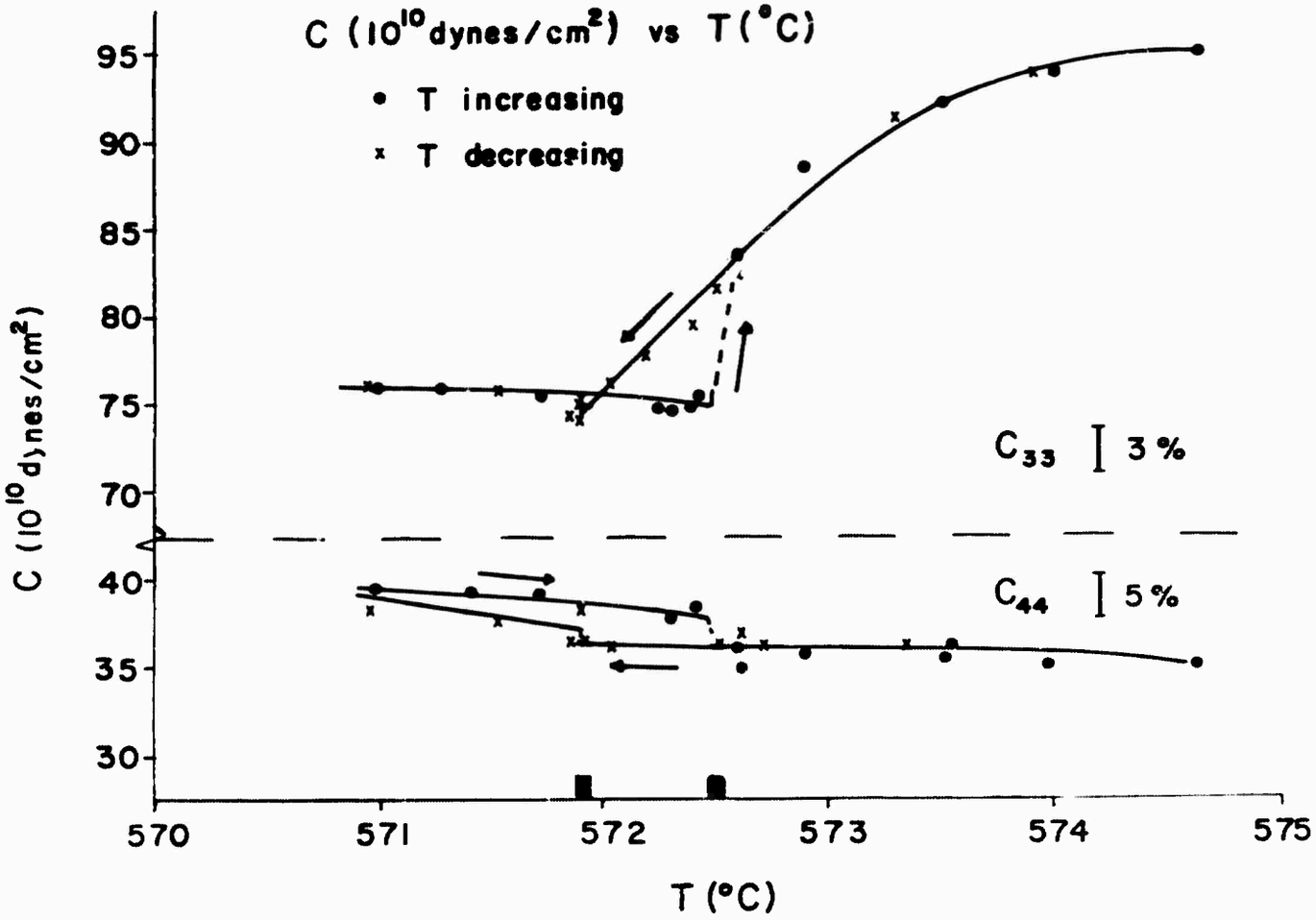

Fig. IV-11. C_{33} and C_{44} (10^{10} dynes/cm^2) vs T (°C) in the transition temperature region calculated from the measured temperature dependence of [001]-L and [001]-T, respectively. The arrows indicate the direction of the temperature change.

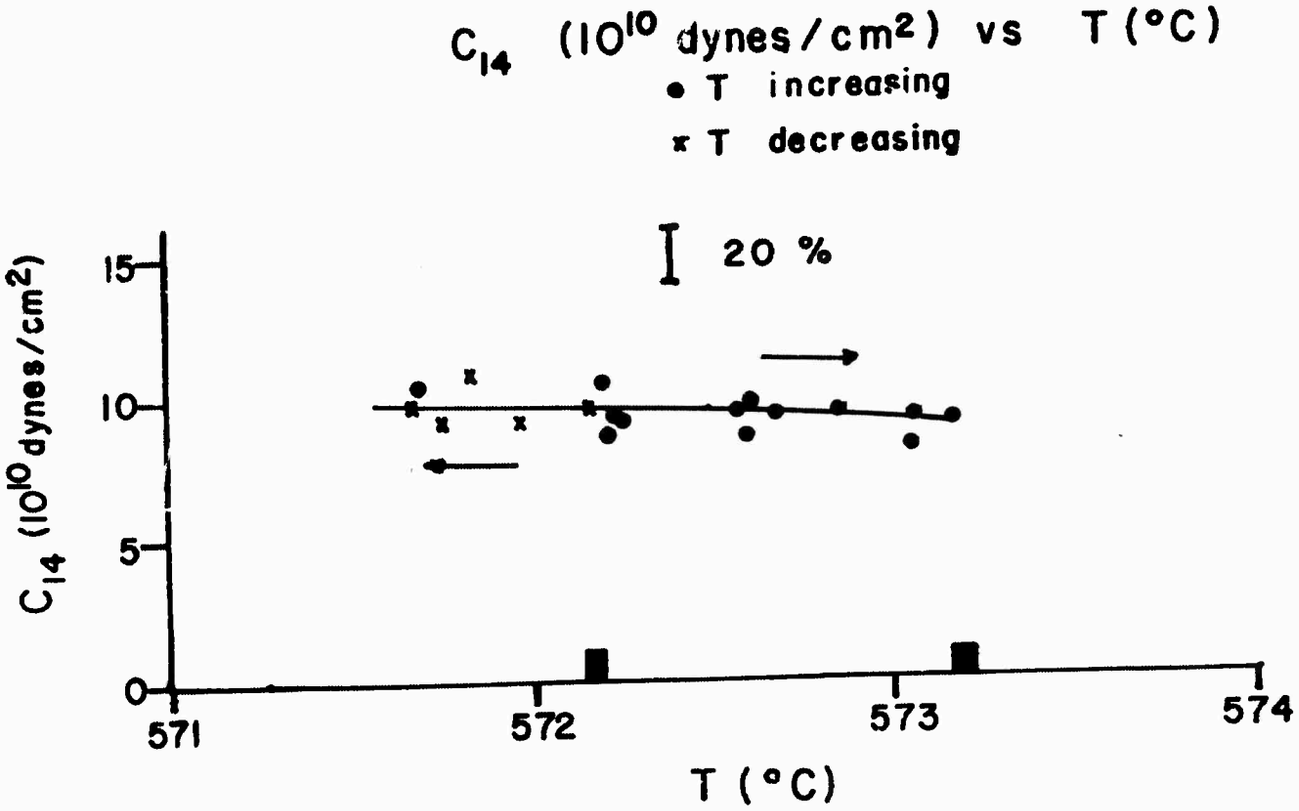

Fig. IV-12. C_{14} (10^{10} dynes/cm^2)vs T (°C) in the transition temperature region calculated from subtraction of the measured [010]-L and [010]-T_2 frequencies, and the measured C_{11}. The arrows indicate the direction of the temperature change.

$$T_{\alpha\beta} = 573.6 \pm .6°C$$

$$T_{\beta\alpha} = 572.6 \pm .5°C$$

Thus a hysteresis of about 1 C° was observed. This hysteresis implies that the transition may well be first order, rather than second order as predicted by Ginzburg (31).

The sudden increase in the Rayleigh scattered light ($\sim 10^4$ times the room temperature intensity) occurs at the same frequency as the unshifted light within the resolution of the Brillouin experiments ($\sim .06$ cm^{-1}). There was no observed spectral structure to the opalescence. Thus in the Brillouin experiment we see no mode whose frequency approaches zero and the observed opalescence is not due to any soft acoustic mode.

C. RAYLEIGH SCATTERING IN THE ALPHA-BETA TRANSITION REGION

In the Raman and Brillouin experiments the intense Rayleigh scattering in the transition region was spectroscopically indistinguishable from pure elastic scattering. Since the spectral linewidth of the "critical opalescence" was too small to measure with either the Raman spectrometer or the Brillouin interferometer, we next considered performing a light-beating experiment of the type used to measure the Rayleigh linewidth in critical opalescence in fluids (105). This experiment was never performed since we discovered during preliminary visual observations of the scattering column that the "critical opalescence" is, in fact, <u>elastic</u> scattering.

When laser light is scattered from a stationary target, the scattered light exhibits a characteristic granular pattern. If the target moves

slowly, the granularity also appears to move. If the target moves so rapidly that the granularity changes in a time shorter than the response time of the eye, the granularity disappears, and one sees a uniform scattered intensity distribution. (This effect, which arises from the spatial coherence of laser light, was discussed by Rigden and Gordon in 1962 (106).)

We observed that when the crystal was below the transition temperature, the scattering column appeared to be homogeneous. (A photograph of the scattering column with 15 min exposure is shown in Fig. IV-13a. The bright specks are crystal imperfections.) When the crystal was heated to the transition temperature the "fog zone" which appeared did not look uniform, but exhibited the characteristic granularity associated with elastic scattering (107). Once the fog zone started to traverse the crystal its progress could not be halted. It took 2 to 3 min for the fog zone to pass through the crystal. Fig. IV-13b is a photograph of the scattering column in the fog zone with 2 sec exposure. The granularity is apparent in the photograph.

In Fig. IV-13c we show a photograph with 5 min exposure in the beta phase. In addition to the specks caused by imperfections, there is some residual structure visible which slowly disappears as the temperature is further increased. On cooling, the above sequence is reversed, with the fog zone reappearing at a lower temperature, as we indicated earlier.

The persistence of static granularity for many seconds in the light scattered from the fog zone suggests that the intense scattering is completely elastic, originating from some essentially static phenomenon rather than from thermodynamic fluctuations of the order parameter. A

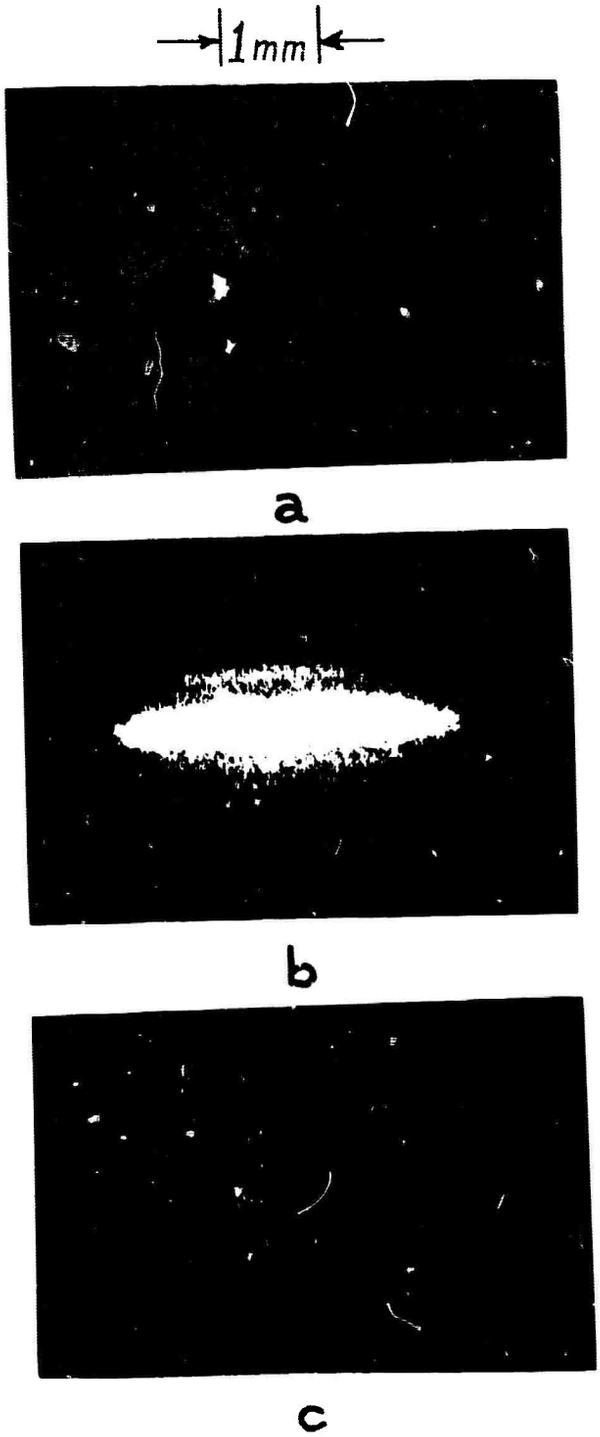

Fig. IV-13. Photographs of the scattering cclumn in crystalline quartz illuminated by a 6328 A He-Ne laser beam. (a) $T < T_t$, 15 min exposure; (b) $T = T_t$, 2 sec exposure; (c) $T > T_t$, 5 min exposure.

possible explanation of this effect was suggested by Young who performed extensive X-ray measurements on quartz through the alpha-beta transition (20). Young found that as the transition is approached from below, the structure separates into domains of Dauphiné (or electrical) twins. The twins, which are related by 180° rotation about the C axis, correspond to opposite signs of the order parameter η (see Ch. I). As the transition is approached, the domain size decreases and the density of domain walls increases. Young suggested that the development of Dauphiné twins is a special type of transition in the long range order which starts a few degrees below the alpha-beta transition and continues until the crystal is completely twinned, i.e., equal volumes of each twin. Within each twinned region the short range order of either the α_1 or α_2 (Fig. I-4) configuration is preserved. The completely twinned state, in which the long range order transition has gone as far as it can and still be termed long range, may be considered as a special kind of intermediate state. This complete twinning occurs at the start of the alpha-beta transition proper which is a transition of short range order.

The large increase in the light scattering presumably arises from inhomogeneous strains present in domain walls which perturb the dielectric constant locally leading to large light scattering efficiencies, an effect which we have previously observed in ferroelectric TGS (108). Thus, it is the domain walls produced by the microtwinning which would be responsible for the observed opalescence.

Another possible source of the inhomogeneities in the index of refraction in the quartz crystal causing the "opalescence" near the transition temperature is the formation of beta quartz regions inside

the alpha quartz crystal. This type of nucleation is possible if the transition is first order. On heating the crystal near T_t beta quartz can exist in a metastable state within the alpha quartz structure. (Conversely, on cooling from the beta phase, alpha quartz can exist in a metastable state in the beta quartz structure.) Since the indices of refraction of beta and alpha quartz differ, the regions of beta quartz will scatter light. An analogous effect could occur in a fluid just below the condensation temperature in the absence of gravity. The fluid might break up into droplets which would produce anomalous scattering. Such an effect would occur most strongly very close to T_t since it would only become energetically possible as the surface tension vanishes. In the case of quartz, the droplets--beta "droplets"--are locked in position in the alpha quartz "fluid."

We can estimate the size of the beta regions within the alpha quartz structure from a measurement of the intensity of the scattered light at the transition temperature. We assume spherical regions of volume V and index of refraction n_β in a medium with an index of refraction n_α. If $|n_\alpha - n_\beta| = |\Delta n| \ll 1$ we apply the Rayleigh-Gans criterion and calculate the Rayleigh ratio (109):

$$R = \frac{\pi^2}{\lambda_o^4} (n_\alpha^2 - n_\beta^2)^2 \frac{V}{2} \text{ cm}^{-1}$$

$$= \frac{\pi^2}{\lambda_o^4} 2n^2 (\Delta n)^2 V \text{ cm}^{-1}$$

where we have assumed that at the temperature where the maximum scattering occurs the spherical beta regions occupy half of the scattering

volume. We set this equal to the measured Rayleigh ratio of the light scattered by quartz at T_t (eq. I-26):

$$R = 2.0 \times 10^{-3}\text{cm}^{-1} = \frac{\pi^2}{\lambda_o^4} 3 \times 10^{-21}\text{cm}^{-1} \qquad (\lambda_o = 6328\ \text{Å})$$

Using the measured values of n and Δn near T_t (I-25) we can solve for V and find the radius of the beta regions within the alpha structure. The results of this calculation yield a radius for the beta region of $r \sim 500$ Å. (In a similar manner we could have assumed we were cooling the crystal and calculated the size of the alpha regions within the beta structure.) This result is consistent with the results of Yakovlev et al, who observed a λ^{-4} dependence of the scattered intensity within the fog zone and deduced that any optical non-uniformities were smaller in size than the wavelength of light (35).

Recent small angle X-ray scattering experiments performed on quartz revealed no excess scattering during the phase transition (110). This result favors the first of the above explanations because the X-rays are insensitive to the microtwinning of the type Young suggested since the electron densities of the two Dauphiné twins are the same, while the X-ray scattering was observed at sufficiently small angles (< 1/4°), so that the regions of beta quartz (of the size estimated above) would have produced additional scattering near the transition temperature.

D. CONCLUSIONS

On the basis of the Raman, Brillouin, and Rayleigh observations, we conclude:

1. Because of the static granularity of the light scattered from the fog zone, we believe that quartz does <u>not</u> exhibit critical

opalescence in the usual sense of diverging fluctuations of the order parameter, despite the excellent agreement between the observed scattering intensity and the theoretical prediction based on the assumption of critical point fluctuations.

2. The intense scattering which is observed near the transition temperature is due to static inhomogeneities of the index of refraction of the quartz crystal. These may be a consequence of the extensive microtwinning of the Dauphiné type that occurs near the transition, or the formation, on heating, of regions of beta quartz within the alpha quartz structure. The results of recent X-ray experiments suggest the former explanation.
3. The hysteresis observed in the Raman and Brillouin experiments suggest that the transition is first order rather than second order. However, this distinction is not really adequate since the phenomenon of micro-domain formation considerably complicates the description of the transition.

CHAPTER V

SUMMARY AND CONCLUSIONS

The temperature dependent Raman and Brillouin scattering spectra of crystalline quartz have been studied with special emphasis on the alpha-beta phase transition region.

In the Raman experiments we studied the Raman active A_1 and E vibrational modes. Scott and Porto (45) showed that the LO-TO degeneracies of some of the E modes were lifted due to long range electrostatic interactions arising from the oscillating electric field associated with the infrared activity of the E modes. Our results agree with those of Scott and Porto. Also, the frequencies of the E modes were measured as a function of temperature and showed little change with increasing temperature.

Theoretical considerations (31) and early temperature dependent Raman studies of quartz (23) showed that the frequency of one of the A_1 vibrations, the 207 cm^{-1} mode, decreased toward zero as the transition temperature was approached from below. Our studies revealed an extra line of A_1 symmetry (frequency at room temperature: 147 cm^{-1}) whose frequency decreased toward zero as the transition temperature was approached. In addition, above the transition temperature, in the beta phase, there was an extra line of A_1 symmetry. Scott (57) suggested that the extra line in the alpha and beta phases is a second order Raman line. He attributed the anomalous temperature dependent behavior of the

first and second order Raman lines to anharmonic coupling between the "soft" zone center, 207 cm^{-1} excitation and the two zone edge acoustic excitations. In the transition region, the low frequency line is the "soft" zone center phonon. The frequency of this phonon did not go to zero at the transition temperature but decreased to a finite value of 30 cm^{-1} and disappeared from our spectra. Coincident with this disappearance a region of increased elastic scattering traversed the crystal. Because the frequency of the soft mode does not decrease continuously to zero at the transition temperature, the observed "opalescence" is not due to diverging fluctuations associated with the "soft" optic mode as had been proposed by Ginzburg (31). On cooling, the low frequency A_1 vibration reappears at a temperature 1 C° lower than the temperature at which it disappears on heating.

In the temperature dependent Brillouin scattering experiments we found good agreement between the elastic constants measured by light scattering and the elastic constants measured by ultrasonic techniques. Thus no frequency dispersion in the elastic constants is apparent. In the transition region, none of the frequencies of the acoustic modes studied approached zero as the transition temperature was approached. Thus the observed "opalescence" is not due to any diverging fluctuations associated with acoustic vibrations. The hysteresis observed in the Raman and Brillouin experiments suggests that quartz undergoes a first order phase transition as opposed to a second order transition proposed by Ginzburg.

Observations of the Rayleigh scattered light in the transition region showed that the large increase in the elastic scattering ($\sim 10^4$), the so-called opalescence, was due to a static process as opposed to the dynamic process associated with true critical opalescence. The large increase in scattered light at the transition temperatures was due to inhomogeneities in the index of refraction created by either the extensive microtwinning of the Dauphiné, or electric, type as reported by Young in his X-ray analysis of the phase transition of quartz (20), or due to the formation of regions of beta quartz, on heating, within the alpha quartz structure.

APPENDIX A

PROPERTIES OF ALPHA AND BETA QUARTZ

1. Chemical (1)	Alpha 25°C			Beta 600°C			
Formula	SiO_2			SiO_2			
Formula weight	60.09 amu			60.09 amu			
Density	2.65 gm/cm^3			2.54 gm/cm^3			
2. Crystallographic	Alpha			Beta			
Space group (2)							
Left handed	$D_3^6(P3_221)$			$D_6^5(P6_422)$			
Right handed	$D_3^4(P3_121)$			$D_6^4(P6_222)$			
Point group (2)	D_3 (32)			D_6 (622)			
Lattice constants							
a	4.9128 Å at 25° (ref 111)			5.01 Å at 600°C (ref 2)			
c	5.4042 Å at 25° (ref 111)			5.47 Å at 600°C (ref 2)			
Atomic Positions (112)	Alpha			Beta			
	(Left handed Structures)						
Silicons							
S_{16}- 1	u	0	0	1/2	0	0	
S_{45}- 2	-u	-u	1/3	1/2	1/2	1/3	
S_{23}- 3	0	u	2/3	0	1/2	2/3	
Oxygens							
O_1 - 4	x	y	z	x	x/2	1/6	
O_5 - 5	y-x	-x	z+1/3	-x/2	-x	1/2	
O_3 - 6	-y	x-y	z+2/3	-x/2	x/2	5/6	
O_6 - 7	x-y	-y	-z	x/2	-x/2	5/6	
O_2 - 8	y	x	2/3-z	x/2	x	1/2	
O_4 - 9	-x	y-x	1/3-z	-x	-x/2	1/6	

(Continued)

Fractional Coordinates (8)	Alpha - 25°C	Beta - 600°C
u	.4705 (ref 111)	
x	.4152	.4137 (ref. 20)
y	.2678	
z	.1184	
Bond lengths		
$S_{16} - O_7$ 1-4	1.603 Å (ref 111)	1.594 Å (ref 20)
$S_{16} \quad O_3$ 1-6	1.611	1.59
$O_3 - O_4$ 6-9	2.635	2.63
$O_1 - O_3$ 4-6	2.641	2.63
$O_1 - O_4$ 4-9	2.613	2.56
$O_1 - O_6$ 4-7	2.613	2.56
Bond angles		
$O_1 - S_{16} - O_3$ 4-1-6	110.04° (ref 111)	
$O_3 - S_{16} - O_4$ 6-1-9	109.16	
$O_1 - S_{16} - O_6$ 4-1-7	108.74	
$O_1 - S_{16} - O_4$ 4-1-9	108.8	
$S_{16} - O_1 - S_{23}$ 1-4-3	143.9	152.8° (ref 20)

3. Electrical Properties	Alpha - 25°C	Beta - 600°C
Dielectric constants		
ε_1 (0)	4.32 (ref 54)	4.4 (ref 113)
ε_1 (∞)	2.356	
ε_{11} (0)	4.56	4.6
ε_{11} (∞)	2.383	

(Continued)

	Alpha - 20°C (ref 8)	Beta - 585°C (ref 27)
Piezoelectric Strain constants: d_{hm} (in units of 10^{-8} $\frac{\text{statcoul}}{\text{dyne}}$ = 1/3 x 10^{-10} cm/volt)	$\begin{bmatrix} 6.9 & -6.9 & . & -2.0 & . & . \\ . & . & . & . & 2.0 & 2x6.9 \\ . & . & . & . & . & . \end{bmatrix}$	$\begin{bmatrix} . & . & . & -5.69 & . & . \\ . & . & . & . & 5.69 & . \\ . & . & . & . & . & . \end{bmatrix}$
Piezoelectric Stress constants: e_{hm} (in units of 10^{4} $\frac{\text{statcoul}}{\text{dyne}}$ = 1/3 x 10^{-1} coul/m^2)	$\begin{bmatrix} 5.2 & 5.2 & . & 1.2 & . & . \\ . & . & . & . & -1.2 & 2x5.2 \\ . & . & . & . & . & . \end{bmatrix}$	$\begin{bmatrix} . & . & . & -2.0 & . & . \\ . & . & . & . & 2.0 & . \\ . & . & . & . & . & . \end{bmatrix}$

4. Optical Properties	Alpha 25°C	Beta - 580°C
Refractive index (1)		
$n_{\perp}$	1.5428 (at 6278 Å)	1.5314 (at 6278 Å)
n_{11}	1.5519	1.5389
Optical rotatory power	18.48 °/mm (at 6368 Å)	---

(Continued)

Pockel's, photoelastic, or elasto-optic constants (75, 76)

Alpha

.138	.250	.259	-.029	.	.
.250	.138	.259	.029	.	.
.258	.258	.098	.	.	.
-.042	.042	.	-.069	.	.
.	.	.	.	-.069	-.042
.	.	.	.	-.029	-.056

Beta

●		●	.	.	.
	●		.	.	.
●		●	.	.	.
.	.	.	●	.	.
.	.	.	.	●	.
.	.	.	.	.	X

● Non-zero values not known.

●—● Equal values

X = 1/2 (P_{11} - P_{12}).

5. Elastic Properties

Elastic stiffness C_{mn} (in units of 10^{10} dynes/cm^2)

Alpha - 25°C (74)

86.87	7.09	11.92	18.02	.	.
7.09	86.87	11.92	-18.04	.	.
11.92	11.92	10.57	.	.	.
18.04	-18.04	.	58.18	.	.
.	.	.	.	58.18	18.04
.	.	.	.	18.04	39.89

Beta - 578°C (92)

90.0	-10.0	12.8	.	.	.
-10.0	90.0	12.8	.	.	.
12.8	12.8	91.5	.	.	
.	.	.	36.5	.	.
.	.	.	.	36.5	.
.	.	.	.	.	50.0

(Continued)

Elastic compliance S_{mn} (in units of $10^{-12}cm^2/dyne$)	Alpha - 20°C (92)	Beta - 578°C (92)
	$\begin{bmatrix} 127.7 & -18.2 & -12.4 & -45.0 & . & . \\ -18.2 & 127.7 & -12.4 & 45.0 & . & . \\ -12.4 & -12.4 & 96.8 & . & . & . \\ -45.0 & 45.0 & . & 200.2 & . & . \\ . & . & . & . & 200.2 & 45.0 \\ . & . & . & . & 45.0 & 291.8 \end{bmatrix}$	$\begin{bmatrix} 115.4 & 15.4 & -18.3 & . & . & . \\ 15.4 & 115.4 & -18.3 & . & . & \\ -18.3 & -18.3 & 114.4 & . & . & . \\ . & . & . & 274.0 & . & . \\ . & . & . & . & 274.0 & . \\ . & . & . & . & . & 200.0 \end{bmatrix}$
Attenuation of Sound (MHz)	31 MHz for x phonon at 30 GHz (ref 81)	-

6. Thermal Properties	Alpha - 0°C (1)	Beta - 600°C (1)
Specific heat (heat capacity	.166 cal/gm	.271 cal/gm
Latent heat in transition	--86 cal/mole (ref 25)--	
Volume change in transition	--.11 cm^3/mole (ref 25)--	

APPENDIX B

OVEN, TEMPERATURE CONTROL, AND TEMPERATURE MEASUREMENT

OVEN

There were several unusual considerations in designing an oven for light scattering experiments near the alpha-beta phase transition of crystalline quartz (573°C): 1) Temperature stability and control of ±0.01°C was sought with a minimum of thermal gradients across the sample region; 2) There had to be two colinear ports to allow light to enter and leave the sample region. A third port was necessary to observe the light scattered at 90° to the incident beam; and 3) Crystalline quartz fractures when heated too rapidly through the transition temperature region. This cracking can be minimized if the temperature of the crystal is changed slowly (6).

With these considerations in mind, a double oven structure with a high thermal mass was constructed. Fig. B-1 shows a cross section of the oven. The outer container is a stainless steel can 15.5 inches in diameter. Harbison-Walker refractory cement was poured into the can making a wall thickness of 3.5 inches. This large thermal mass prevents us from heating the crystal too quickly. The outer heater consists of two Kanthol (REH-1) heating elements placed on top of each other and connected in series. Inside the outer heater is a stainless steel heat shield used to smooth out temperature gradients. The inner heater is a single Kanthol (REH-40) cylindrical heating element with holes in it to

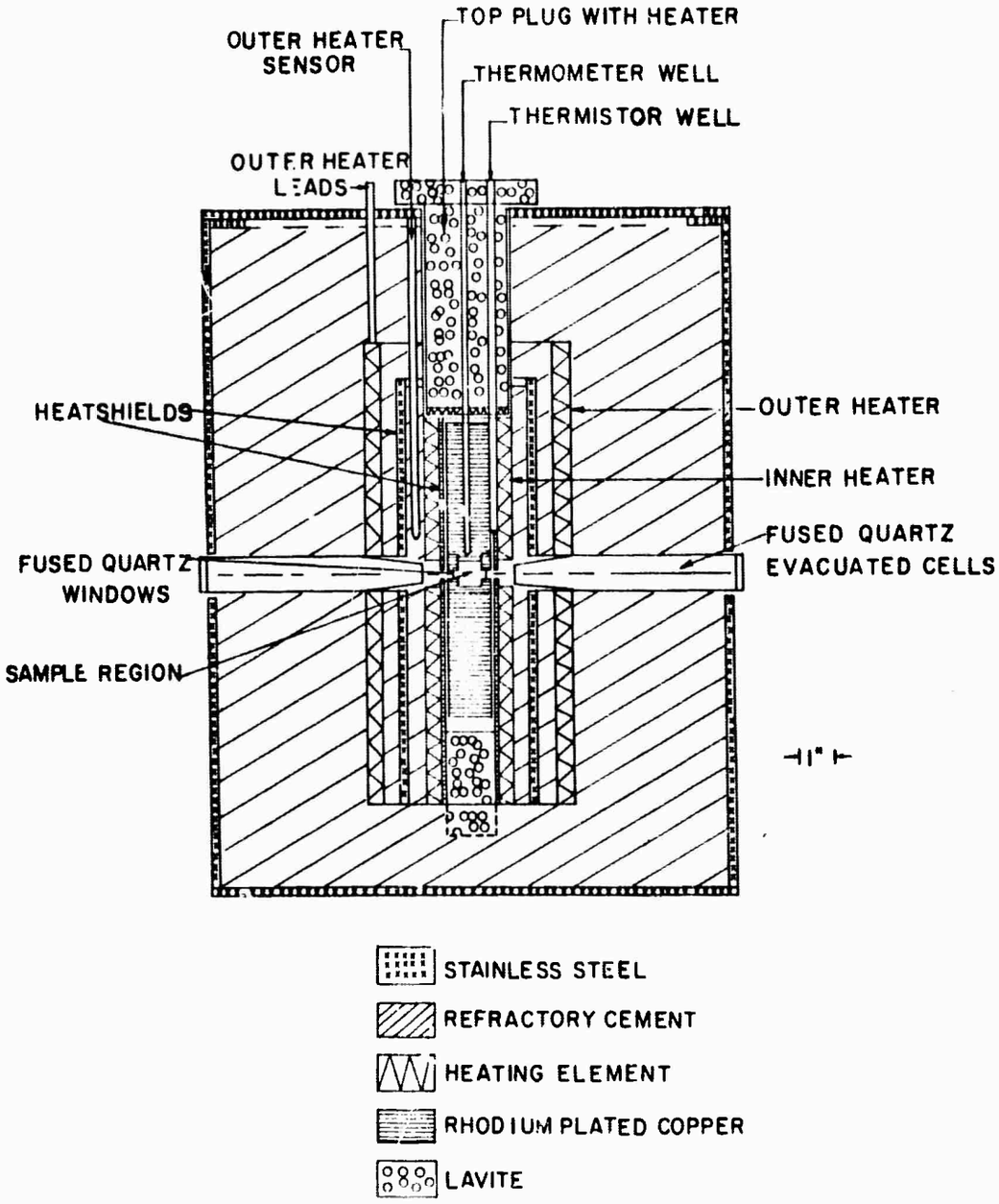

Fig. B-1. Cross section of the oven used in the experiments. The observation port is out of the plane of the paper.

allow the light to enter and leave the sample region. A hollow, Rhodium plated, 1.25 inch diameter copper tube serves as an inner heat shield which fits inside the Kanthol element and smooths out the temperature gradients. The use of a good thermal conductor like copper is strategic in reducing the temperature gradients near the sample region. The temperature gradients are estimated at 0.02°C/mm in the sample region. The Rhodium plating prevents oxidation of the copper at elevated temperatures. There are 6.5 mm holes in the heat shield for light input and output. A solid Rhodium plated copper cylinder is fastened to the inner wall of the inner heat shield to support the sample holder. The sample holder is a solid cylinder of copper, 1 inch in height, 1.25 inch in diameter with a 11/16 x 13/16 inch hole for the crystal. There are three 5 mm diameter holes in this piece to allow the light to pass through the sample and to be observed. Fused quartz windows, 1/.6 inch thick, 5 mm diameter, cover these holes to reduce air currents. Evacuated fused quartz cells, which allow light to pass through but limit any thermal loss by convection, extend out from the sample region to the outside section of the stainless steel can. Another solid, Rhodium plated copper cylinder fits snugly into the sample holder and seals the sample region. Thus the sample region is essentially surrounded by copper with heat being supplied from the sides. The heat loss due to the rising of the heated air was compensated for by a lavite plug with a heater embedded in the end plate. The plug fits into the hole at the top of the oven and a constant amount of heat is supplied to the heater (20 watts).

TEMPERATURE CONTROL

A block diagram of the temperature control and measuring apparatus is shown in Fig. B-2. The outer heater raises the ambient temperature of the sample region to 550°C. Thus only a small amount of power need be applied to the inner heater to increase the temperature of the sample to the transition temperature: 573°C.

A Variac (Powerstat 2260) is used to limit the 220 V.A.C. line voltage applied to the primary of the transformer. The Kanthol heating elements have a very low resistance (less than one ohm) and a step down transformer (220:32) is necessary to reduce the voltage applied to the heaters. The maximum power rating of the outer heater is 1 kW at 32 V and 33 A. A Partlow time proportional controller (Model LFES) activates a mercury relay in the secondary of the transformer. The sensor of the Partlow controller is a steel tube encapsulating liquid mercury which expands and moves a temperature indicator which has a microswitch mounted on it. As the temperature indicator approaches the set temperature the microswitch makes contact with a rotating cam (2 rpm) attached to the set arm of the controller. The microswitch activates the mercury relay and turns the outer heater off for a portion of the cycle. This controller alone is able to control the oven within ± 5 C° at 550°C.

A Fisher Proportional Controller (Model No. 15-177-50V2) with a thermistor sensor controls the power supplied to the inner Kanthol heating element. Since this heating element has a very low resistance a transformer is required to step down (110:8) the 110 V.A.C. output of the controller. The inner heater has a maximum power rating of 280 watts at 8 V and 35 A. The controller is essentially an A. C. bridge with the

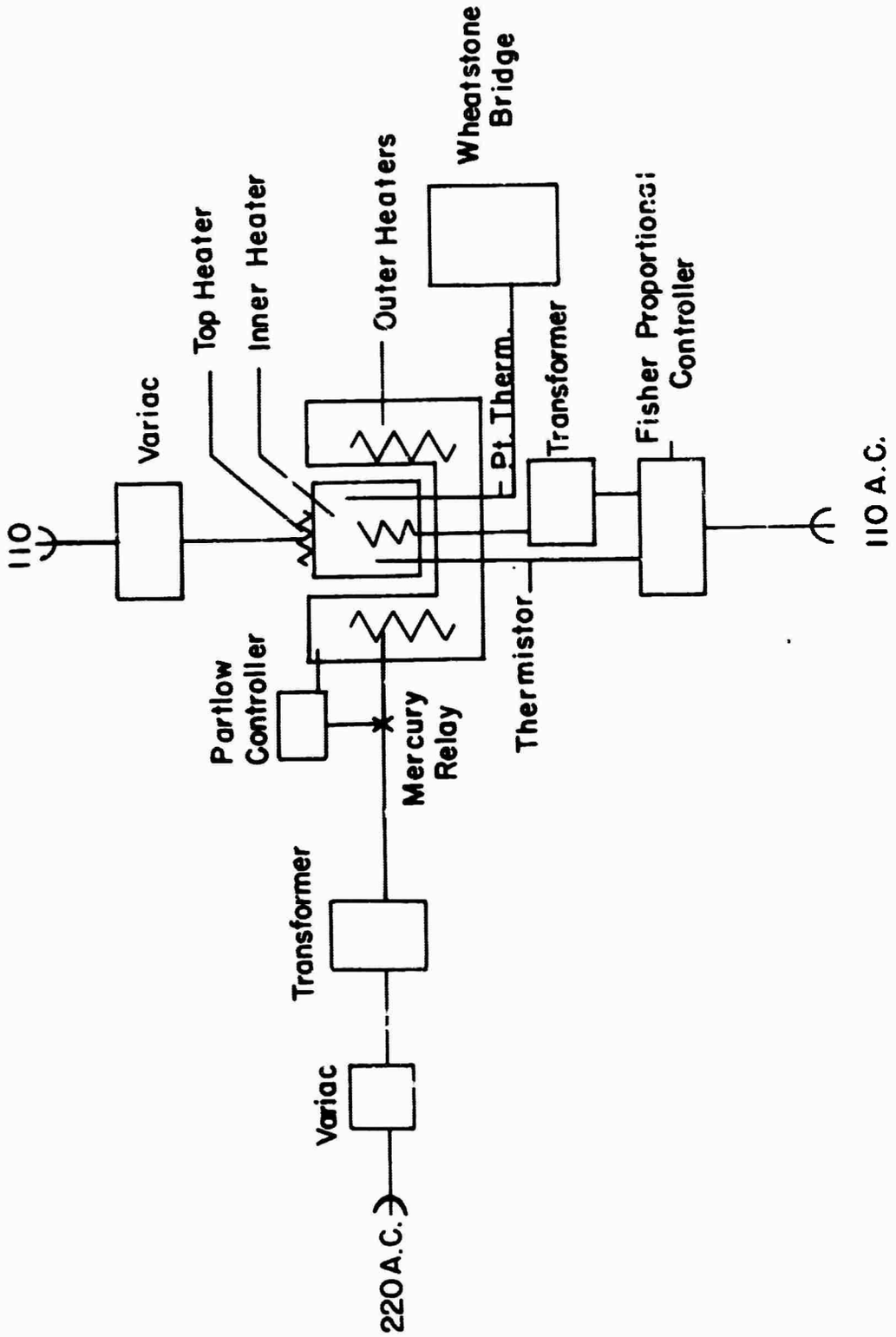

Fig. B-2. Block diagram of the temperature control and measurement system.

thermistor as the variable arm. The error signal from the bridge is amplified and is used to trigger two SCR's which limit the output of the controller. The availability of a thermistor that can withstand a temperature of 600°C in an oxidizing atmosphere is the limiting factor in our temperature stability. The thermistor used was supplied by Carborundum Co. and has a resistance of ∿300 ohms at 575°C. The temperature stability of the oven is 0.03°C/hr. Since no spectrum took more than 10 minutes to record, the temperature is essentially constant during the recording of the spectra.

In the transition region the temperature can be changed by .03 C° increments. Each time the temperature is changed by 1 degree or less, 45 minutes to an hour is allowed for the oven to equilibrate.

TEMPERATURE MEASUREMENT

A Rosemount Engineering Company Platinum resistance thermometer (Model No. 104M48ACHT) is used for temperature measurement. Its resistance is measured by an equal ratio arm (1 KΩ), laboratory constructed Wheatstone Bridge. The adjustable arm of the bridge is a General Radio Decade box (Model No. 1432-W) with variable resistance from .01 ohm to 9999.99 ohms. The null detector is a Honeywell Electronic Null detector (Model No. 10411-WG). The resistance of the thermometer in the transition temperature region is approximately 1230 ohms and the slope of the R vs T curve is .75 Ω/°C. Thus a .01 ohm change corresponds to a change in temperature of .0075 C°. Our sensitivity was limited by the amount of current we could supply to the thermometer without appreciable self heating. The overall sensitivity of the temperature measuring system at 573°C is 0.02°C.

The absolute accuracy of the temperature measured is within ± 1 C°. No effort was made to compensate for the lead resistance or changes in the lead resistance as the temperature of the oven is raised. The triple point resistance of the Platinum thermometer with all the leads used in the experiment was checked and found to be within 0.3 ohm (=0.2°C) of the calibrated value. The thermometer is an immersion type and has an element length of 2 inches. Since the thermometer is placed above the sample the temperature read is averaged over a region above the sample. However, since the sample and the thermometer are surrounded by copper, and since the thermal gradients are very small, the temperature read by the thermometer is close to that of the crystal. Also our measured transition temperatures agree very well with other published values of the transition temperature (1).

Summarizing the performance of the temperature control and measurement of our system:

1. The sensitivity of the temperature control in the transition region is 0.03°C.
2. The absolute accuracy of the temperature measurement is within ±1°C.
3. The relative sensitivity of the temperature measurement in the transition region is 0.02°C.

NOTES

1. R. B. Sosman, The Properties of Silica (The Chemical Catalogue Co., Inc., New York, 1927), and The Phases of Silica (Rutgers University Press, New Jersey, 1965).

2. R. W. G. Wyckoff, Crystal Structures (John Wiley and Sons, Inc., New York, N. Y., 1965).

3. Proc. IRE 37, 1378 (1949).

4. H. A. McKinstry, Mineral Industries 34, 1 (1965).

5. C. Kittel, Introduction to Solid State Physics (John Wiley and Sons, Inc., New York, 1967).

6. C. Frondel, Am. Mineralogist 30, 447 (1945).

7. L. A. Thomas and W. A. Wooster, Proc. Roy. Soc. A208, 43 (1951).

8. W. G. Cady, Piezoelectricity (Dover Publications, New York, N. Y., 1964).

9. J. F. Nye, Physical Properties of Crystals (Oxford University Press, London, 1957).

10. F. A. Jenkins, and H. E. White, Fundamentals of Optics (McGraw-Hill Book Co., Inc., New York, N. Y., 1957).

11. G. Mayer, Ph.D. Thesis, University of Paris (1959) (Unpublished).

12. For a rigorous theoretical treatment of the normal mode problem see M. Born and K. Huang, Dynamical Theory of Crystal Lattices (Oxford University Press, London, 1954).

13. D. A. Kleinman and W. G. Spitzer, Phys. Rev. 125, 16 (1962).

14. V. Heine, Group Theory in Quantum Mechanics (Pergamon Press, New York, N. Y., 1960), and M. Tinkham, Group Theory and Quantum Mechanics (McGraw-Hill Book Co., New York, N. Y., 1964).

15. D. F. Hornig, J. Chem. Phys. 16, 1063 (1948), and H. Winston and R. S. Halford, J. Chem. Phys. 17, 607 (1949).

16. S. Bhagavantam and T. Venkatarayudu, Proc. Indian Acad. Sci. A9, 224 (1939).

17. J. Murphy, H. H. Caspers and R. A. Buchanan, J. Chem. Phys. 40, 743 (1969).

18. International Tables for X-ray Crystallography, Vol. I (The Kynoch Press, Birmingham, England, 1965).

19. L. D. Landau and E. M. Lifshitz, Statistical Physics (Addison-Wesley Publishing Co., Inc., Reading, Massachusetts, 1958).

20. R. A. Young, U. S. Air Force Office of Scientific Research, Final Report No. AFOSR-2569 (unpublished) and Defense Department Documentation Center, Report No. AD 276-235, 1962 (unpublished).

21. B. D. Saksena, Proc. Indian Acad. Sci. A12, 93 (1940).

22. S. M. Shapiro, D. C. O'Shea and H. Z. Cummins, Phys. Rev. Letters 19, 261 (1967).

23. P. K. Narayanaswamy, Proc. Indian Acad. Sci. A26, 527 (1947); A28, 417 (1948).

24. M. A. Mosesmann, and K. S. Pitzer, J. Am. Chem. Soc. 63, 2348-2356 (1941) and N. N. Sinel'nikov, Dokl. Akad. Nauk. SSSR. 92, 369 (1952).

25. A. J. Majumbdar, H. A. McKinstry and R. Roy. J. Phys. Chem. Solids 25, 1487 (1964).

26. A. H. Jay, Proc. Roy. Soc. (London) A142, 237 (1933).

27. R. K. Cook and P. G. Weissler, Phys. Rev. 80, 712 (1950).

28. J. V. Atanasoff and P. J. Hart, Phys. Rev. 59, 85 (1941).

29. K. P. Sinha and A. P. B. Sinha, Indian J. Pure Appl. Phys. 2, 91 (1964).

30. M. E. Fisher, Repts on Prog. in Phys. 30, 615 (1967).

31. V. L. Ginzburg and A. P. Levanyuk, J. Phys. Chem. Solids 6, 51 (1958), and Zh. Eksperim. i Theor. Fiz. 39, 192 (1960) [translation: Soviet Phys.-JETP 12, 138 (1961)]; V. L. Ginzburg, Usp. Fiz. Nauk. 77, 621 (1962) [translation: Soviet Phys.-Usp. 5, 649 (1963)].

32. L. P. Kadanoff et al, Rev. Mod. Phys. 39, 395 (1967).

33. I. L. Fabelinski, Molecular Scattering of Light (Plenum Press, Inc., New York, N. Y., 1968).

34. A. Einstein, Ann. Physik 33, 1275 (1910).

35. A. Yakovlev, T. S. Velichkina and L. F. Mikheeva, Dokl. Akad. Nauk. SSSR 106, 675 (1956) [translation: Soviet Phys.-Doklady 1, 215 (1956)] and Kristallografiya 1, 91 (1956); I. A. Yakovlev and T. S. Velichkina, Usp. Fiz. Nauk. 63, 411 (1957) [translation: Advan. Phys. Sci. 63, 552 (1957)].

36. R. Loudon, Proc. Roy Soc. (London) A275 , 218 (1963).

37. R. Loudon, Adv. in Physics 13, 423 (1964).

38. S. Mizushima, Handbuch der Physik 26, 171 (1958).

39. G. S. Landsberg and L. I. Mandel'shtam, Z. Physik 50, 769 (1928).

40. K. S. Krishnan, Nature 122, 477 (1928).

41. F. Rasetti, Nuovo Cimento 9, 72 (1932).

42. R. S. Krishnan, Nature 155, 452 (1945).

43. C. V. Raman and T. M. K. Nedungadi, Nature 145, 147 (1940).

44. V. G. Zubov and L. P. Osipova, Kristallografiya 6, 418 (1961) [Translation: Soviet Phys.-Crystallography 6, 330 (1961)].

45. J. F. Scott and S. P. S. Porto, Phys. Rev. 161, 903 (1967).

46. T. C. Damen, S. P. S. Porto and B. Tell, Phys. Rev. 142, 570 (1966).

47. J. F. Scott, L. E. Cheesman and S. P. S. Porto, Phys. Rev. 162, 834 (1967).

48. J. F. Scott and S. Oshioda, Light Scattering in Solids (G. B. Wright, ed., Springer Verlag, New York, 1969), paper A-4.

49. P. E. Tannenwald and D. L. Weinberg, I EEE.J. Quantum Electronics QE-3, 334 (1967).

50. R. H. Lyddane, R. G. Sachs and E. Teller, Phys. Rev. 59, 673 (1941).

51. The following derivation is similar to the derivation in M. Born and K. Huang, Dynamical Theory of Crystal Lattices (Oxford University Press, London, 1959), pp. 82ff.

52. W. Cochran and R. A. Cowley, J. Phys. Chem. Solids 23, 447 (1962).

53. A. S. Barker, Jr., Phys. Rev. 136, A1290 (1964).

54. W. G. Spitzer and D. A. Kleinman, Phys. Rev. 121, 1324 (1961).

55. A. S. Pine and P. E. Tannenwald, Phys. Rev. (to be published).

56. R. S. Krishnan, Proc. Indian Acad. Sci. 22A, 329 (1945).

57. J. F. Scott, Phys. Rev. Letters, 21, 907 (1968).

58. M. M. Elcombe, Ph.D. Thesis, Cambridge University, 1966 (unpublished; and Proc. Phys. Soc. (London) 91, 947 (1967).

59. J. D. Axe and G. Shirane, Washington, D.C. APS. Meeting April 1969. Bull. Am. Phys. Soc. (to be published).

60. V. Dvorák, Phys. Rev. 167, 525 (1968).

61. E. M. Brody and H. Z. Cummins, Phys. Rev. Letters 21, 1263 (1968).

62. A. A. Maradudin and A. E. Fein, Phys. Rev. 128, 2589 (1962).

63. K. N. Pathek, Phys. Rev. 139, A1569 (1965).

64. R. A. Cowley, Phil. Mag. 11, 673 (1965).

65. W. Cochran, Adv. in Physics 9, 387 (1960).

66. L. Brillouin, Ann. Phys. 17, 88 (1922).

67. H. Mueller, Proc. Roy. Soc. (London) A166, 425 (1938).

68. G. B. Benedek and K. Fritsch, Phys. Rev. 144, 647 (1966).

69. R. W. Gammon and H. Z. Cummins, Technical Report No. 2, AROD Contract No. DA-31-124-ARO-D-400 (1967); and R. W. Gammon, Ph.D. Thesis, Johns Hopkins University (1967) (Unpublished).

70. H. Z. Cummins, "Laser Light Scattering Spectroscopy," in International School of Physics "Enrico Fermi XLII Course, Varenna 1967" (Academic Press, New York, N. Y.) (in press).

71. L. D. Landau and E. M. Lifshitz, Theory of Elasticity (Addison-Wesley Publishing Co., Inc., Reading, Mass., 1959).

72. G. W. Farnell, Can. J. Phys. 39, 65 (1961).

73. The positive directions of X, Y, or Z were not known. When directions are referred to it is understood that the sign may be (+) or (-). For most phonons studied the velocity depended only on the square of components of the phonon propagation direction and, thus, was insensitive to sign.

74. H. J. McSkimin, J. Acoust. Soc. Am. 34, 1271 (1962).

75. The known Pockel's coefficients are tabulated in Landolt-Bonstein, Group III, Vol. I, Elastic, Piezoelectric, Piezooptic and Electro-optic Constants of Crystals (Springer-Verlag, New York, 1966).

76. F. Pockels. Lehrbuch der Kristalloptik (Teibner, Leipzig, 1960).

77. E. Gross, Nature 126, 201 (1930).

78. R. S. Krishnan, Proc. Indian Acad. Sci, 22A, 329 (1945).

79. R. S. Krishnan, Nature 159, 740 (1947), Proc. Indian Acad. Sci. 26A, 399 and 450 (1947); R. S. Krishnan and V. Chandrasekharan, Proc. Indian Acad. Sci. 31A, 427 (1950); V. Chandrasekharan, Proc. Nat. Inst. Sci. 19, 597 (1953).

80. S. M. Shapiro, R. W. Gammon and H. Z. Cummins, Appl. Phys. Letters 9, 157 (1966).

81. G. E. Durand and A. S. Pine, IEEE J. Quantum Electronics, QE-1, 523 (1968).

82. R. S. Krishnan, Proc. Indian Acad. Sci. 41A, 91 (1955).

83. A. Perrier and R. Mandrot, Compt. Rend. 175, 622 (1922).

84. R. Bechman, Proc. Phys. Soc. (London) B64,323 (1951).

85. S. Bhagavantam, Proc. Indian Sci. Congr. 33rd Congr. Part II (1946).

86. O. Nomoto, Proc. Phys.-Math. Soc. Japan 25, 240 (1943).

87. I. Koga, M. Aruga and Y. Yoshinaka, Phys. Rev. 109, 1467 (1958).

88. R. Bechmann, Phys. Rev. 110, 1060 (1958).

89. H. J. McSkimin, P. Andreatch, and R. N. Thurston, J. Appl. Phys. 36, 1624 (1965).

90. J. V. Atanasoff and P. J. Hart, Phys. Rev. 59, 85 (1941).

91. V. G. Zubov, Dok. Akad. Nauk. SSSR 107, 392 (1956) [Translation: Sov. Phys.-Dokl. 1, 187 (1956)].

92. V. G. Zubov and M. M. Firsova, Kristallografiya 7, 469 (1962) [Translation: Sov. Phys.-Crystallogr. 7, 374 (1962)].

93. J. V. Atanasoff and E. W. Kammer, Phys. Rev. 59, 97 (1941).

94. E. W. Kammer, T. E. Pardue and H. F. Frissel, J. Appl. Phys. 19, 265 (1948).

95. V. G. Zubov and M. M. Firsova, Dokl. Akad. Nauk. SSSR 109, 493 (1956) [Translation: Sov. Phys-Dokl. 1, 441 (1956)].

96. R. Y. Chiao and B. P. Stoicheff, J. Opt. Soc. Am. 54, 1286 (1964).

97. H. Z. Cummins and R. W. Gammon, J. Chem. Phys. 44, 2785 (1966).

98. For a complete discussion of the properties of the Fabry-Perot used in this experiment see Ref. 69.

99. R. W. Gammon, Pvt. Communication.

100. S. M. Shapiro and H. Z. Cummins, Phys. Rev. Letters, 21, 1578 (1968).

101. L. D. Landau and I. M. Khalatnikov, Dokl. Akad. Nauk. SSSR 96, 469 (1954); and Collected Works of L. D. Landau, edited by D. Ter Haar (Gordon and Breach Publishers, Inc., New York, N. Y., 1967), p. 626.

102. E. J. O'Brien and T. A. Litovitz, J. Appl. Phys. 35, 180 (1964).

103. R. W. Gammon and H. Z. Cummins, Phys. Rev. Letters 17, 193 (1966).

104. M. L. Keith and O. F. Tuttle, Am. J. Sci., Bowen Volume, 203 (1952).

105. H. L. Swinney and H. Z. Cummins, Phys. Rev. 171, 152 (1968).

106. J. D. Rigden and E. I. Gordon, Proc. IRE 50, 2367 (1962).

107. The first observation of this in our laboratory was by Robert Gammon.

108. S. M. Shapiro, R. W. Gammon and H. Z. Cummins, Appl. Phys. Letters 10, 113 (1967).

109. H. C. Van de Hulst, Light Scattering by Small Particles (John Wiley and Sons, New York, N. Y., 1957).

110. H. Brumberger, W. Claffey, N. G. Alexandropoulos, and D. Hakim, Phys. Rev. Letters 22, 537 (1969); and W. Claffey, Private Communication.

111. R. A. Ycung and B. Post, Acta Cryst. 15, 337 (1962).

112. The subscripts denote which segments of the hexagonal cell (Figs. I-2 and I-5) the atoms border or are located in. The numbers are the notation of Saksena (21) and Kleinman and Spitzer (13). In the coordinate system used, X and Y make an angle of 120° with one another and Z is perpendicular to X and Y (see Chapter I).

113. V. G. Zubov, M. M. Firsova and T. M. Molokovo, Kristallografiya 8, 112 (1962) [Translation: Sov. Phys.-Crystallogr. 8, 85 (1963)].